Investigation of volatile gas sensors integrated on flexible and wearable substrates with functional nanomaterials

by

Hyejin Park

A dissertation submitted to the Graduate Faculty of
Auburn University
in partial fulfillment of the
requirements for the Degree of
Doctor of Philosophy

Auburn, Alabama
Aug 01, 2015

Keywords: ZnO nanorods, graphene oxide, gas sensors, wearable devices

Approved by

Dong-Joo Kim, Chair, Professor of Materials Engineering
Barton C. Prorok, Professor of Materials Engineering
Zhongyang Cheng, Professor of Materials Engineering
Helen Koo, Assistant Professor of Consumer and Design Sciences

Abstract

In this dissertation, development of gas sensors on wearable substrates was studied to overcome the limitations, e.g., high-temperature process for fabricating sensing material, high sensing temperature, insufficient sensitivity and selectivity. The approach to overcome these limitations was focused on developing coating methods on fabrics, catalyst doping, and investigation of alternative sensing materials. A representative metal oxide with good semiconducting properties, ZnO (3.37 eV band gap), was explored as a sensing material. Thin films of the ZnO material were coated on sensor platforms by different deposition techniques: sputtering, sol-gel, dip-pad-cure method, and electrophoretic deposition and their properties were studied. Additionally, ZnO nanorod structure was grown by thermolysis-assisted chemical solution deposition on ZnO seed layer to enhance the sensing performance by using nanostructure. Among these deposition methodologies, dip-pad cure method was found to be suitable to coat ZnO at low temperature on fabric substrates.

To lower sensing temperature from several hundred Celsius (i.e. 300 °C) to room temperature in semiconductor oxide sensors, the effects of catalyst on gas sensing mechanism and performance were studied. Additionally, composition gradient effects on gas sensing behavior to improve gas selectivity were explored by adapting different metal elements. The combination of two metallic catalysts by varying their concentrations in a sensor platform was investigated: platinum and palladium combination and platinum and titanium combination. Since the amount and island size of catalysts strongly influence structural

modification of metal oxide materials, the sensing properties can be changed. Therfore, the fundamental study of catalyst elements and their effects on change in concentration were conducted to realize chemical gas sensor module with improved selectivity and sensitivity under multiple gas combination.

Another approach to reduce sensing temperature of semiconductor oxides is to utilize non-traditional oxide materials. As a new sensing material, graphene oxide was used due to its good semiconducting and chemical properties. Graphene oxide presents conducting or insulating properties according to its reduction condition. Therefore, reduction of graphene oxide was studied to achieve room temperature gas detection reported in the literature. However, exploration of non-treated graphene oxide, i.e. pristine graphene oxide, was rarely conducted. This study investigated the use of non-treated graphene oxide for gas sensors, and its reduction behavior on electrical properties such as N-P transition was studied.

Finally, the combinatorial or composite structure was investigated with SnO_2 nanostructure and graphene oxide to enhance gas selectivity. The ratio of graphene oxide to SnO_2 was changed as the amount of SnO_2 was added. To explore how they interact to improve the gas sensing behavior, the combined structure was also modified, for examples bimorph structure and multilayer structure.

Acknowledgments

I would like to express the deepest appreciation to my academic advisor Dr. Dong-Joo (Daniel) Kim to whom this dissertation could not have completed without his encouragement and support. He not only guided me throughout the research effort but also encouraged me over the course of the Ph.D. pursuit and in overcoming personal obstacles since joining his research group.

I would like to express my deepest gratitude to my committee members, Dr. ZhongYang Cheng, Dr. Bart Prorok, and Dr. Helen Koo for their valuable suggestions and guidance. I also would like to show thanks to my group alumni and members, Dr. Hosang Ahn, Dr. Seon-bae Kim, Dr. Seokhee Lee, Mr. Jaeyoung Jeong, Ms. Yoonsung Chung, Ms. Eunji Lee, and Mr. Soohyun Ahn for their co-work and help during the last four and a half years. Especially, I would like to give my thanks to Dr. Joo Hyon Noh for his effort in setting up the equipment and developing software to measure the gas sensing properties, which saved me considerable time and made the experiments much easier.

Lastly, my family is the reason why I live and study here in U.S. I would like to say thank you to my parents: Young-ik Park, Hyun-min Park; my husband and my son: Chanyoung Park and Mason W. Park; my brother Kukkwon Park, and Soo-kwon Park whom I love. Without their love and support during my study, I could not have reached this point.

Table of Contents

List of Tables

List of Figures

List of Abbreviations

ZnO	Zinc Oxide
SnO_2	Tin Oxide
GO	Graphene Oxide
r-GO	Reduced Graphene Oxide
Pt	Platinum
Ti	Titanium
Pd	Palladium
HMT	Hexamethylenetetramine
DEA	Diethanolamine
MEA	Monoethanolamine
ITO	Indium Tin Oxide
PET	Polyethylene Terephthalate
PVD	Physical Vapor Deposition
DPC	Dip-Pad Cure
EPD	Electrophoretic Deposition
SEM	Scanning Electron Microscopy
XRD	X-ray Diffraction
EDS	Energy Dispersive X-ray Spectroscopy
XPS	X-ray Photoelectron Spectroscopy
FTIR	Fourier Transform Infrared Spectroscopy
VOC	Volatile Organic Compound

UV	Ultra Violet
SOI	Silicon On Insulator
DC	Direct Current
RF	Radio Frequency
MFC	Mass Flow Controller
MEMS	MicroElecroMechanical Systems

CHAPTER 1. INTRODUCTION

1.1 Background and motivation

Gas sensors are widely used in various fields of food market, construction, and automobile industry, to medical field to prevent the accident from unexpected gas flow [1,2,3]. The fabrication of gas sensors on traditional silicon-based substrates has made sensors more portable even as small as a micro-chip. For example, the utilization of SOI, silicon on insulator, enables electronic devices to be miniaturized and brings enormous research and development opportunities in the electronics. Gas sensors have also been developed based on silicon-based wafers where the electrode's structure and shape are easily changed to improve the sensing performance [4]. As gas sensors expand their applications, the attempt to adopt alternate and functional substrates has been focused. ITO (indium tin oxide) glass is one of the examples as a functional substrate for electronics [5]. Adaption of gas sensors on flexible substrates such as polyimide and PET (polyethylene terephthalate) films is another example to install gas sensors in the complex place, where the sensors on solid substrates are hard to be installed [6].

As the demands of gas sensors increase in the medial industry, research on the investigation of wearable substrates has been attracted attentions. Especially in the medical industry, development of gas sensors to detect gasses on the patient's breath can be very important to monitor and ensure the patient's health conditions [7]. Approaches to embed or carry electronics on human skin promote to explore other types of flexible substrates such as membranes and fabrics. In terms of using fabrics, wearable electronic devices have been explored especially for various medical purposes. It may be possible to monitor patients'

health condition all day as wearing the electronic devices in a part of the cloth. In this respect, embedding gas sensing components on the fabrics has been focused. However, using fabric substrates to embed electrical components still have limitations such as high-temperature process, and high working temperature [8].

1.2 Objectives of research

In this dissertation, developing of gas sensors on wearable substrates was studied to overcome the limitations, e.g., high-temperature process, high sensing working temperature, poor sensitivity and low selectivity. The approach to overcome these limitations was focused on developing coating methods on fabrics, catalyst doping, and alternative sensing materials. A representative metal oxide with good semiconducting properties, ZnO, was focused (E_g = 3.37 eV) in addition to alternate SnO_2, graphene oxides and their composite structure.

1. Process development at low deposition temperature: ZnO material was coated on sensor platforms by different deposition techniques: sputtering, sol-gel, dip-pad-cure (DPC) method, and electrophoretic deposition (EPD). The ZnO nanorods were grown by thermolysis-assisted chemical solution deposition on the ZnO seed layer. Among these deposition methodologies, suitable coating methods working at low temperature were employed for fabric substrates. Then, properties of ZnO deposited via different methods were compared to support the suitable deposition methods on wearable substrates.

2. Catalyst effect by compositional gradient to lower the operating temperature and to enhance the selectivity: To lower sensing temperature from several hundred Celsius

to room temperature of semiconductor oxide sensors and to improve the gas selectivity, compositional gradient of catalysts was explored based on the catalyst effects on gas sensing mechanism and performance. Two metals having different catalytic activities were utilized: Platinum (Pt) and palladium (Pd). The thickness of the catalyst layer kept constant, and only the composition (ratio of the components) was changed to investigate the effect of the catalyst composites [4].

3. Alternative sensing materials to achieve room temperature gas sensing on wearable substrates: Another approach to reduce sensing temperature of semiconductor oxides was to utilize non-traditional oxide materials. As a new sensing material, graphene oxide was used due to its good semiconducting and chemical properties. Graphene oxide is well known as conducting or insulating properties according to its reduction condition. Non-treated graphene oxide and its reduction were studied to understand transition behavior of the electrical properties and further to construct semiconducting graphene oxides for gas sensing application.

4. Combinatorial structure for gas selectivity: Finally, a single chip array sensor was developed to discriminate types of gas mixture. Beyond metal catalysts, oxide composite was investigated to achieve room temperature gas sensors with oxide catalytic effect. The array was designed by fabricating gradient combination of graphene oxide and other metal oxides such as ZnO and SnO_2. Such a gradient structure was investigated and applied for the gas sensing layer to improve the sensitivity and selectivity from one chip.

1.3 Dissertation structure

This dissertation consists of 8 chapters including an introduction to conclusions of this research. Each chapter covers details that are listed below.

Chapter 1 introduces how this dissertation contributes to scientific and engineering fields providing the motivation, research objectives and dissertation structure.

Chapter 2 supports the purpose of this dissertation based on the literature survey: deposition methods of ZnO, effects of a composition gradient of catalyst on the properties of semiconductor oxides, use of graphene oxide as a gas sensor, and combinatorial structure of oxide compounds.

Chapter 3 describes the experimental set up of the research: a process to prepare solutions/suspensions to deposit the sensing materials and to fabricate the gas sensing devices.

Chapter 4 describes the exploration of various types of deposition methods of ZnO and property changes of ZnO based on the deposition types. Investigation of coating methods on wearable substrates was discussed.

Chapter 5 demonstrates the effect of a compositional gradient of catalysts by changing the ratio of metal catalysts on gas sensing behaviors.

Chapter 6 covers the material study of non-treated graphene oxide and its reduced state after thermal reduction for gas sensing behaviors.

Chapter 7 discusses the combined structure from graphene oxide and metal oxide for enhancing gas selectivity.

Chapter 8 summarizes the achievements attained over the course of this research and future research directions that may further advance the field.

References

1. Funazaki N, Hemmi A, Ito S, et al. Application of semiconductor gas sensor to quality control of meat freshness in food industry. *Sensors and Actuators B: Chemical.* 1995;25(1):797-800.
2. Kawamura K, Kerman K, Fujihara M, Nagatani N, Hashiba T, Tamiya E. Development of a novel hand-held formaldehyde gas sensor for the rapid detection of sick building syndrome. *Sensors and Actuators B: Chemical.* 2005;105(2):495-501.
3. Oto K, Shinobe A, Manabe M, Kakuuchi H, Yoshida Y, Nakahara T. New semiconductor type gas sensor for air quality control in automobile cabin. *Sensors and Actuators B: Chemical.* 2001;77(1):525-528.
4. Müller G, Friedberger A, Kreisl P, Ahlers S, Schulz O, Becker T. A MEMS toolkit for metal-oxide-based gas sensing systems. *Thin Solid Films.* 2003;436(1):34-45.
5. Nogami M, Maeda T, Uma T. A methanol gas sensor based on inorganic glass thin films. *Sensors and Actuators B: Chemical.* 2009;137(2):603-607.
6. Kim YS. Microheater-integrated single gas sensor array chip fabricated on flexible polyimide substrate. *Sensors and Actuators B: Chemical.* 2006;114(1):410-417.
7. Yamazoe N. Toward innovations of gas sensor technology. *Sensors and Actuators B: Chemical.* 2005;108(1):2-14.
8. Morrison SR. Selectivity in semiconductor gas sensors. *Sensors and actuators.* 1987;12(4):425-440.

CHAPTER 2. LITERATURE BACKGROUND

2.1. Process development to adapt gas sensors on wearable substrates.

Science and technology are continuously focusing on the miniaturization of electronic machines or devices using nano-fabrication on silicon substrates [1,2]. Efforts to realize soft portable electronic devices such as wearable devices, electronic papers, and chip smart cars became a possible route to revolutionize modern society [3,4]. Fabrics can be good substrates for constructing electronic systems with another functionality, such as protection of the body against the harmful environment and collection of body's status and conditions [5,6]. Among multifunctional inorganic materials, ZnO is a great candidate material having good semiconductor properties including a band gap of 3.37 eV and 60 meV of exciton binding energy [7]. Additionally, ZnO has much attention due to great UV blocking properties even from lower UV wavelength range (UV-A, 100 – 280 nm) to higher range (UV-C, 320 – 400 nm) [5,7]. Therefore, ZnO impregnated fabrics have been demonstrated for UV protection, clothing colors, and anti-odor function in recent study in terms of functionalized garments [6,9,10,11].

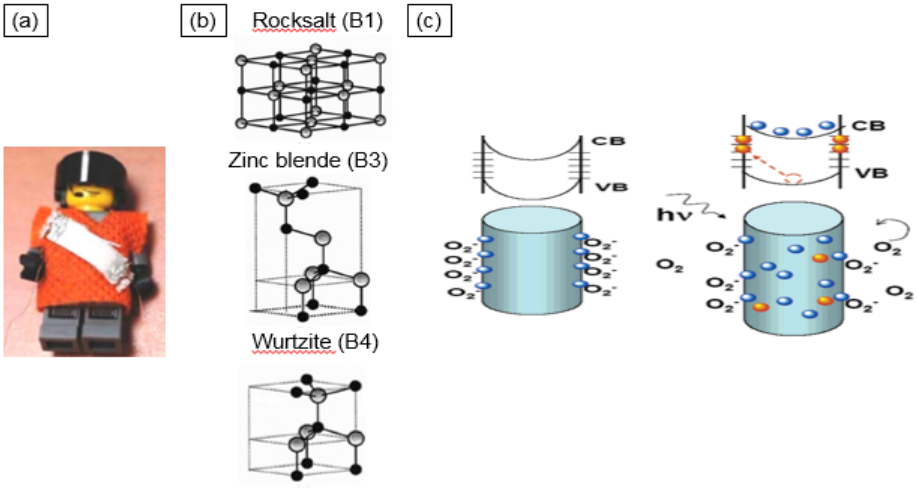

Figure 2-1. (a) A photograph of working device on fabric, (b) ZnO crystal structures, and (c) band gap structure changing by photonic source [5,12,13].

Multifunctional ZnO can be deposited by solution-based route such as dip-pad-cure (DPC), hydrothermal, and thermolysis assisted chemical solution method as well as other physical deposition methods. However, the use of fabric materials as a substrate for functional systems remains a critical challenge due to issues with developing more robust and cheaper fabrication of inorganic materials on fabrics [6]. Exploring new properties and advancing fabrication of ZnO for the functional garment will demand morphological control of ZnO nanostructures on fabrics. The environmental constraint of fabrics such as temperature and pressure can be another consideration. For the development of functionalized garments with ZnO, studies on process development are necessary.

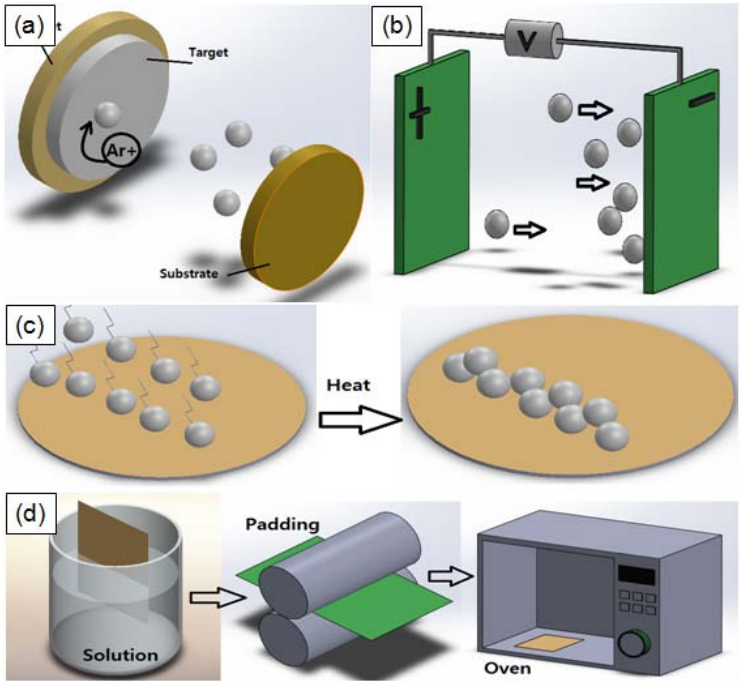

Figure 2-2. Illustrations of ZnO coating processes: (a) sputter deposition, (b) electrophoretic deposition (EPD), (c) sol-gel deposition, and (d) dip-pad-cure coating (DPC).

Physical vapor deposition (PVD) is one of the most common deposition methods for thin films. Among PVD, sputter deposition can operate at room temperature under high-pressure condition. For uniform film deposition, vacuum condition requires several tens mTorr in pressure [14-18]. Power can be supplied by DC (direct current) and RF (radio frequency) to interact target materials with Ar gas in a chamber. This interaction results in generating plasma (ionized gas) to transfer the target molecules to the substrates. To deposit thin film via sputter deposition, substrates can be varied from very rigid substrates to flexible substrates owing to its low operating temperature. However, this process can be more favorable to deposit a thin film on flat surface area since the film does not cover whole substrates if the substrates have a complex shape.

Table 2-1. Deposition conditions of ZnO via physical vapor deposition, sputter method.

Ref.	Type	Pressure, mTorr	Time, min	Power, W	Temperature, °C	O_2/Ar	Substrate
[14]	DC	12 – 25	10 – 70	50 – 100	RT – 450		Stainless steel
[15]	RF	5 – 30	5 – 30	100 – 200	RT	0.1	Si wafer
[16]	RF	50	5 – 30	200	RT	0.3	Si wafer
[17]	RF	6 – 45	30 – 60	150 – 300	RT	0.1	PET
[18]	RF	2 – 7		25 – 125	RT – 100		PAN

The sol-gel process, one of the solution-based methods, allows ZnO grains to have preferred orientation. The process has an intermediate step to elaborate a solid material from a solution by using sol or gel. This process has benefits of glasses and ceramics and direct thin film formation from the solution. To synthesize solid materials, the sol-gel process contains two main chemistry reactions based on the transformation of molecular precursors into an oxide network: by hydrolysis and condensation reactions. Through these processes, the material, especially ZnO, can be formed with preferred orientations [19]. However, the hydrolysis and condensation reactions to form ZnO require fairly high temperature over 300 °C. It can limit selection in substrates as summarized in Table 2-2. Even though the sol-gel has advantages to change the morphologies of materials by a change in precursors or additives, the high operating temperature to evaporate organic solvents remains as challenges in terms of adaptability.

Table 2-2. Deposition conditions of ZnO via sol-gel coating.

Ref.	Precursor	Alcohol	Additive	Pre-heat, °C	Post-heat, °C	Substrate
[19]	ZAD	MeOH	-	80	500 – 575	Pyrex
[20]	ZAD	EtOH	DEA	400	400 – 800	Quartz
[21]	ZAD	2-PrOH	MEA	250	650	Glass
[22]	ZAD	PVA	-	120	600	Si (100)
[23]	ZAD	2-ME	MEA	300	700	SiN_x/Si
[24]	ZAD	EG	Glycerol	100	200 – 600	Glass

Electrophoretic deposition (EPD), another solution-based method, is well known as colloidal process from suspensions. One of the unique characteristics of EPD is pre-synthesized powder-based deposition working at room temperature. Once the powders are charged in the suspension by any charging agent, they are attracted to the substrates, which have conductivity. Two parallel electrodes are required to deposit the charged particles by applied voltage in the suspensions. EPD is frequently used to deposit ZnO layer owing to its short formation time, simple apparatus irrespective of substrate shape, no binder requirement, and working at ambient conditions. However, the substrates need to be conductive for EPD process. To overcome this limitation, modified voltage application such as AC power supply has been adapted, but it results in low efficiency in film deposition.

Table 2-3. Deposition conditions of ZnO via electrophoretic deposition (EPD).

Ref.	Type	Conditions	Treatment	Substrate
[25]	DC	10 to 100 V for 5 – 25 min	400 °C annealing for 15 hr	Cu foil
[26]	DC	10 mA for 1 hr	-	Stainless steel sheet
[27]	DC	30 V for 7 min	390 sintering for 15 min	FTO glass
[28]	AC	10 mHz – 100 Hz for 5 min	-	Au electrodes on glass
[29]	DC	14 V for 40 min	-	Carbon fabric
[30]	DC	-	-	Carbon fabric

Dip-pad-cure coating is the fourth method introduced to coat ZnO on wearable substrates. This method is based on chemical solution route at lower formation temperature. The principle of the dip-pad-cure coating method is as same as dip coating [31]. Zinc acetate dehydrate, and an OH provider completely melt in alcohol solvent forming Zn(OH). Then, the Zn(OH) is transformed to ZnO during the curing process. The only difference is that the substrates are passing through a padder, which has two rollers to squeeze the substrates with a certain pressure. This means that devices on flexible substrates are suitable to adapt this process. Through the padding step, the coating layers are easily penetrating to all surfaces of the substrates instead of coating on only exposed area. As proven, the formation temperature of ZnO is fairly low as 170 °C, which is high enough temperature for the wearable substrates to be endured [1,8,32-35].

Table 2-4. Deposition conditions of ZnO via dip-pad-cure (DPC) coating method.

Ref.	Materials	Solvent	Dipping time, min	Curing temperature, °C	Substrate
[32]	ZAD + NaOH	Ethanol	2	170 for 10 min	cotton
[33]	ZAD + TEA	2-MeOH		150	Fabric
[34]	ZAD + NaOH	Ethanol	5	170 for 10 min	Cotton/PET/Nylon
[1]	ZAD + NaOH	Methanol	10	170 for 10 min	PET
[8]	ZAD + TEA	IPA	10	95 for 8 hr	Nylon
[35]	ZAD + NH_3	H_2O	10	120 for 1 hr	Cotton

Four types of ZnO seed layer coating methods are introduced above, and brief characteristics of each process are summarized in Table 2-5. Based on the literature background and summaries, solution-based fabrication of inorganic materials on fabric materials can be good approach instead of physical vapor deposition or chemical vapor deposition [2]. It is also known that the structure properties of ZnO (size, crystallinity, and shape) can be easily altered by parameters in solution-based process [9]. Especially, DPC coating seems to be most favorable to coat ZnO thin films for gas sensing layer owing to its low process temperature and uniform thin layer formation. However, little attention has been paid to the investigation of ZnO nanostructures driven by fabric types and their properties. In this section, not only process comparison is performed to coat ZnO on wearable substrates, but ZnO nanoparticles and nanorods also are grown on various fabrics such as cotton, PET, and nylon by chemical solution process. The growth behaviors of ZnO nanostructures on fabrics and their properties are characterized.

Table 2-5. Summaries of deposition methods of ZnO seed layer [35-38].

	Sputter	Sol-gel	EPD	DPC
Working Condition	Coating at RT High vacuum pressure	Coating at RT Pyrolysis at 300 °C	Coating at RT	Coating at RT
Treatment	No treatment	Annealing at 600 °C	No treatment	Cured at 150 °C
Pros	Uniform deposition	Uniform deposition	Simple process Complex shape	Deposition in complex shape
Cons	Only deposited on exposed area	High working temperature	Poor adhesion Conductive Substrate	Formation of ZnO at low temperature

2.2. Compositional gradient effect of catalysts on gas sensing performance to reduce operating temperature and to enhance gas selectivity.

Semiconducting metal oxides, such as WO_3, SnO_2, and ZnO, have been attracting a sustained interest for gas sensing applications because of their excellent gas responses [4,12]. Especially, ZnO is one of those semiconductors that has been widely investigated over the past decades in some commercially available gas sensors for a variety of combustible and toxic gas detections [3,5]. Most ZnO gas sensors use either thin film technologies or 3-D nanostructures to enhance their sensing ability. While the first-generation gas sensors have been investigated as the early gas detection to prevent fire and gas hazards, efforts to research

and develop ZnO based gas sensors have still to be devoted to achieve multiple gases sensing detections with greatly improved sensing performance. Especially, use of gas sensors has become broaden, and adapting gas sensing components on garments has been explored for medical purposes. Meanwhile, efforts to overcome the limitation of semiconducting gas sensors such as high operating temperature have been focused [39,40]. Most of semiconducting gas sensors including ZnO based sensors require several hundred degree to activate the molecules to react with surface gases. However, this high operating temperature is not suitable to adapt gas sensors on patient's garment to monitor their health conditions. There have been several approaches to reduce the operating temperature of gas sensing devices by controlling the band gap of semiconducting materials or changing structure of coated layer [40,41]. But, these approaches are not sufficient by reducing the working temperature of the sensors only several tens of degree. The most feasible approach in this respect seems to develop catalysts on supporting materials [39]. Adapting catalysts is the well known approach to increase active sites so that it promotes not only to react with surface gasses at a lower temperature but also enhance gas selectivity towards a variety of gasses.

Figure 2-3 below illustrates the concepts of sensing mechanism of semiconducting materials (especially n-type semiconductor) and effects of catalysts on the supporting materials. In Figure 2-3 (a), individual grains of n-type semiconductor in electrical contact are described. Specifically, each grain adsorbs oxygen on the surface, where the conduction band is generated at the near-surface region as adsorbed oxygen has extracted the conduction electrons from the materials leading to an insulating surface layer. Therefore, for conduction, the electrons inside of grains need to jump to the next grain by passing through the insulating layer.

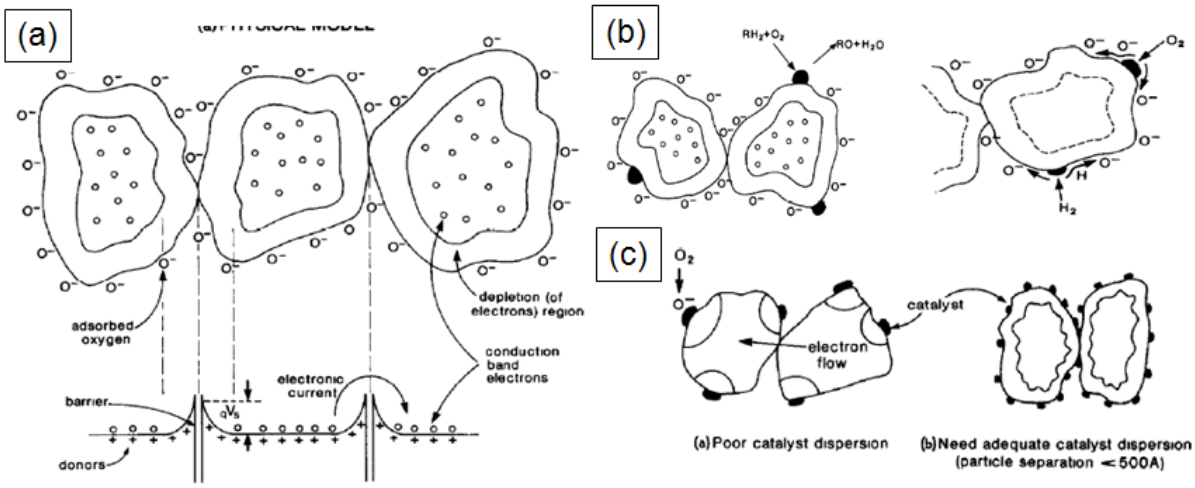

Figure 2-3. Schematic diagrams of (a) sensing mechanism of pure metal oxide, (b) spill-over mechanism of catalyst on the surface of metal oxide, and (c) Fermi energy control of catalyst on the surface of metal oxide [39].

Based on the illustration, the insulating layer is related to oxygen concentration (O_2 or O^-) and the generated layer is directly expressed as a barrier (V_s). Then, the concept of qV_s is where V_s increases as the concentration of O^- increases and the density of electrons (N_s) are given by the Boltzmann equation as shown in Equation (2): N_d is the density of donors, k is Boltzmann coefficient, and T is temperature. Therefore, the more amount of oxygen exists on the surface; the higher barrier is generated, and the fewer electrons can be transferred to the next grains resulting in higher resistance of the material. The term of RH_2 in Equation (3) refers to reducing agent representing catalysts on the surface. The concentration of RH_2 involves in controlling the concentration of O^- to modify the conductance barrier. Therefore, the existence of catalysts on the metal oxide surface plays an important role in gas sensing performances.

$$O_2 + 2e^- \rightarrow 2O^- \quad (1)$$

$$N_s = N_d \exp(-qV_s/kT) \quad (2)$$

$$RH_2 + 2O^- \rightarrow RO + H_2O + 2e^- \quad (3)$$

Once the catalysts are considered as important parameters to enhance gas sensing performances, understanding of the catalyst mechanisms is required. Two main mechanisms are introduced in the literature as shown in Figure 2-3 (b) and (c) called “spill-over” and “Fermi energy control.” Following Equations (4) – (7) explain how the concentration of oxygen is controlled by spill-over mechanisms. When the catalysts induce hydrogen and oxygen dissociation, it speeds up the overall reaction. Therefore, the resistance of the devices decreases rapidly as the concentration of catalysts (reducing agent) increases. Then, it results in the electrons to jump to the next grains easily.

$$2Pt\cdot + H_2 \rightarrow 2Pt\text{-}H \quad (4)$$

$$2Pt\cdot + O_2 \rightarrow 2Pt\text{-}O \quad (5)$$

$$2H\cdot + O^- \rightarrow H_2O + e\text{-} \quad (6)$$

$$RH_2 + 2O^- \rightarrow RO + H_2O + 2e^- \quad (7)$$

Fermi energy control is directly related to the migration of catalysts to the intergranular contacts with good dispersion. As the catalysts react with surface oxygen, it automatically removes the electrons from the semiconducting material with affecting the depletion of electrons. A few catalysts only affect small changes in depletion layer but adequate catalysts contribute to the overlap of the depletion regions and to extend to the intergranular contacts as shown in Figure 2-3 (c). These phenomena influence to the Fermi energy level and the surface barrier at the same time. Therefore, it is important to adjust the amount and dispersion

of catalysts on the surface of semiconductors.

Table 2-6 supports the effect of catalysts on metal oxide gas sensing behaviors. It has been proven that the catalysts enhance the gas response and lower the sensing temperature. However, these results still did not reach the room temperature gas sensing by the catalysts and the investigation was only focused on single catalyst behaviors on the metal oxide. In this section, the research will be more focused on the operating temperature to demonstrate gas sensors on wearable substrates and effect of combined catalysts with composition gradients. To explore the composition gradient of catalysts, Pt and Pd mixture and Pt and Ti combination were performed as the ratio of the metal catalysts were changed with distance [50-55].

Table 2-6. Effect of catalysts on gas response and sensing temperature.

Ref.	Materials	Catalysts	Methods	Target gas	Gas response	Sensing Temp (°C)
[42]	WO_3	Pd, Pt, Au	Sputter/evaporation	NO_2/NO	Pd: x 4 Pt: x 2 Au: x 3	Pd: -100 Pt: -150 Au: -100
[43]	SnO_2	Pt	Pulsed laser	CO	x 2.5	-100
[44]	ZnO	Ru, Rh, Pt, Au	Chemical precipitation/ sintering	C_2H_6OH/ C_4H_{10}/ H_2	Ru: x 12 Pt: x 4.7 Ag: x 2	Ru: -170 Pt: -70

[45]	SnO_2	Pd	Vapor grown	O_2/H_2	x 10	-
[46]	$SnO_{1.8}$	Ag	Aerosol route	Ethanol	x 3	-
[47]	ZnO	Cu	Sputter	CO	x 2.7	-150
[48]	SnO_2	Pt	Sputter	CH_4/H_2	x 2	-
[49]	ZnO	Au	Carbothermal route	NO_2	x 2	-150

2.3. Exploration of alternative materials to achieve room temperature detection.

Graphene, a monolayer of graphite, has been attracted in recent years due to its outstanding mechanical, thermal, and electrical properties [56,57]. Graphene has extremely high electron mobility and excellent electron transport at room temperature for applications in various electric devices including gas sensors [58,59]. The derivatives of graphene have also been investigated to improve the device performance. Graphene oxide (GO), a graphene sheet decorated with oxygen functional groups such as epoxy group (R-O-R), hydroxyl (R-OH), and carboxyl group (R-COOH), can be an ideal derivative for gas sensing application because GO contains a diverse range of surface sites whose density is easily controlled [60,61]. GO is made by the Hummers method mostly using natural graphite flake to make GO. This method makes it possible to obtain chemically modified graphene in large scale production. On the other hand, electrical conductivity becomes weaker (6×10^{-5} S/m) due to the oxygen-containing groups. Table 2-7 shows that several researches based on pure graphene gas sensors fabricated by traditional methods such as scotch tape. They demonstrated room temperature gas sensors are owing to excellent electrical properties of graphene such as easy electron transfer through double carbon bondings [64,65]. Additionally, many groups

explored the reduction of graphene oxide for the mass production of modified graphene and demonstrated gas sensing performance at room temperature. These groups showed feasible gas sensing performance with r-GO owing to its functionalization as well as mass production of the films. Such functionalization can be obtained by many different ways including thermal reduction that converts GO from an insulator to a semiconductor [62]. The reduction can modify the number of active sites reacting with gas molecules and its influence on electric transport. Therefore, most works reporting on gas sensing were focused on reduced or modified GO rather than pristine or non-treated GO [57,59,63].

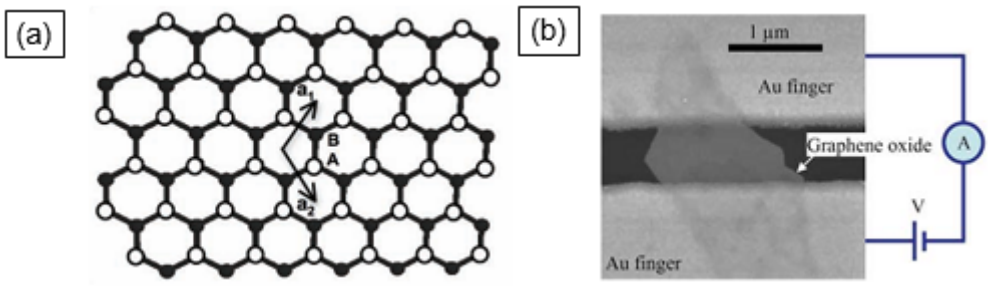

Figure 2-4. (a) Schematic of the crystal structure of graphene oxide and (b) SEM image of a GO sheet bridging the electrodes [56,59].

Table 2-7. Researches of gas sensor development based on graphene oxide.

Ref.	Reduction Conditions	Working Temp (°C)	Gas type	ppm
[59]	Hydrazine	RT	NO_2	100
[63]	600 °C in H_2 and NH_3	RT	NO_2	10
[64]	Pure graphene	RT	NO_2	100
[65]	Pure graphene	22 – 60	CO_2	100

[66]	120 °C for 1 hr	150	NH_3	65
[67]	Hydrothermal	RT	NO_2	2
[68]	Plasma reduction	RT	CO_2	750
[69]	Not treated	RT	H_2	1000
[70]	Hydrazine	RT	NH_3	50

Reduction process has been performed, and understanding of reduction process to control the electrical and sensing properties of GO is important. Three main reduction methods are reported to transform GO to graphene: chemical reduction, optical reduction, and thermal reduction as discussed in the introduction section. Chemical reduction of GO is conducted by using chemical reagents at room temperature or by moderate heating. Chemical reagents for the reduction are hydrazine, metal hydrides, and HI. These chemicals help to change the ratio of GO and C/O to convert GO to r-GO. Hydrazine is soluble in polymer DMH or ammonia as a surfactant to reduce GO. However, it is hazardous chemical reagent [59,70]. NaH, $LiAlH_4$, and $NaBH_4$ are examples of metal hydrides and especially $NaBH_4$ is the most effective for the reduction of C=O species but this reduction requires H_2SO_4 pretreatment [71]. HI is well known and most effective chemical reagents for reduction [72]. To overcome the harmful environmental conditions of chemical reduction, thermal reduction has been attracted. This method is conducted after obtaining GO powder or films. Firstly, it occurs over 2000 °C to form GO powder within very short time. However, the temperature becomes lower to 1000 °C to obtain GO films under Ar and H_2 atmosphere as increasing reduction time. This high temperature is required to evaporate most of the oxygen groups; however, recent researches take lower temperature below 1000 °C to get the intermediate state (r-GO) to

explore its semiconducting properties. Table 2-8 shows the advantages and disadvantages of each reduction method. Based upon this consideration, the thermal reduction has been adapted for this dissertation. Additionally, Figure 2-5 shows how to analyze the conversion of GO to r-GO by reduction methods.

Table 2-8. Advantages and disadvantages of each reduction methods [56,59,73]

	Advantages	Disadvantages
Chemical reduction	Low-temperature process	Toxic environment
Optical reduction	Low-temperature process	Poor results in transform
Thermal reduction	Non-toxic environment	High temperature

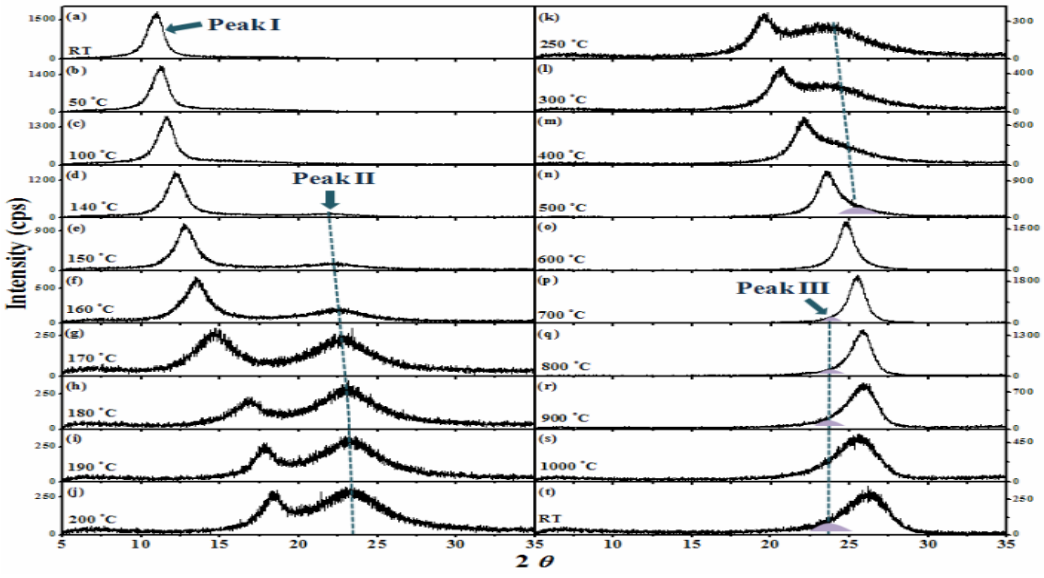

Figure 2-5. Individual XRD plots of graphene oxide/graphene films obtained at RT to 1000 °C [74].

Based on these backgrounds, gas sensing performance and behavior of non-reduced GO

films have been rarely emphasized. Additionally, the transition in gas sensing behavior by thermal reduction has also not been a focus. In this paper, we report the gas sensing behaviors of non-reduced GO. Then, n-p transition in the gas sensing behavior of GO films with thermal reduction is reported. The bond structure and phase change from GO to r-GO are suggested to explain gas sensing properties of GO and r-GO films. The prototype to combine GO and reduced GO by simple heat treatments would provide practical solutions to construct a sensor array with selective and sensitive recognition of various gasses.

2.4. Investigation of combinatorial structure for gas selectivity.

As discussed in previous section, GO is obtained by Hummers methods with various oxygen functional groups, having hydroxyl and epoxies functional groups on their basal planes as well as carbonyl and carboxyl groups located at the sheet edges [60,61]. This results in the large-scale synthesis of graphene sheets having comparable properties. However, modified GO for graphene sheet could not reach 100 % to match its properties. To overcome and compensate challenges, GO based composites have paid attention. These nanocomposites have been reported as a radical alternative to conventionally filled nanomaterials [75]. According to the hydrophilic nature of GO, GO in aqueous solution is not compatible with most organic materials. Therefore, inorganic materials such as ZnO and SnO_2 are good candidates to make nanocomposites. One of the advantages of the nanocomposites is enhancing electrical properties by increasing charge carrier or mobility of electrons. This phenomenon also contributes to overcoming the challenges of r-GO based gas sensors as well as metal oxide gas sensors as summarized in Table 2-9. Additionally, illustration of the composite and the crystallographic unit cell of the selected metal oxides were shown in Figure 2-6.

Table 2-9. Advantages and disadvantages of r-GO and Metal oxide gas sensors [56-58,76,77].

	Benefits	Challenges
r-GO	▪ High surface area (2600 m^2/g) ▪ Excellent semiconductor ▪ Good electrical properties ▪ RT sensing	▪ Instability ▪ Long recovery time ▪ Varies with surface defect
Metal Oxide	▪ Stability ▪ Good semiconductor ▪ Good sensitivity ▪ Low production cost	▪ Higher operating temperature

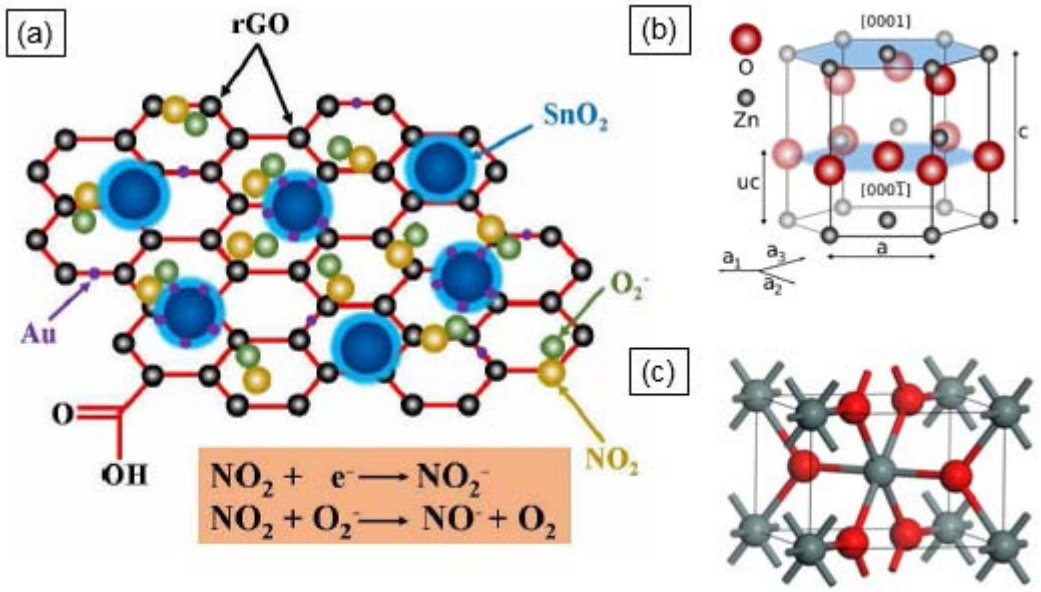

Figure 2-6. Schematic of (a) the proposed gas sensing mechanism of r-GO/SnO_2 by NO_2 gas and crystallographic structure of (b) ZnO and (c) SnO_2 [76-78].

Investigation of the r-GO and metal oxide composites was conducted to explore the gas sensing properties. Layer by layer structure and intercalation structures were fabricated via

different methods as shown in Table 2-10. These articles reported that enhancement in properties of the composite is owing to the high surface area and excellent electrical properties of r-GO and the interaction between the r-GO and the metal oxide. However, most researches were focused on r-GO films combining with metal oxide, and the specific explanation of the interaction between two oxides was not clarified yet. Therefore, non-treated GO and metal oxide composite were investigated, and the gas sensing mechanism of the composites was specified. Moreover, the research showed the improvement in gas response as catalytic effect and gas selectivity to VOC gases.

Table 2-10. Trends of gas sensor development of r-GO and metal oxide mixture.

Ref.	Materials	Structure	Method	Sensing type	Gas type	Conditions
[79]	r-GO + ZnO	Layer	Spray – hydrothermal	n-type	H_2S	2 ppm @ RT
[80]	r-GO + WO_3	Mixture	Drop coating	p-type	Alcohol	100 – 200 ppm @ 300 °C
[81]	r-GO + SnO_2	Mixture	Drop coating	p-type	Propanol	@ 513 K
[82]	r-GO + ZnO	Layer	Drop coating	p-type	Ethanol	10 – 50 ppm @ 300 °C
[83]	r-GO + SnO_2	Layer	Mini-arc reactor	p-type	NH_2	1 – 100 ppm @ 300 °C
[67]	r-GO + Cu_2O	Mixture	Hydrothermal	p-type	NO_2	0.4 – 2 ppm @ RT

[84]	r-GO + WO_3	Layer	Drop coating	p-type	NO_2	5 ppm @ 250 °C
[85]	r-GO + ZnO	Mixture	Spin coating	p-type	CO	22 ppm @ RT
[86]	r-GO + SnO_2	Mixture	Hydrothermal	p-type	NH_2	10 – 50 ppm @ RT
[87]	r-GO + SnO_2	Mixture	Painting	n-p type	NO_2	8 ppm @ 250 °C

References

1. Zhou Z, Zhao Y, Cai Z. Low-temperature growth of ZnO nanorods on PET fabrics with two-step hydrothermal method. *Applied Surface Science*. 2010;256(14):4724-4728.
2. Wang R, Xin JH, Tao XM, Daoud WA. ZnO nanorods grown on cotton fabrics at low temperature. *Chemical physics letters.* 2004;398(1):250-255.
3. Seesaard T, Khunarak C, Kerdcharoen T, Kitiyakara T. Development of an electronic nose for detection and discrimination of exhaled breath of hepatocellular carcinoma patients. Paper presented at: Systems, Man, and Cybernetics (SMC), 2012 IEEE International Conference on2012.
4. Ko YH, Kim MS, Park W, Yu JS. Well-integrated ZnO nanorod arrays on conductive textiles by electrochemical synthesis and their physical properties. *Nanoscale research letters.* 2013;8(1):1-8.
5. Lim Z, Chia Z, Kevin M, Wong A, Ho G. A facile approach towards ZnO nanorods conductive textile for room temperature multifunctional sensors. *Sensors and*

Actuators B: Chemical. 2010;151(1):121-126.

6. Broasca G, Borcia G, Dumitrascu N, Vrinceanu N. Characterization of ZnO coated polyester fabrics for UV protection. *Applied Surface Science.* 2013.
7. Ates ES, Unalan HE. Zinc oxide nanowire enhanced multifunctional coatings for cotton fabrics. *Thin Solid Films.* 2012;520(14):4658-4661.
8. Athauda TJ, Ozer RR. Nylon fibers as template for the controlled growth of highly oriented single crystalline ZnO nanowires. *Crystal Growth & Design.* 2013.
9. Xue C-H, Wang R-L, Zhang J, Jia S-T, Tian L-Q. Growth of ZnO nanorod forests and characterization of ZnO-coated nylon fibers. *Materials Letters.* 2010;64(3):327-330.
10. Sivakumar P, Balaji S, Prabhawathi V, Neelakandan R, Manoharan P, Doble M. Effective antibacterial adhesive coating on cotton fabric using ZnO nanorods and chalcone. *Carbohydrate polymers.* 2010;79(3):717-723.
11. Wani A, Shah M. A unique and profound effect of MgO and ZnO nanoparticles on some plant pathogenic fungi. 2012.
12. Özgür Ü, Alivov YI, Liu C, et al. A comprehensive review of ZnO materials and devices. *Journal of applied physics.* 2005;98(4):041301.
13. Soci C, Zhang A, Xiang B, et al. ZnO nanowire UV photodetectors with high internal gain. *Nano letters.* 2007;7(4):1003-1009.
14. Hoon J-W, Chan K-Y, Krishnasamy J, Tou T-Y, Knipp D. Direct current magnetron sputter-deposited ZnO thin films. *Applied Surface Science.* 2011;257(7):2508-2515.
15. Chen M-T, Ting J-M. Sputter deposition of ZnO nanorods/thin-film structures on Si. *Thin Solid Films.* 2006;494(1):250-254.
16. Chiou W-T, Wu W-Y, Ting J-M. Growth of single crystal ZnO nanowires using sputter deposition. *Diamond and Related Materials.* 2003;12(10):1841-1844.
17. Deng B, Yan X, Wei Q, Gao W. AFM characterization of nonwoven material

functionalized by ZnO sputter coating. *Materials Characterization.* 2007;58(10):854-858.

18. Fernández S, Martínez-Steele A, Gandía J, Naranjo F. Radio frequency sputter deposition of high-quality conductive and transparent ZnO: Al films on polymer substrates for thin film solar cells applications. *Thin Solid Films.* 2009;517(10):3152-3156.

19. Znaidi L, Soler Illia G, Benyahia S, Sanchez C, Kanaev A. Oriented ZnO thin films synthesis by sol–gel process for laser application. *Thin Solid Films.* 2003;428(1):257-262.

20. Natsume Y, Sakata H. Zinc oxide films prepared by sol-gel spin-coating. *Thin Solid Films.* 2000;372(1):30-36.

21. Kim Y-S, Tai W-P, Shu S-J. Effect of preheating temperature on structural and optical properties of ZnO thin films by sol–gel process. *Thin Solid Films.* 2005;491(1):153-160.

22. Zhang Y, Lin B, Sun X, Fu Z. Temperature-dependent photoluminescence of nanocrystalline ZnO thin films grown on Si (100) substrates by the sol–gel process. *Applied Physics Letters.* 2005;86(13):131910-131910-131913.

23. Ohyama M, Kouzuka H, Yoko T. Sol-gel preparation of ZnO films with extremely preferred orientation along (002) plane from zinc acetate solution. *Thin Solid Films.* 1997;306(1):78-85.

24. Yoon SH, Liu D, Shen D, Park M, Kim D-J. Effect of chelating agents on the preferred orientation of ZnO films by sol-gel process. *Journal of materials science.* 2008;43(18):6177-6181.

25. Wang Y-C, Leu C, Hon M-H. Preparation of nanosized ZnO arrays by electrophoretic deposition. *Electrochemical and solid-state letters.* 2002;5(4):C53-C55.

26. Wong EM, Searson PC. ZnO quantum particle thin films fabricated by electrophoretic deposition. *Applied Physics Letters.* 1999;74(20):2939-2941.

27. Yin X, Liu X, Wang L, Liu B. Electrophoretic deposition of ZnO photoanode for plastic dye-sensitized solar cells. *Electrochemistry Communications.* 2010;12(9):1241-1244.

28. Khiabani PS, Marzbanrad E, Zamani C, Riahifar R, Raissi B. Fabrication of In< sub> 2</sub> O< sub> 3</sub> based NO< sub> 2</sub> gas sensor through AC-electrophoretic deposition. *Sensors and Actuators B: Chemical.* 2012;166:128-134.

29. An Q, Rider AN, Thostenson ET. Electrophoretic deposition of carbon nanotubes onto carbon-fiber fabric for production of carbon/epoxy composites with improved mechanical properties. *Carbon.* 2012;50(11):4130-4143.

30. Rodriguez AJ, Guzman ME, Lim C-S, Minaie B. Synthesis of multiscale reinforcement fabric by electrophoretic deposition of amine-functionalized carbon nanofibers onto carbon fiber layers. *Carbon.* 2010;48(11):3256-3259.

31. Valle G, Hammer P, Pulcinelli S, Santilli C. Transparent and conductive ZnO: Al thin films prepared by sol-gel dip-coating. *Journal of the European Ceramic Society.* 2004;24(6):1009-1013.

32. Xu B, Cai Z. Trial-manufacture and UV-blocking property of ZnO nanorods on cotton fabrics. *Journal of applied polymer science.* 2008;108(6):3781-3786.

33. Tsuzuki T, Wang X. Nanoparticle coatings for UV protective textiles. *Research journal of textile and apparel.* 2010;14(2):9-20.

34. Park H, Tong F, Sujan A, et al. Growth of nanostructured ZnO on wearable fabrics for functional garment. *Materials Letters.* 2014;118:47-50.

35. Xu L, Zhuang W, Xu B, Cai Z. Superhydrophobic cotton fabrics prepared by one-step water-based sol–gel coating. *Journal of the Textile Institute.* 2012;103(3):311-319.

36. Znaidi L. Sol–gel-deposited ZnO thin films: a review. *Materials Science and Engineering: B.* 2010;174(1):18-30.

37. Besra L, Liu M. A review on fundamentals and applications of electrophoretic deposition (EPD). *Progress in materials science.* 2007;52(1):1-61.

38. Ozgur U, Hofstetter D, Morkoc H. ZnO devices and applications: a review of current status and future prospects. *Proceedings of the IEEE.* 2010;98(7):1255-1268.

39. Morrison SR. Selectivity in semiconductor gas sensors. *Sensors and Actuators.* 1987;12(4):425-440.

40. Barsan N, Koziej D, Weimar U. Metal oxide-based gas sensor research: How to? *Sensors and Actuators B: Chemical.* 2007;121(1):18-35.

41. Zhang Y, Xu J, Xiang Q, Li H, Pan Q, Xu P. Brush-like hierarchical ZnO nanostructures: synthesis, photoluminescence and gas sensor properties. *The Journal of Physical Chemistry C.* 2009;113(9):3430-3435.

42. Penza M, Martucci C, Cassano G. NO< sub> x</sub> gas sensing characteristics of WO< sub> 3</sub> thin films activated by noble metals (Pd, Pt, Au) layers. *Sensors and Actuators B: Chemical.* 1998;50(1):52-59.

43. El Khakani M, Dolbec R, Serventi A, et al. Pulsed laser deposition of nanostructured tin oxide films for gas sensing applications. *Sensors and Actuators B: Chemical.* 2001;77(1):383-388.

44. Xu J, Shun Ya, Pan Q, Qin J. Sensing characteristics of double layer film of ZnO. *Sensors and Actuators B: Chemical.* 2000;66(1):161-163.

45. Kolmakov A, Klenov D, Lilach Y, Stemmer S, Moskovits M. Enhanced gas sensing by individual SnO2 nanowires and nanobelts functionalized with Pd catalyst particles. *Nano letters.* 2005;5(4):667-673.

46. Joshi RK, Kruis FE. Influence of Ag particle size on ethanol sensing of SnO 1.8: Ag

nanoparticle films: a method to develop parts per billion level gas sensors. *Applied Physics Letters.* 2006;89(15):153116-153116-153113.

47. Gong H, Hu J, Wang J, Ong C, Zhu F. Nano-crystalline Cu-doped ZnO thin film gas sensor for CO. *Sensors and Actuators B: Chemical.* 2006;115(1):247-251.

48. Murata N, Suzuki T, Kobayashi M, Togoh F, Asakura K. Characterization of Pt-doped SnO 2 catalyst for a high-performance micro gas sensor. *Physical Chemistry Chemical Physics.* 2013;15(41):17938-17946.

49. Nguyen H, Quy C, Hoa N, Hieu N. A design of high performance gas sensor array with discrete islands of Au catalyst for increasing of zinc oxide nanowire junctions. Paper presented at: Solid-State Sensors, Actuators and Microsystems (TRANSDUCERS & EUROSENSORS XXVII), 2013 Transducers & Eurosensors XXVII: The 17th International Conference on2013.

50. Dolbec R, El Khakani M, Serventi A, Saint-Jacques R. Influence of the nanostructural characteristics on the gas sensing properties of pulsed laser deposited tin oxide thin films. *Sensors and Actuators B: Chemical.* 2003;93(1):566-571.

51. Dolbec R, El Khakani M. Sub-ppm sensitivity towards carbon monoxide by means of pulsed laser deposited SnO 2: Pt based sensors. *Applied Physics Letters.* 2007;90(17):173114-173114-173113.

52. Xu J, Han J, Zhang Y, Sun Ya, Xie B. Studies on alcohol sensing mechanism of ZnO based gas sensors. *Sensors and Actuators B: Chemical.* 2008;132(1):334-339.

53. Ponzoni A, Comini E, Sberveglieri G, et al. Ultrasensitive and highly selective gas sensors using three-dimensional tungsten oxide nanowire networks. *Applied Physics Letters.* 2006;88(20):203101.

54. Guo P, Pan H. Selectivity of Ti-doped In< sub> 2</sub> O< sub> 3</sub> ceramics as an ammonia sensor. *Sensors and Actuators B: Chemical.* 2006;114(2):762-767.

55. Guidi V, Boscarino D, Casarotto L, et al. Nanosized Ti-doped MoO< sub> 3</sub> thin films for gas-sensing application. *Sensors and Actuators B: Chemical.* 2001;77(1):555-560.

56. Zhu Y, Murali S, Cai W, et al. Graphene and graphene oxide: synthesis, properties, and applications. *Advanced materials.* 2010;22(35):3906-3924.

57. Some S, Kim Y, Yoon Y, et al. High-Quality Reduced Graphene Oxide by a Dual-Function Chemical Reduction and Healing Process. *Scientific reports.* 2013;3.

58. Fowler JD, Allen MJ, Tung VC, Yang Y, Kaner RB, Weiller BH. Practical chemical sensors from chemically derived graphene. *Acs Nano.* 2009;3(2):301-306.

59. Lu G, Ocola LE, Chen J. Gas detection using low-temperature reduced graphene oxide sheets. *Applied Physics Letters.* 2009;94(8):083111.

60. Wu S, Yin Z, He Q, Huang X, Zhou X, Zhang H. Electrochemical deposition of semiconductor oxides on reduced graphene oxide-based flexible, transparent, and conductive electrodes. *The Journal of Physical Chemistry C.* 2010;114(27):11816-11821.

61. Becerril HA, Mao J, Liu Z, Stoltenberg RM, Bao Z, Chen Y. Evaluation of solution-processed reduced graphene oxide films as transparent conductors. *Acs Nano.* 2008;2(3):463-470.

62. Yang D, Velamakanni A, Bozoklu G, et al. Chemical analysis of graphene oxide films after heat and chemical treatments by X-ray photoelectron and Micro-Raman spectroscopy. *Carbon.* 2009;47(1):145-152.

63. Jeong HY, Lee D-S, Choi HK, et al. Flexible room-temperature NO 2 gas sensors based on carbon nanotubes/reduced graphene hybrid films. *Applied Physics Letters.* 2010;96(21):213105-213105-213103.

64. Ko G, Kim H-Y, Ahn J, Park Y-M, Lee K-Y, Kim J. Graphene-based nitrogen dioxide

gas sensors. *Current Applied Physics.* 2010;10(4):1002-1004.

65. Yoon HJ, Jun DH, Yang JH, Zhou Z, Yang SS, Cheng MM-C. Carbon dioxide gas sensor using a graphene sheet. *Sensors and Actuators B: Chemical.* 2011;157(1):310-313.

66. Gautam M, Jayatissa AH. Gas sensing properties of graphene synthesized by chemical vapor deposition. *Materials Science and Engineering: C.* 2011;31(7):1405-1411.

67. Deng S, Tjoa V, Fan HM, et al. Reduced graphene oxide conjugated Cu2O nanowire mesocrystals for high-performance NO2 gas sensor. *Journal of the American Chemical Society.* 2012;134(10):4905-4917.

68. Hafiz SM, Ritikos R, Whitcher TJ, et al. A practical carbon dioxide gas sensor using room-temperature hydrogen plasma reduced graphene oxide. *Sensors and Actuators B: Chemical.* 2014;193:692-700.

69. Wang J, Singh B, Park J-H, et al. Dielectrophoresis of graphene oxide nanostructures for hydrogen gas sensor at room temperature. *Sensors and Actuators B: Chemical.* 2014;194:296-302.

70. Wang Y, Zhang L, Hu N, et al. Ammonia gas sensors based on chemically reduced graphene oxide sheets self-assembled on Au electrodes. *Nanoscale research letters.* 2014;9(1):251.

71. Shen J, Shi M, Li N, et al. Facile synthesis and application of Ag-chemically converted graphene nanocomposite. *Nano Research.* 2010;3(5):339-349.

72. Pei S, Zhao J, Du J, Ren W, Cheng H-M. Direct reduction of graphene oxide films into highly conductive and flexible graphene films by hydrohalic acids. *Carbon.* 2010;48(15):4466-4474.

73. Wu J, Becerril HA, Bao Z, Liu Z, Chen Y, Peumans P. Organic solar cells with solution-processed graphene transparent electrodes. *Applied Physics Letters.*

2008;92(26):263302.

74. Huh SH. *Thermal reduction of graphene oxide*: INTECH Open Access Publisher; 2011.

75. Stankovich S, Dikin DA, Dommett GH, et al. Graphene-based composite materials. *Nature.* 2006;442(7100):282-286.

76. Ahn H, Park J-H, Kim S-B, Jee SH, Yoon YS, Kim D-J. Vertically aligned ZnO nanorod sensor on flexible substrate for ethanol gas monitoring. *Electrochemical and solid-state letters.* 2010;13(11):J125-J128.

77. Wang B, Zhu L, Yang Y, Xu N, Yang G. Fabrication of a SnO2 nanowire gas sensor and sensor performance for hydrogen. *The Journal of Physical Chemistry C.* 2008;112(17):6643-6647.

78. Zhang H, Wang L, Zhang T. Reduced graphite oxide/SnO 2/Au hybrid nanomaterials for NO 2 sensing performance at relatively low operating temperature. *RSC Advances.* 2014;4(101):57436-57441.

79. Cuong TV, Pham VH, Chung JS, et al. Solution-processed ZnO-chemically converted graphene gas sensor. *Materials Letters.* 2010;64(22):2479-2482.

80. Akhavan O, Choobtashani M, Ghaderi E. Protein degradation and RNA efflux of viruses photocatalyzed by graphene–tungsten oxide composite under visible light irradiation. *The Journal of Physical Chemistry C.* 2012;116(17):9653-9659.

81. Song H, Zhang L, He C, Qu Y, Tian Y, Lv Y. Graphene sheets decorated with SnO2 nanoparticles: in situ synthesis and highly efficient materials for cataluminescence gas sensors. *Journal of Materials Chemistry.* 2011;21(16):5972-5977.

82. Akhavan O. Photocatalytic reduction of graphene oxides hybridized by ZnO nanoparticles in ethanol. *Carbon.* 2011;49(1):11-18.

83. Mao S, Cui S, Lu G, Yu K, Wen Z, Chen J. Tuning gas-sensing properties of reduced

graphene oxide using tin oxide nanocrystals. *J. Mater. Chem.* 2012;22(22):11009-11013.

84. Srivastava S, Jain K, Singh V, et al. Faster response of NO2 sensing in graphene–WO3 nanocomposites. *Nanotechnology.* 2012;23(20):205501.

85. Singh G, Choudhary A, Haranath D, et al. ZnO decorated luminescent graphene as a potential gas sensor at room temperature. *Carbon.* 2012;50(2):385-394.

86. Neri G, Leonardi SG, Latino M, et al. Sensing behavior of SnO 2/reduced graphene oxide nanocomposites toward NO 2. *Sensors and Actuators B: Chemical.* 2013;179:61-68.

87. Lin Q, Li Y, Yang M. Tin oxide/graphene composite fabricated via a hydrothermal method for gas sensors working at room temperature. *Sensors and Actuators B: Chemical.* 2012;173:139-147.

CHAPTER 3. EXPERIMENTAL SET UP

3.1. Device fabrication

Three types of substrates were used to characterize deposited sensing materials and fabricate devices to measure gas sensing properties: Si wafer, polyimide film, and fabrics. 4” SiO_2/Si wafers were selected as reference substrates, which are rigid and form amorphous structure. Polyimide films were representative substrates as flexible substrates. It was chosen as an intermediate step to adapt gas sensing devices to wearable substrates. Fabrics were target substrates to embed sensing components. Cotton, nylon, and polyester were used to coat sensing materials and adapt electrodes on them. Fabrics are greatly flexible and have excellent mechanical properties such as elongation, and resistance [1]. Table 3-1 covers mechanical properties of generally woven fabrics. However, it still has several disadvantages as a substrate: high absorption rate toward solvent and low melting point to be burnt or damaged [3]. Long-chains of polymer make fabrics then it is weak against heating. Therefore, heating is most concern to handle the wearable substrates.

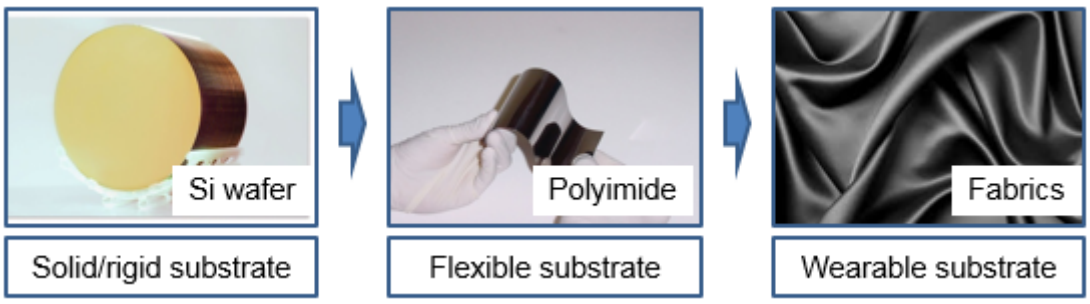

Figure 3-1. Change of research focus on substrates from Si wafer to wearable substrates.

Table 3-1. Mechanical properties of general woven fabrics [2].

Reinforcement type	Flat tape
Young's modulus E (GPa)	6.2
Failure strength $\boldsymbol{\sigma_F}$ (MPa)	370
Failure strain $\boldsymbol{\varepsilon_F}$ (%)	16
Density $\boldsymbol{\rho}$ (kg/m^3)	932
M_n	56,100
M_2	325,000
Tape width (mm)	2.5
Tape thickness (mm)	0.046
Filament bundle diameter (mm)	-
Denier (g for 9000 m)	1030

Once substrates were selected, conductive electrodes must be patterned on the substrates to measure the change of electrical signal. A variety shape of electrodes had been used for bulk and micro system, however, as devices become miniaturized, electrodes having large capacitance have been considered in small scale. Therefore, interdigitated electrodes were patterned on substrates rather than patterning dots to measure the resistance through sensing layers. The interdigitated electrodes were designed to enlarge the surface area in same dimension resulting in larger conductivity [4]. The arrays of electrodes were engraved on 75 x 75 x 0.5 mm stainless steel plate as shown in Figure 3-2 (a). The each electrode had 500 μm width and 400 μm distance between electrodes. The size of one device was 10 x 5 mm. Each

device was cut by cutting tools such as diamond cutter for the SiO_2/Si wafer to coat a sensing layer on the top of the electrodes for sensing performances.

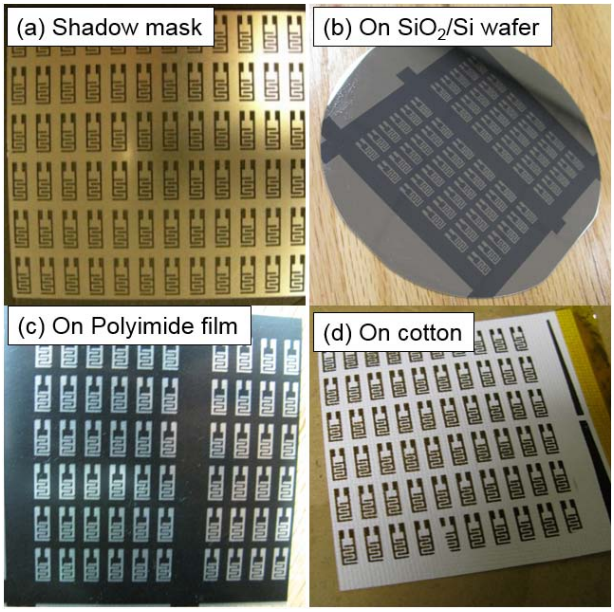

Figure 3-2. Images of (a) shadow mask of interdigitated electrodes and (a) patterned electrodes on SiO_2/Si wafer, (c) on polyimide film, and (d) on cotton paper.

Before patterning the interdigitated electrodes, the substrates were cleaned using ultra-sonicator (Brason, 3510) in ethanol and D.I water for 5 min. each. The cleaned and dried substrates were now ready to be used as substrates. The substrates were placed inside of the magnetron-sputter chamber (Discovery 18, Denton Vacuum) as described in Figure 3-3. Pt target (Lasker, 99.9 %) was used as electrode materials, which has good electrical conductivity and resistance to being oxide [5]. However, for Si wafer, Ti (Lasker, 99.9 %) target was also required as an adhesion layer between the substrate and Pt layer. Once the chamber vacuum became below 5 x 10^{-5} mTorr, sputter deposition was ready to perform under Ar atmosphere. RF sputter was conducted to coat Ti layer (10 nm) if it was required, then, DC sputter was performed to deposit Pt layer (100 nm) over the substrate (detail

deposition conditions were listed in Table 3-2). Now, the gas sensing platform was ready to have sensing layers on the top of the electrodes.

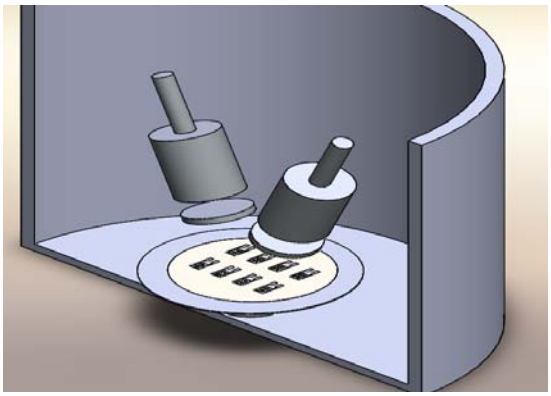

Figure 3-3. Schematic diagram of inside of the sputter chamber

Table 3-2. Sputter deposition conditions for material preparations.

	Power type	Power (W)	Time (sec)	Estimate thickness (nm)	Ar (sccm)	O_2 (sccm)	Working Pressure (mTorr)
Pt	D.C.	100	300	100	25	0	4.3
Ti	R.F.	400	25	10	25	0	4.3
ZnO	R.F.	80	2500	80	20	2	5.0
Pd	R.F.	100	30	42	25	0	4.3

3.2. ZnO deposition

Four types of deposition methods were employed to coat ZnO seed layer: sputter deposition, sol-gel coating, electrophoretic deposition (EPD), and dip-pad-cure (DPC)

coating. Then, ZnO nanorods were grown via thermolysis assisted chemical solution method.

3.2.1. Sputter deposition

ZnO ceramic target (Lasker, 99.9 %) was prepared to use the Discovery 18 sputter machine. The target was installed in RF position. Most of the dielectric materials are recommended to use RF power to take out molecules from the target [6]. The distance from the target to substrate kept in 4". The process vacuum condition was below 5 x 10^{-6} mTorr and the pressure inside of the chamber while deposition kept as 5.0 mTorr to supply sufficient electrical properties of ZnO. Also, argon and oxygen gas were used simultaneously in the ratio of 20:2 to supply enough oxygen amount to perform the stable and more stoichiometric ZnO films [7]. 80 W of power was supplied to coat 80 nm of ZnO films as a seed layer (details were described in Table 3-2).

3.2.2. Sol-gel deposition

Zinc acetate dihydrate (Aldrich, $(C_2H_3O_2)_2Zn\text{-}2H_2$) was dissolved in 2-methoxyethanol (Aldrich, $C_3H_8O_2$) with different chelating agents, i.e. diethanolamine (DEA, Aldrich, $HN(CH_2CH_2OH)_2$) or monoethanolamine (MEA, Aldrich, $NH_2CH_2CH_2OH$). The molar ratio of zinc acetate and the chelating agent was 1:1 and the concentration of the precursor solution were 0.5M. The solution was stirred at 80 °C for one hr to get the homogeneous solution and cooled at room temperature for 24 hrs. The pre-synthesized solution was dropped on the substrates and coated by spin coater (WS-400-LITE, Laurell Technologies Corporation), rotated at 3000 rpm for 30 sec. Pyrolysis was performed by preheating the substrate at 250 – 300 °C for 10 min to evaporate organic solvents and to break the network chains to form ZnO

[8]. The spin-coating containing preheating procedure was repeated three times to get 80 nm thickness. Then the films were annealed at 600 °C for one hr in a furnace.

3.2.3. Electrophoretic deposition (EPD)

Commercial ZnO nanoparticles (Aldrich, 100nm) were purchased. 0.6 wt% of ZnO suspension was prepared in 60 ml isopropyl alcohol (Aldrich, IPA). 0.1 g of PEI (Aldrich, polyetherimide, $(C_{37}H_{24}O_6N_2)_n$) was used as charging agent to ionize ZnO nanoparticles in IPA [9]. The suspension was ultrasonication for 30 min before use to obtain a well-dispersed suspension. This stable suspension was kept for 5 hrs. 1 x 1 cm of stainless steel plate was chosen as a counter and working electrode. The distance between two electrodes was kept as 1 cm. The electrodes were immersed into the suspension, and constant voltage (100V) was provided to attract the charged ZnO nanoparticles from the suspension by a power supplier (Agilent, 6645A). The Deposition time was one min to obtain one μm thickness. After deposition, the coated layers were dried in ambient conditions overnight.

3.2.4. Dip-pad-cure (DPC) deposition

Woven cotton (138 ± 2 g/m^2), PET (62 ± 2 g/m^2), and nylon (65 ± 2 g/m^2) with fiber thickness of about 17 μm were used. These fabrics were ultrasonicated in ethanol and water for 5 min. These were then dried at 50 °C overnight and cooled to room temperature prior to ZnO growth. A transparent nanosol of ZnO was synthesized to grow a seed layer. Zinc acetate dehydrate (Aldrich, $(C_2H_3O_2)_2Zn\text{-}2H_2$, 0.04 M) and sodium hydroxide (Aldrich, NaOH, 0.12 M) were dissolved in ethanol for 2 hrs at 60 °C. Coating ZnO seed layer on fabrics using the ZnO nanosol was performed DPC method in the ambient conditions. The cleaned pieces of

fabrics were immersed in the ZnO nanosol for 5 min. and the piece was then padded with a padder with constant pressure, 10 kg/m^2. The padded fabrics were air dried for 20 min at room temperature and cured at 150 °C for 10 min to remove the organic solvent [10].

3.2.5. Thermolysis assisted chemical solution methods

Zinc nitrate hexahydrate (Fisher Scientific, $Zn(NO_3)_2 \cdot 6H_2O$, 0.01M) and hexamethylenetetramine (Aldrich, HMT, $C_6H_{12}N_4$, 0.01M) were dissolved in 400 ml deionized (DI) water, followed by mixing for 24 hrs under stirring at room temperature. The substrates were immersed in the prepared solution, and the solution was dipped in a hot water bath (Iso Temp 202, Fisher Scientific) for 4 hrs at 85 °C to grow ZnO nanorods. After 4 hrs, the substrates were rinsed with DI water then dried in the ambient conditions. In this manner, ZnO nanorods were grown to c-axis preferred orientation as described in L. Vayssieres group [11].

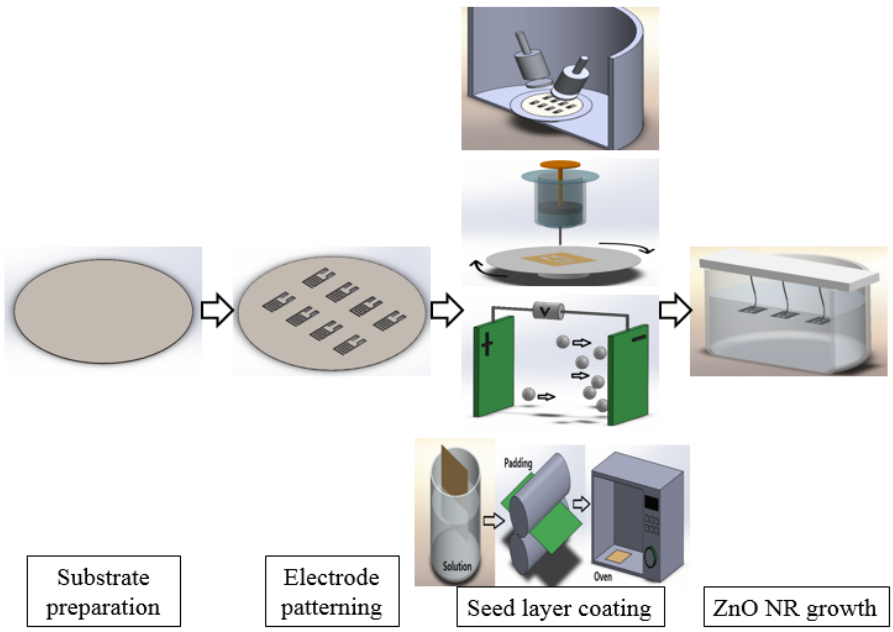

Figure 3-4. Illustrations of fabrications of ZnO based gas sensing device.

3.3. SnO_2 deposition

To deposit SnO_2 nanoparticles by EPD, commercial nanoparticles were purchased. The size of SnO_2 was 20 nm and 450 nm to compare. To perform EPD to coat SnO_2 nanoparticles uniformly, the particles were added to a various solvent such as isopropyl alcohol, ethanol, and water to obtain stable condition. Selection of solvent was one of the most important factors to obtain stable suspensions. In the case of dielectric constant, the proper range for EPD was between 12 to 25. Below that number, the deposition would fail because of insufficient dissociative power, while above the number, the high ionic concentration in the suspension reduced the size of the double layer region and electrophoretic mobility [9]. For deposition, 0.1 wt % of SnO_2 suspension was prepared in 60 mL IPA. The charging agent was used with PEI. The mixed suspension was unltrasonicated for one hr to get a well-dispersed suspension. 1x1 cm stainless steel or electrode patterned polyimide films were prepared as substrates. DC power supplier was connected to each working and counter electrode to provide electrical field. The distance between working and the counter electrode was 1 cm. Applied voltage was varied from 50 V to 100 V to get uniform films for 1 min. After deposition for several min., the coated films were dried overnight under ambient condition.

Table 3-3. Information of solvent used for EPD process [9, 12].

	Dielectric constant	Polarity index	Conductivity
Water	80.4	9.0	Not specified
Ethanol	24.3	5.2	
Acetone	20.7	6.2	

IPA	17.9	3.9

3.4. Graphene oxide deposition

Three deposition methods were employed to coat graphene oxide (GO, Graphene Supermarket®) films: drop coating, spin coating, and EPD. After coating the GO films, the thermal reduction was selected to obtain reduced graphene oxide (r-GO) films.

3.3.1. Drop coating

To coat GO on the electrode patterned substrates, drop coating was firstly used since aqueous GO suspension was known to be hydrophobic. Using a syringe, a droplet of GO suspension (0.1mL) was dropped on a glass piece and a patterned substrate and dried overnight at room temperature.

3.3.2. Spin coating

Spin coating was also employed to obtain a thin layer of GO. It is well understood that the slippery hydrophobic surface of glass or oxide layer will exhibit a low contact hysteresis to make a water droplet with graphene flakes roll off easily [13]. Thus, three steps of spin coating were conducted to spread the dispersion gradually and to prevent rolling off. The deposition condition was adjusted based on the literature and spin speed is 500, 800, and 1600 rpm for 30 sec each in sequence with 12.5 g/L of graphene oxide solution [14,16]. For low concentration of GO solution, the speed of spin coating was reduced down to 125 rpm

for 30 sec and then gradually increased. A few drops of the GO suspension were cast onto the substrate using three different spin speeds for higher concentration: 250 rpm, 400 rpm, and 800 rpm for 30 sec each. The deposited GO films were dried at room temperature for 24 hrs. Then, all samples were dried overnight at room temperature.

Table 3-4. Reported conditions on spin coating of graphene oxide [14 – 18]

Group	Solvent	Concentration	Process approach		
J. Liu (2010)	Methanol		400 rpm		
H.A. Becerril (2008)	Water	15 g/L	500 rpm (30s)	800 rpm (30s)	1600 rpm (30s)
J. Wu (2008)	Water	15 g/L	500 rpm (30s)	800 rpm (30s)	1600 rpm (30s)
S. Wu (2010)	Methanol	0.5 g/L	4000 rpm		
V.C. Tung (2009)	Methanol	1 g/L	1000 ~ 2000 rpm		

3.3.3. Electrophoretic deposition (EPD)

Commercial GO solutions dispersed in water were used. Typical flake size is 0.3 to 5 μm and thickness is one atomic layer. Three different concentration including 0.5 g/L and 5.0 g/L were examined to find optimal deposition conditions of GO films. A piece of stainless steel and polyimide films were used as a substrate for EPD process. The substrates were cleaned with ultra-sonication in acetone for 10 min to eliminate dust and oil on the surface of the substrates. Pt electrodes were patterned on the polyimide film by sputter deposition method

for a resistance measurement to detect gasses layer. To coat GO on each substrate, EPD was employed. Well dispersed and charged GO flakes are ready to be attracted by the electric force. Negatively charged flakes were attracted to positive electrode for coating. Under certain voltage (10 V and 5 V for 0.5 g/L GO and 5.0 g/L GO respectively) for 1 min, the coated films were dried overnight at room temperature under ambient condition.

3.3.4 Thermal treatment

After drying the coated samples at ambient conditions, the thermal reduction was conducted to control the amount of functional groups in GO thin films. The thermal reduction was typically performed using a tube furnace (Lindberg/Blue M) with flowing Ar gas (200 kPa). A series of samples were prepared by annealing at 50 °C, 100 °C, 150 °C, 200 °C, or 500 °C for 1hr. Then the samples were taken out from the furnace right after one hr thermal reduction. The samples were placed in the air to cool them down overnight. The desiccators were used to store the reduced samples to minimize the influence of environmental humidity.

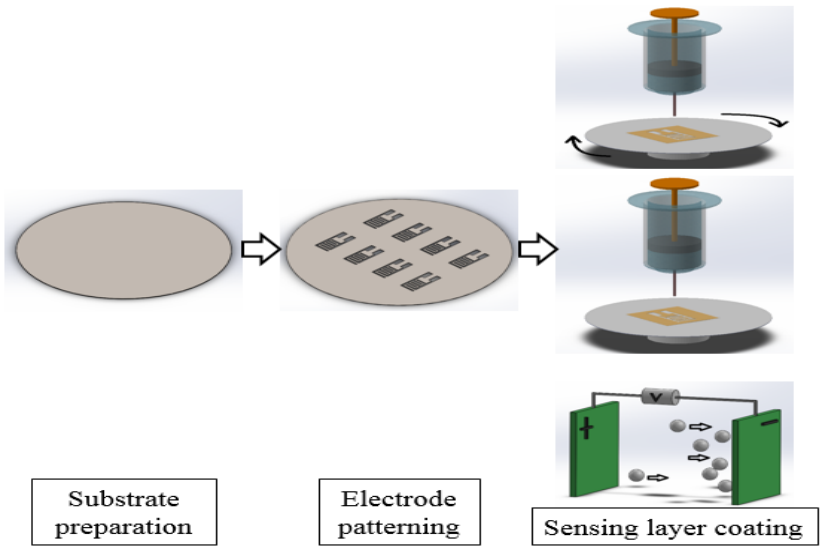

Figure 3-5. Illustrations of device fabrications with GO layers.

3.5. Materials characterization

The morphologies of thin film surface were characterized by SEM (scanning electron microscopy, JEOL), and the crystalline structure of the films were analyzed by XRD (X-ray diffractometer) and Raman spectroscopy. EDS (electron dispersive spectroscopy) was employed for material compositions. Profilometer (Veeco, Dektak 150) was used to measure the film thickness. Chemical bonding structure was analyzed by FTIR (Fourier transformation infrared) and XPS (X-ray photoelectron spectroscopy). Solvent evaporation and bonding change were analyzed by DSC (Differential scanning calorimetry). The UV-Vis diffuse reflectance spectroscopy (Avantes) was used to analyze the reflectance and band gap information of the samples. I-V measurement was also conducted to investigate the electrical properties of the samples.

Table 3-5. XRD specification.

Wavelength	Range	Step size	X-ray
1.54 A	5 ~ 50 °	0.25	40kV/20mA

Table 3-6. Specification of Raman spectroscopy

Grating #	Range	Exposure time	Slit size
2400	325 ~ 441.56 nm	20 sec	0.1 mm

Table 3-7. Specification of FTIR spectroscopy

Spectral resolution	Range	Wavelength precision	Minimum signal to

			nose ratio
< 1 cm^{-1}	500 ~ 4000 cm^{-1}	0.01 cm^{-1}	20000:1

3.6. Gas sensing measurement

Gas sensing behaviors were measured as described in Figure 3-6. The system used gas bubbles as a gas delivery control method. Two gas cylinders, which were oxygen and nitrogen, were prepared to generate the bubbles in the system. The amount and flow rate of the gasses were controlled by a MFC (mass flow controller). Once the air mixture was flew into the liquid source, spherical bubbles were generated and flow into the gas chamber. The resistance change of the sensor was measured by a Keithley 2400 source meter. Two conductive pin points located in the interdigitated electrode were used to extract the resistance signals, and the data was recorded on a personal computer running the custom Labview software. The sensing temperature could be controlled by a temperature controller if it were required. Then, the gas responses were calculated by following equation (1):

$$\text{Gas response} = R_i/R_g \quad (1)$$

, where R_i is initial resistance and R_g is the resistance of the gas atmosphere [15].

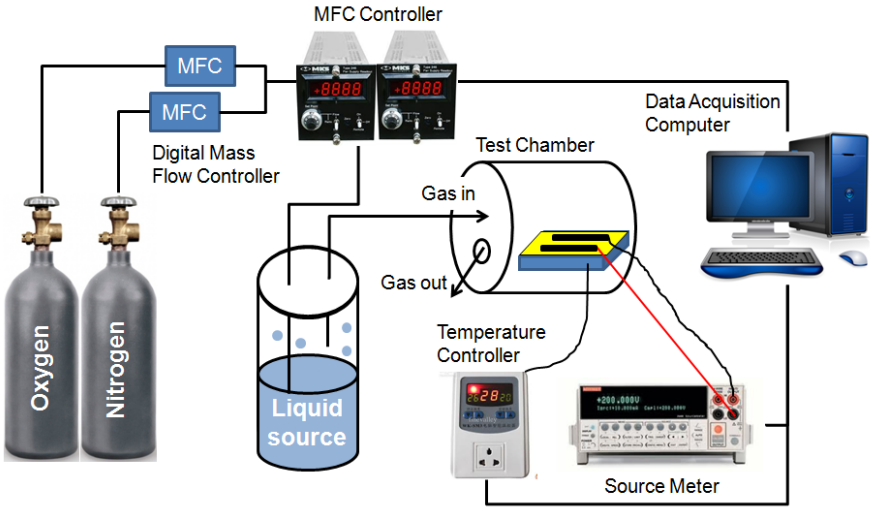

Figure 3-6. Schematic diagram of configured parts, gas cylinders, temperature controller, MFC (Mass Flow Controller), and data acquisition computer run by NI Lab VIEW.

Table 3-8. Information of organic gases for gas sensing performance.

	Molecular Formula	Polarity	Groups	Concentration, ppm
Ethanol	C_2H_6O	5.2	Non-benzene	100
Formaldehyde	CH_2O		Non-benzene	100
Toluene	C_7H_8	2.4	Benzene	100
Styrene	C_8H_8	Non	Benzene	100
Xylene	C_8H_{10}	2.5	Benzene	200
Benzene	C_6H_6	Non	Benzene	200

References

1. Bassett RJ, Postle R, Pan N. Experimental methods for measuring fabric mechanical properties: A review and analysis. *Textile research journal.* 1999;69(11):866-875.

2. Hine P, Ward I, Jordan N, Olley R, Bassett D. The hot compaction behaviour of woven oriented polypropylene fibres and tapes. I. Mechanical properties. *Polymer.* 2003;44(4):1117-1131.

3. Choi K, Cho G, Kim P, Cho C. Thermal storage/release and mechanical properties of phase change materials on polyester fabrics. *Textile research journal.* 2004;74(4):292-296.

4. Kim H, Jeong Y-G, Chun K. Improvement of the linearity of a capacitive pressure sensor using an interdigitated electrode structure. *Sensors and Actuators A: Physical.* 1997;62(1):586-590.

5. Chen A, Holt-Hindle P. Platinum-based nanostructured materials: synthesis, properties, and applications. *Chem. Rev.* 2010;110(6):3767-3804.

6. Fung T-C, Abe K, Kumomi H, Kanicki J. Electrical instability of RF sputter amorphous In-Ga-Zn-O thin-film transistors. *Display Technology, Journal of.* 2009;5(12):452-461.

7. Hinze J, Ellmer K. In situ measurement of mechanical stress in polycrystalline zinc-oxide thin films prepared by magnetron sputtering. *Journal of Applied Physics.* 2000;88(5):2443-2450.

8. Yoon SH, Liu D, Shen D, Park M, Kim D-J. Effect of chelating agents on the preferred orientation of ZnO films by sol-gel process. *Journal of materials science.* 2008;43(18):6177-6181.

9. Besra L, Liu M. A review on fundamentals and applications of electrophoretic deposition (EPD). *Progress in materials science.* 2007;52(1):1-61.

10. Park H, Tong F, Sujan A, et al. Growth of nanostructured ZnO on wearable fabrics for functional garment. *Materials Letters.* 2014;118:47-50.

11. Vayssieres L. Growth of arrayed nanorods and nanowires of ZnO from aqueous

solutions. *Advanced Materials.* 2003;15(5):464-466.

12. Reichardt C. Empirical Parameters of Solvent Polarity as Linear Free-Energy Relationships. *Angewandte Chemie International Edition in English.* 1979;18(2):98-110.

13. Jeong HY, Kim JY, Kim JW, et al. Graphene oxide thin films for flexible nonvolatile memory applications. *Nano letters.* 2010;10(11):4381-4386.

14. Fowler JD, Allen MJ, Tung VC, Yang Y, Kaner RB, Weiller BH. Practical chemical sensors from chemically derived graphene. *Acs Nano.* 2009;3(2):301-306.

15. Lu G, Ocola LE, Chen J. Gas detection using low-temperature reduced graphene oxide sheets. *Applied Physics Letters.* 2009;94(8):083111.

16. Wu J, Becerril HA, Bao Z, Liu Z, Chen Y, Peumans P. Organic solar cells with solution-processed graphene transparent electrodes. *Applied Physics Letters.* 2008;92(26):263302.

17. Wu S, Yin Z, He Q, Huang X, Zhou X, Zhang H. Electrochemical deposition of semiconductor oxides on reduced graphene oxide-based flexible, transparent, and conductive electrodes. *The Journal of Physical Chemistry C.* 2010;114(27):11816-11821.

18. Becerril HA, Mao J, Liu Z, Stoltenberg RM, Bao Z, Chen Y. Evaluation of solution-processed reduced graphene oxide films as transparent conductors. *Acs Nano.* 2008;2(3):463-470.

CHAPTER 4. PROCESS DEVELOPMENT TO ADAPT GAS SENSORS ON WEARABLE SUBSTRATES.

4.1. Process development of ZnO

Four deposition methods to coat ZnO seed layer were investigated: sputter deposition, sol-gel coating, electrophoretic deposition (EPD), and dip-pad-cure (DPC) coating. ZnO seed layer was deposited on various substrates such as nylon fabrics, stainless steel, or SiO_2/Si wafer according to the applicability of each processing method. After coating ZnO seed layer, ZnO nanorods were grown on the seed layer to make the 3-D structure of gas sensing layer for improvement on sensing performance [1].

Figure 4-1 shows SEM images of ZnO seed layer deposited via RF-sputter with 80 W for 2500 sec under 20:2 Ar to O_2 atmosphere and ZnO nanorods on the seed layer and nylon fabrics. Even though sputter deposition requires high vacuum conditions such as 5 x 10^{-6} mTorr, ZnO nanoparticles were successfully formed with 80 nm thickness on nylon fabrics with good adhesion at room temperature. As taking the seed layer as nucleation assistance, ZnO nanorods were grown with good coverage on the surface of the woven fabrics with 1.5 μm in length and 100 nm in diameter. However, as described in the literature, thin films deposited by sputter have coverage limitation, which means that only exposed area, can be coated [2]. Therefore, such woven fabrics having complicated structure are hard to be coated with uniform coverage via sputter deposition.

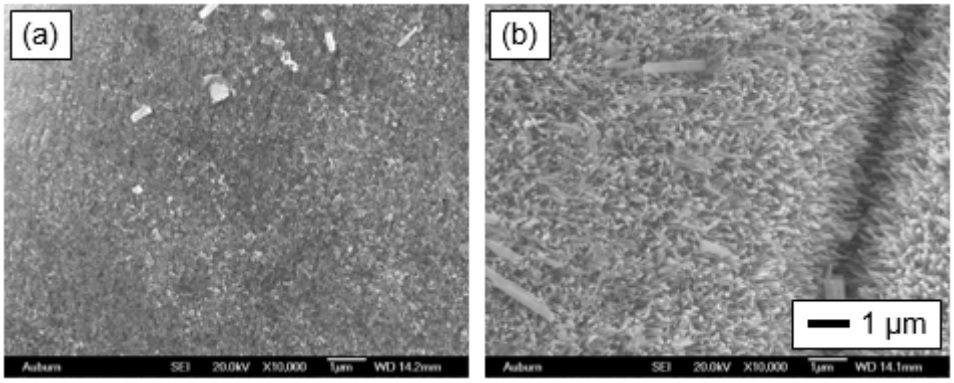

Figure 4-1. SEM images of (a) ZnO seed layer (x10k) deposited by RF-sputter method and (b) ZnO nanorods (x10k) on the seed layer on nylon fabrics.

The second approach to deposit ZnO thin films was a sol-gel method on SiO_2/Si wafer. Figure 4-2 presents morphology of ZnO thin films and ZnO nanorods on the seed layer. Via sol-gel process, ZnO seed layer was deposited with around 80 nm in thickness after 5 repeated processes. Each grain and grain boundary were observed clearly with high magnifications. In spite of uniform deposition on the substrates, pores were observed from the sol-gel film. The reaction mechanism was described from (1) – (4) equations. This reaction contains hydrolysis at the reaction (2) to (3) and condensation process at the reaction (3) to (4). As shown in Figure 4-2 (b), c-axis oriented ZnO nanorods were grown on the ZnO seed layer by sol-gel process. The ZnO grains from sol-gel method had also preferred orientation to c-axis, but sol-gel approach has process limitation to demand pyrolysis and post-annealing to evaporate the organic solvent and form ZnO nucleation sites [3]. Such limit requires higher working temperature such as 300 °C for pyrolysis and 500 °C for post-annealing, which is the reason SiO_2/Si wafer was employed for the deposition test. Therefore, sol-gel deposition is not suitable to apply to common wearable substrates.

$$C_2H_6O_4Zn + NH_3O \quad (1)$$

$$Zn^{2+} + H_2O \quad (2)$$

$$HOZn^{2+} + HO^- \quad (3)$$

$$ZnO \quad (4)$$

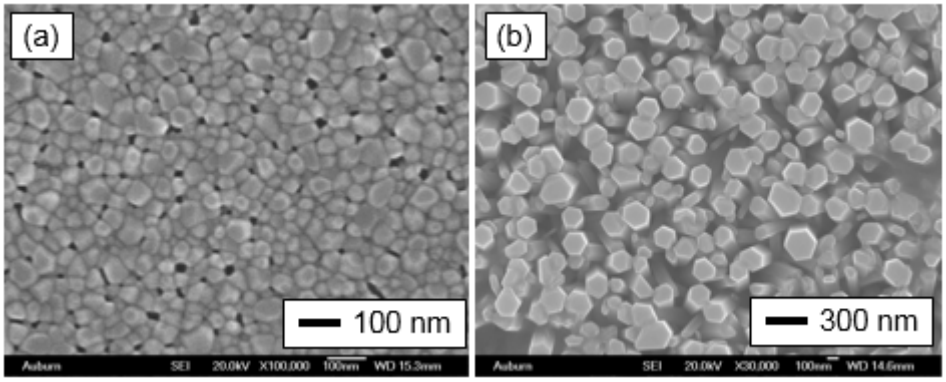

Figure 4-2. SEM images of (a) ZnO seed layer (x100k) deposited by sol-gel method and (b) ZnO nanorods (x30k) on the seed layer.

To overcome temperature limitation of the sol-gel method, EPD was applied to apply to wearable substrates. Figure 4-3 displays topography of ZnO nanoparticles via EPD and ZnO nanorods grown on the nanoparticles. Under 100 V for 1 min, ZnO nanoparticles (100 nm) were well attached on stainless steel substrates. The film thickness was measured with around one μm, which is fairly thick as a seed layer. In this EPD method, different topography of ZnO nanorods was observed. ZnO nanorod shape was hard to find in Figure 4-3 (b). This result is mainly due to non-preferred orientation of ZnO nanoparticles by EPD. Round shape of the nanoparticles can provide nucleation sites and let ZnO nanorods to grow all around the surface. However, space to grow nanorods seems to be limited. The growth of the nanorods only contributed to the increase in the film density by packing pores in the film. Such denser structure may degrade the gas sensing performance by applications as reducing the reaction

sites where the number of sites is much higher in porous 3-D nanostructure [1]. In addition, since EPD requires conductive substrates to attract particles from suspensions [4], it can be limited to fabricate diverse electronic devices.

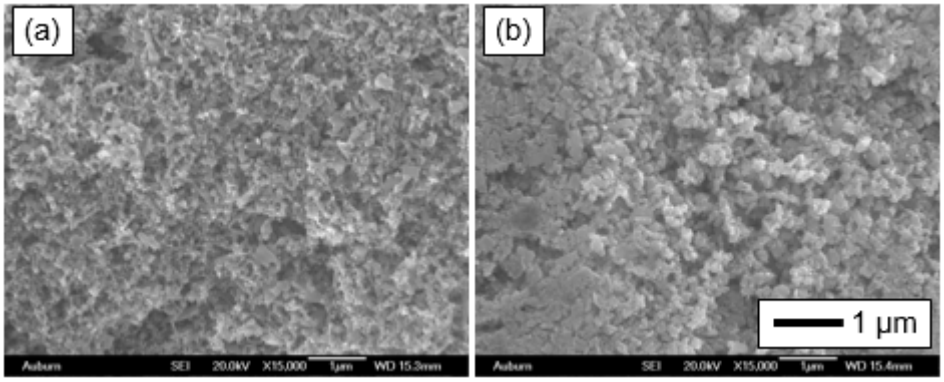

Figure 4-3. SEM images of (a) ZnO seed layer (x15k) deposited by electrophoretic (EPD) method and (b) ZnO nanorods (x15k) on the seed layer.

The other suggested method called DPC was also used to coat ZnO on wearable substrates. Figure 4-4 shows well coated ZnO seed layer via DPC process on nylon fabrics and randomly grown ZnO nanorods on the seed layer. The ZnO seed layer was successfully deposited on nylon fabrics at low temperature such as 150 °C without any damage to substrates. The suggested reaction mechanism was discussed from (5) to (7) equations. This process appears to be very similar to sol-gel process. However, it does not contain hydrolysis and condensation step. The coated ZnO seed layer had 100 nm thickness covered with nanoparticle shape. Due to the particle-like seed layer, ZnO nanorods were randomly grown without preferred orientation. Via DPC coating, ZnO seed layer was fully covered on all surface of woven fabrics regardless of the exposed area. Therefore, ZnO nanorods were able to grow anywhere of fabrics including top, bottom, and side locations with good adhesion. DPC coating method gives a great advantage to coat the sensing layer on the complex shape

of substrates.

$$Zn(OAc)_2 + 2EtOH \rightarrow Zn(Et)_2 + 2AcOH \quad (5)$$

$$Zn(OEt)_2 + H_2O \rightarrow Zn(OH)_2 + 2EtOH \quad (6)$$

$$Zn(OH)_2 \rightarrow ZnO + H_2O \quad (7)$$

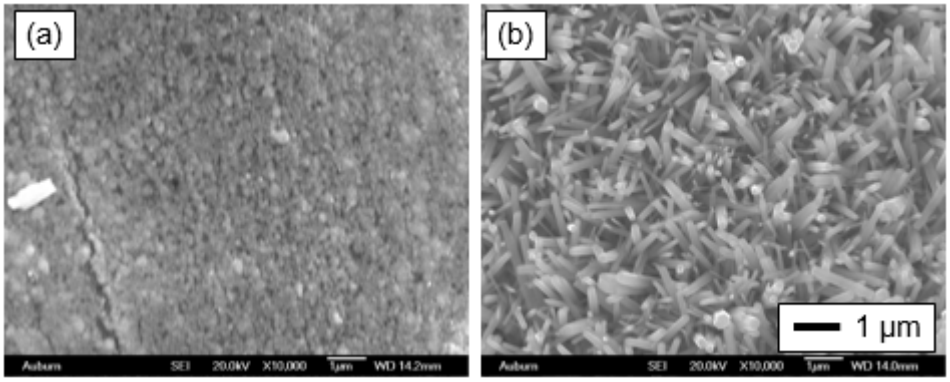

Figure 4-4. SEM images of (a) ZnO seed layer (x10k) deposited by dip-pad-cure (DPC) method and (b) ZnO nanorods (x10k) on the seed layer.

To compare ZnO growth via each deposition method, XRD characterization was performed. Figure 4-5 gives the crystalline information of ZnO seed layers and ZnO NRs on the seed layer. Regardless of deposition methods, three ZnO peaks were observed at 31.7°, 34.4°, and 36.25° representing (100), (002), and (101) planes respectively. Figure 4-5 (a) described the ZnO formation via sputter method. These peaks explained the ZnO formation on nylon substrates were randomly distributed, even though the intensity of (002) peak was slightly higher. ZnO formation by the sputter method provides relatively oriented growth. The randomly oriented growth of ZnO seed layer may result from round surface of the fabric substrates not by the effect of the deposition methods according to the references [2,5]. XRD patterns of ZnO deposited via sol-gel coating show different film orientation as shown in Figure 4-5 (b). A remarkably higher intensity was observed at 34. 4°, (002) plane, comparing

the peak with others at 31.7° and 36.25°. The growth of ZnO towards (002) plane was expected because (002) plane has the lowest energy barrier to form ZnO crystalline. The significant difference was clearly observed after growing ZnO NR on seed layers. The difference in the intensities of the (002) peak and the others was almost 4,000 times. This difference confirmed that the ZnO by sol-gel promoted c-axis growth of ZnO [6] corresponding to the morphology shown in Figure 4-2. Completion of the pyrolysis and post-annealing resulted in only ZnO peaks without intermediate chemicals such as Zn(OH) and any organic solvents. Figure 4-5 (c) explains randomly distributed ZnO nanoparticles deposited via EPD on the flat stainless steel substrates. Fairly strong intensities and random distribution were probably due to the presence of the pre-synthesized nanoparticles from the suspension that helps thick film form with around one μm. Additionally, no binders were detected without heat treatment process. ZnO nanoparticles synthesized by DPC were characterized as shown in Figure 4-5 (d). Randomly oriented ZnO NR peaks were detected, but small (100) peak was observed from the ZnO seed layer. It was due to the thinner layer with sub-nanoscale nanoparticles. As depicted in Figure 4-4, the size of the nanoparticles was less than 20 nm and this weak signal was confirmed by SEM result. However, such thinner layer was sufficient to prove ZnO formation at a lower temperature of 150 °C used for this experiment.

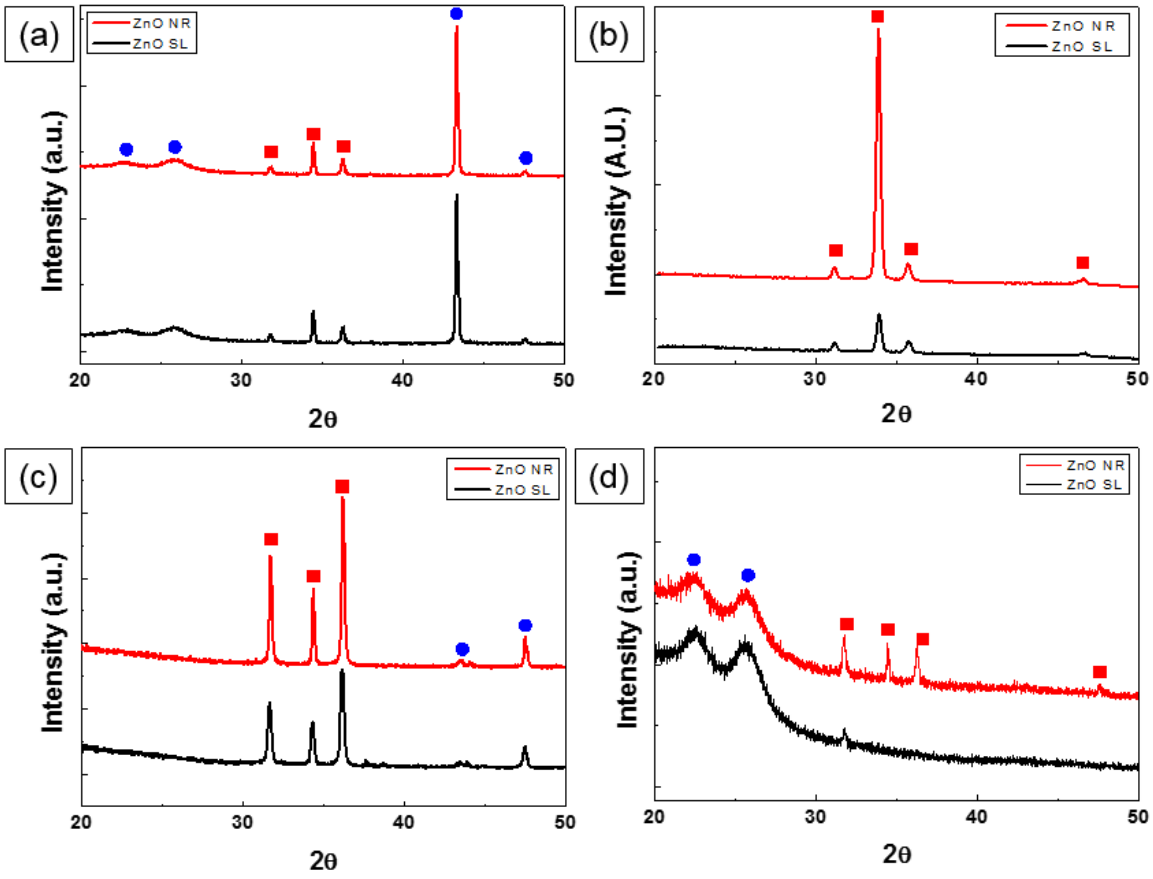

Figure 4-5. XRD spectra of ZnO seed layers (black) and ZnO nanorods (red) on the seed layer via different deposition methods: (a) R.F. sputter, (b) sol-gel, (c) EPD, and (d) DPC. The Red square indicates ZnO and the blue dot represents substrate peak.

Figure 4-6 compares XRD patterns of the ZnO seed layers deposited via different methods. Formation of ZnO was successfully conducted regardless of deposition methods and XRD peak intensities at (100), (002), and (101) planes. However, the preferred orientation of the films and film thickness were varied. For the applications on wearable substrates, sputter deposition, EPD, and DPC coating were favorable methods for low-temperature deposition of ZnO seed layer. In this study, DPC coating was selected owing to its uniform formation of ZnO at fairly lower temperature and excellent coverage on complex substrates.

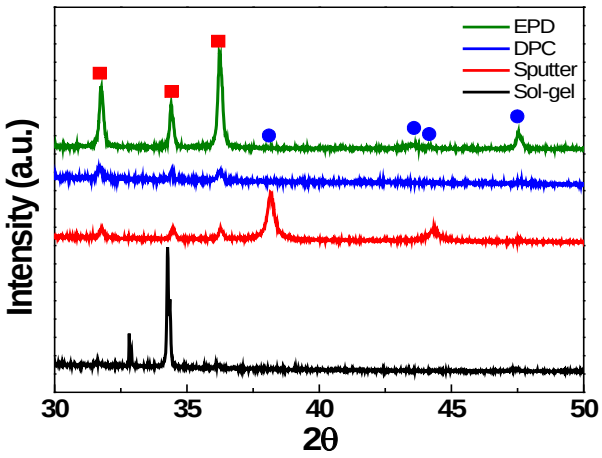

Figure 4-6. Comparison of XRD spectra of the ZnO seed layers deposited by various deposition methods. The Red square indicates ZnO and the blue dot represents substrate peak.

Table 4-1 summarizes advantages and disadvantages of each deposition method for application to wearable substrates. Among four methods, DPC was most favorable to coat ZnO on garments because of lower deposition temperature for ZnO formation.

Table 4-1. Summary of advantages and disadvantages of deposition methods.

	Advantages	Disadvantages
Sputter deposition	Working at RT	High vacuum condition
Sol-gel coating	Good coverage	High curing temperature
Electrophoretic deposition	Working at RT	Thick-film formation
Dip-pad-cure method	Working at lower temperature	Only for flexible substrates

4.2. Adaptability of ZnO sensing layer on wearable substrates

As taking the advantages of DPC coating such as low formation temperature and good coating coverage, DPC coating was employed for further research. To verify the effect of seed layer on fabric substrates, ZnO NR were grown on the pristine substrates and seed layer coated substrates. Figure 4-7 shows coverage of ZnO NR on nylon substrates. Figure 4-7 (a) depicted partially grown ZnO NR on the plain fabrics, however, fully coated ZnO NR was observed on the substrates with ZnO seed layer as shown in Figure 4-7 (b). This observation supported the requirement of seed layer for uniform coating deposition [7].

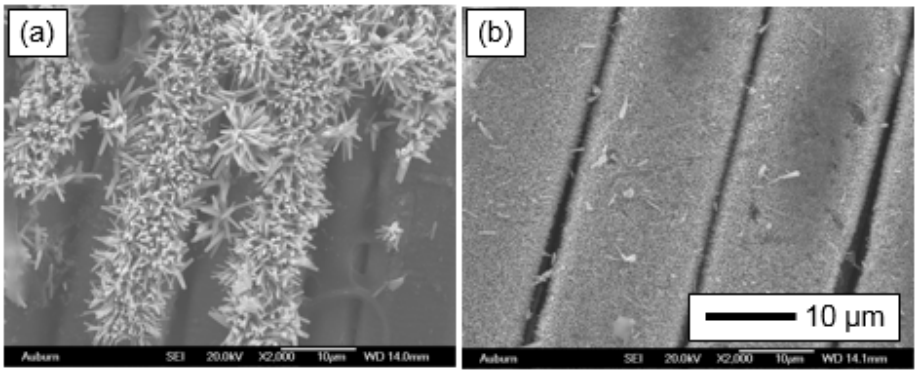

Figure 4-7. SEM images of ZnO nanorods (x10k) on the film without seed layer and with seed layer deposited by dip-pad-cure (DPC) method.

The SEM images were used to observe the surface morphology of fabric substrates and ZnO nanorods grown on various fabrics. Figure 4-8 (a), (b), and (c) show the surface morphology of bare fabrics including cotton, nylon, and PET, respectively. Although weave types show different patterns, the similar width of fibers (around 17 μm) was used to compare the growth of ZnO nanostructures. Uniform coverage of ZnO seed layers and nanorods was obtained for three fabric substrates. Figure 4-8 (d) shows the surface topography of a ZnO

seed layer deposited by a dip-pad-cure method on nylon fabric. Irrespective of fabric types, uniform coating of ZnO seed layers was obtained, and similar topography of the ZnO was observed in this study. ZnO nanorods were then fabricated on bare fabrics and ZnO seeded fabrics. Figure 4-8 (e) shows ZnO nanorods grown without a seed layer. The ZnO nanorods were not uniformly grown on fabrics, and the nanorods were larger due to lower nucleation density. The ZnO nanorods on seeded fabrics show uniform and dense growth along the vertical direction. But the nanorods' dimensions were slightly different depending on fabric type. The size and length of ZnO nanorods on PET are around 50 nm and 1.5 μm each. These typical dimensions of the nanorods were corresponded to the dimensions when similar deposition conditions for ZnO nanorods and seed layers are used on solid substrates [8,9]. However, the diameter of ZnO on nylon shows about three times larger than on the cotton and PET, whereas the length of ZnO on the cotton was shorter than one on the nylon and PET. Since the surface topologies of ZnO seed layers on the three fabrics were similar, the slight difference in the ZnO nanorods' dimensions may be attributed to expansion. Moreover, contraction of fabrics resulting from temperature change and/or possibly solution impregnation during the growth of ZnO nanorods in aqueous solution. Apparently, the uniform growth of ZnO nanorods on fabrics requires a seed layer. It appears that solution growth of ZnO nanorods can be significantly affected by the difference in shape change and soaking solution depending on fabric types.

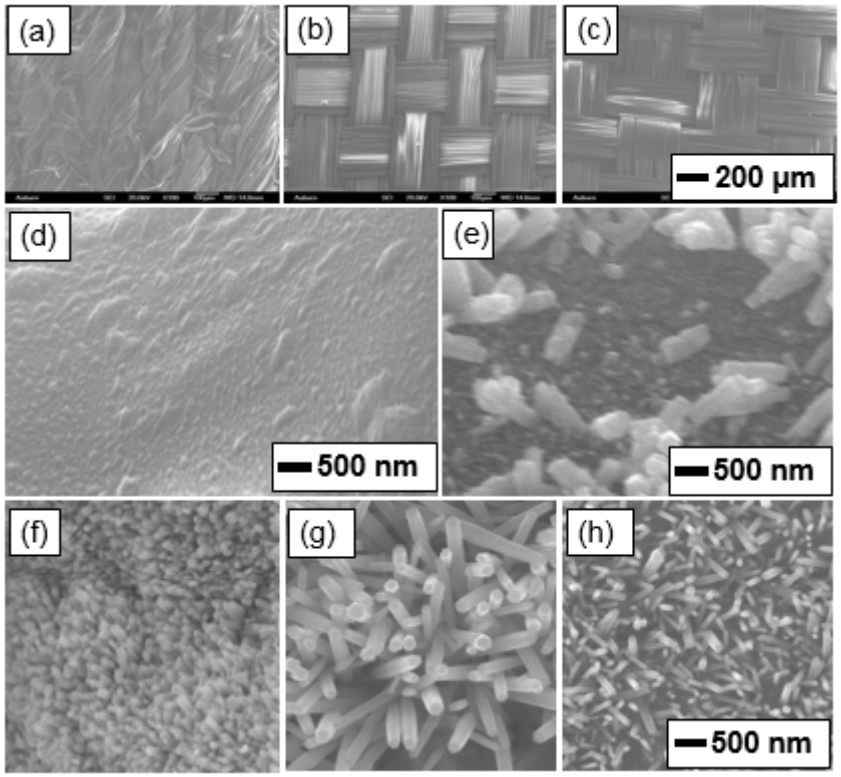

Figure 4-8. SEM images of ZnO nanorods and seed layer on fabrics: bare fabrics (a) of cotton, (b) of nylon, and (c) on PET, (d) ZnO seed layer on nylon, ZnO nanorods (e) without seed layer and with seed layer (f) on cotton, (g) on nylon, and (h) on PET.

XRD analysis was performed to confirm the formation and to examine preferred orientation of ZnO by the dip-pad-cure method on different fabrics. Figure 4-9 (a) shows the peaks of ZnO seed layers on three fabrics. The peaks of the ZnO seed layers were relatively weak due to very thin layers, around 80 nm. But the peaks of ZnO are clearly observed at 2θ = 31.7°, 34.3, and 36.3° after nanorods growth as shown in Figure 4-9 (b). Preferred [002] orientation of ZnO nanorods typically found on solid substrates was not observed due to rougher and more rolling surface of fabrics. The peak intensity of ZnO nanorods on nylon appears to be slightly weaker compared to those on the other substrates probably. It may be due to the slightly lower density of ZnO nanorods on nylon fabrics, as can be seen in the SEM images. XRD and SEM results indicate that low-temperature growth of ZnO seed layers

and nanorods can be obtained by a combined dip-pad-cure method and a chemical solution deposition regardless of fabric types.

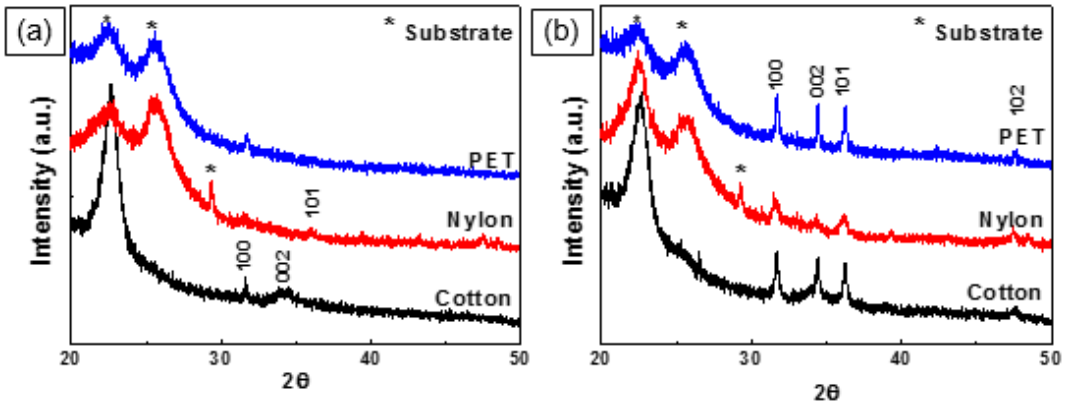

Figure 4-9. XRD spectra of (a) ZnO seed layer and (b) ZnO nanorods on fabrics.

The optical properties of nanostructured ZnO on the fabrics were examined using UV-vis diffuse reflectance spectroscopy. Figure 4-10 (a) shows the diffuse reflectance spectra of bare fabrics and ZnO nanorods grown on the fabrics. Reduction of the UV light reflection was observed at around 410 nm on bare fabrics. ZnO coated fabrics showed another reduction in the UV light reflection at around 380 nm, indicating an increase of UV light absorption due to ZnO nanorods. The absorption spectra of ZnO was expressed as the Kubelka-Munk function [F(R∞)] obtained from diffuse reflectance measurements as shown in Figure 4-10 (b). No specific absorption peaks in the range from 350 to 400 nm was observed from the fabrics. A characteristic absorption peak occurred at around 380 nm corresponding to ZnO [10-12]. The reflectance characteristics can also determine the UV-blocking ability of nanostructured ZnO on fabrics. The absorbance and diffuse reflectance spectra thus demonstrate good absorption ability of ZnO nanorods.

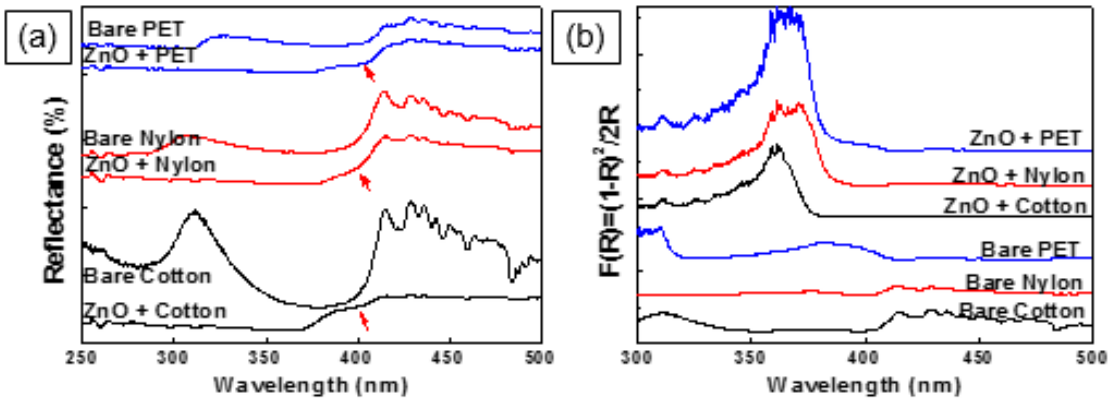

Figure 4-10. Diffuse reflectance spectroscopy of ZnO nanorods on fabrics: (a) reflectance vs. wavelength, and (b) F(R∞) vs. wavelength.

Electrical conductivity of the ZnO seed layer and nanorods on nylon was characterized by I-V measurement in dark condition and at room temperature as shown in Figure 4-11. As with optical properties, electrical conductivity was not significantly affected by fabric type. The I-V characteristic curves of Al/ZnO seed layer and nanorods show nearly ohmic behavior in forward or reverse bias. The linear increase of the current with applied bias is due to the increase of the carrier drift velocity. The electrical current of the ZnO seed layer on nylon was around 0.1 nA at 5V. The current of ZnO nanorods increased to 15 nA at 5V. Such increase can result from the increased surface area by ZnO nanorods. Surface-volume ratio of nanorods contributes to large number of electrons and trapping at surface states affects the transport of charge carriers [13].

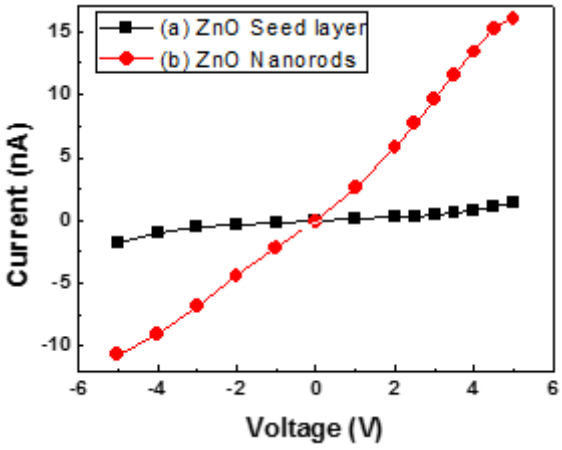

Figure 4-11. I-V measurement of (a) ZnO seed layer/nylon and (b) ZnO nanorods/seed layer/nylon in dark condition and at room temperature.

4.3. Summary and Conclusions

Four deposition methods, i.e. sputter deposition, sol-gel coating, electrophoretic deposition, and dip-pad-cure methods, were pre-selected to coat ZnO seed layer on wearable substrates. ZnO seed layer was successfully coated via each method. Among these coating methods, DPC method was chosen for its good coverage on fabrics and stable ZnO formation at lower temperature (150 °C). Via this technique, ZnO nanostructures were successfully fabricated on wearable substrates such as cotton, nylon and PET. The influence of seed layer was critical to grown ZnO nanorods on fabrics similar to solid substrates. However, non-flat surface and solution absorption during solution growth methods were considered as potential parameters to affect the morphology of ZnO nanorods. XRD result presented ZnO peaks without preferred orientation. The optical property of ZnO nanorods on fabrics showed reduced diffused reflectance near 380 nm by absorbing UV light. Increased electrical conduction was also observed due to the higher surface-volume ratio of the ZnO nanorods. The growth of ZnO nanostructures by low-temperature chemical solution growth can be a

good approach to embed functional ZnO nanostructures into various fabrics for developing functional garments.

References

1. Azad A, Akbar S, Mhaisalkar S, Birkefeld L, Goto K. Solid-state gas sensors: A review. *Journal of the Electrochemical Society.* 1992;139(12):3690-3704.
2. Hoon J-W, Chan K-Y, Krishnasamy J, Tou T-Y, Knipp D. Direct current magnetron sputter-deposited ZnO thin films. *Applied Surface Science.* 2011;257(7):2508-2515.
3. Znaidi L. Sol–gel-deposited ZnO thin films: a review. *Materials Science and Engineering: B.* 2010;174(1):18-30.
4. Besra L, Liu M. A review on fundamentals and applications of electrophoretic deposition (EPD). *Progress in materials science.* 2007;52(1):1-61.
5. Shao D, Gao D, Wei Q, Zhu H, Tao L, Ge M. Structures and properties of the polyacrylonitrile fabric coated with ZnO–Ag composites. *Applied Surface Science.* 2010;257(4):1306-1309.
6. Znaidi L, Soler Illia G, Benyahia S, Sanchez C, Kanaev A. Oriented ZnO thin films synthesis by sol–gel process for laser application. *Thin Solid Films.* 2003;428(1):257-262.
7. Song J, Lim S. Effect of seed layer on the growth of ZnO nanorods. *The Journal of Physical Chemistry C.* 2007;111(2):596-600.
8. Ahn H, Park J-H, Kim S-B, Jee SH, Yoon YS, Kim D-J. Vertically aligned ZnO nanorod sensor on flexible substrate for ethanol gas monitoring. *Electrochemical and solid-state letters.* 2010;13(11):J125-J128.
9. Carcia P, McLean R, Reilly M, Nunes Jr G. Transparent ZnO thin-film transistor fabricated by rf magnetron sputtering. *Applied Physics Letters.* 2003;82(7):1117-1119.

10. Sathishkumar P, Sweena R, Wu JJ, Anandan S. Synthesis of CuO-ZnO nanophotocatalyst for visible light assisted degradation of a textile dye in aqueous solution. *Chemical Engineering Journal.* 2011;171(1):136-140.

11. Bulko JB, Herman RG, Klier K, Simmons GW. Optical properties and electronic interactions of microcrystalline copper/zinc oxide (Cu/ZnO) catalysts. *Journal of Physical Chemistry.* 1979;83(24):3118-3122.

12. Elilarassi R, Chandrasekaran G. Structural, optical and magnetic characterization of Cu-doped ZnO nanoparticles synthesized using solid state reaction method. *Journal of Materials Science: Materials in Electronics.* 2010;21(11):1168-1173.

13. Lim Z, Chia Z, Kevin M, Wong A, Ho G. A facile approach towards ZnO nanorods conductive textile for room temperature multifunctional sensors. *Sensors and Actuators B: Chemical.* 2010;151(1):121-126.

CHAPTER 5. INVESTIGATION OF CATALYTIC EFFECT AND CATALYST GRADIENT ON ZNO FOR GAS SENSING BEHAVIOR

5.1 Material preparation

Fabrication of ZnO nanorods gas sensors was performed as described in Chapter 3. This ZnO NR gas sensors were employed to develop catalyst tuned gas sensors. Platinum (Pt) and Palladium (Pd) were adopted as catalysts to explore the gradient structure of catalyst composition on the ZnO NR sensors. Deposition of the catalysts was conducted by sputter deposition. Each catalyst was deposited using one cathode under the substrate rotation speed 50 to obtain uniform films. Pt was deposited by DC sputtering under 100 W, where as Pd was coated by RF sputtering under 400 W because the surface properties of Pt is much softer than that of Pd. However, when fabricating compositionally gradient structure, some of sputter conditions were changed. The location of Pd and Pt targets kept as same but the rotation speed was changed to 0 instead of 50 to change catalyst composition on different location in a sample [1]. After deposition without substrate rotation, composition was characterized according to the position.

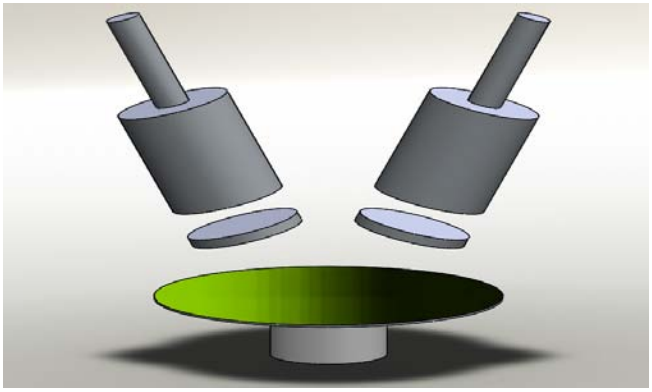

Figure 5-1. Schematic diagram of sputter deposition to deposit compositionally gradient

catalysts.

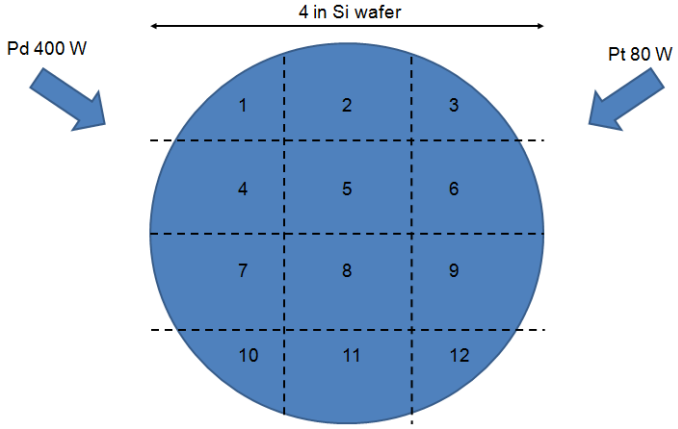

Figure 5-2. Illustration of the catalyst tuned samples according to the locations.

Table 5-1. Sputter deposition conditions of the catalysts.

	Cathode	Power	Gas condition	Deposition time
Pt	DC	100 W	25 sccm Ar	15/30 sec
Pd	RF	400 W	25 sccm Ar	15/30 sec

5.2 Material characterization

Catalyst tuned ZnO NR gas sensor devices were characterized by EDS. Four samples were prepared: 15 sec/30 sec deposited Pt catalyst on ZnO and 15 sec/30 sec deposited Pd catalyst on ZnO respectively. Such catalyst amounts on the ZnO devices were not sufficient to be detected by XRD [2]. Therefore, EDS analysis was employed to examine the composition. As shown in Table 5-2, small amounts of the catalysts were detected. Pt with 0.61 at % was detected out of 99.39 at % of ZnO when the Pt was sputtered for 15 sec. After the sputtering time is increased to 30 sec, more amount of Pt was observed with 1.29 at %.

Similar trend was observed with Pd catalyst. Based on the detected amount of catalysts under same sputtering time, it was estimated that the similar amount of two catalysts was deposited on ZnO devices.

Table 5-2. EDS analysis of Pt and Pd assisted ZnO NR gas sensors (at %).

	15 sec	30 sec		15 sec	30 sec
Pt	0.61	1.29	Pd	0.63	1.34
Zn	46.05	46.30	Zn	46.14	52.39
O	53.34	52.41	O	53.23	46.37

After defining deposition conditions to obtain similar amounts of catalysts by EDS, co-sputter deposition was conducted to obtain the combinatorial structure without rotation of the substrate holder. As marked in Figure 5-2, the composition at each position was analyzed by XRD. The (111) peak of the Pd was detected at 40.119 ° [3] and that of the Pt was detected at 39.794 ° [4]. However, the position of the peaks was shifted depending on sample location. From sample 1 to 3 as shown in Figure 5-2 (a), the peak indicating Pd shifted to the left, where the Pt is dominant. The sample 1 is located just below the Pd target; therefore at sample 1, Pd should be dominant element rather than Pt. However, at sample 3, it is located closer to the Pt target so that the peak was shifted to the left indicating Pt dominant area. As the samples change to the vertical way (e.g. sample 1, 4, 7, 10 as shown in Figure 5-2 (e)), the change in the peak intensity was observed. The result indicated that less amount of the catalysts was deposited as the samples were away from the targets.

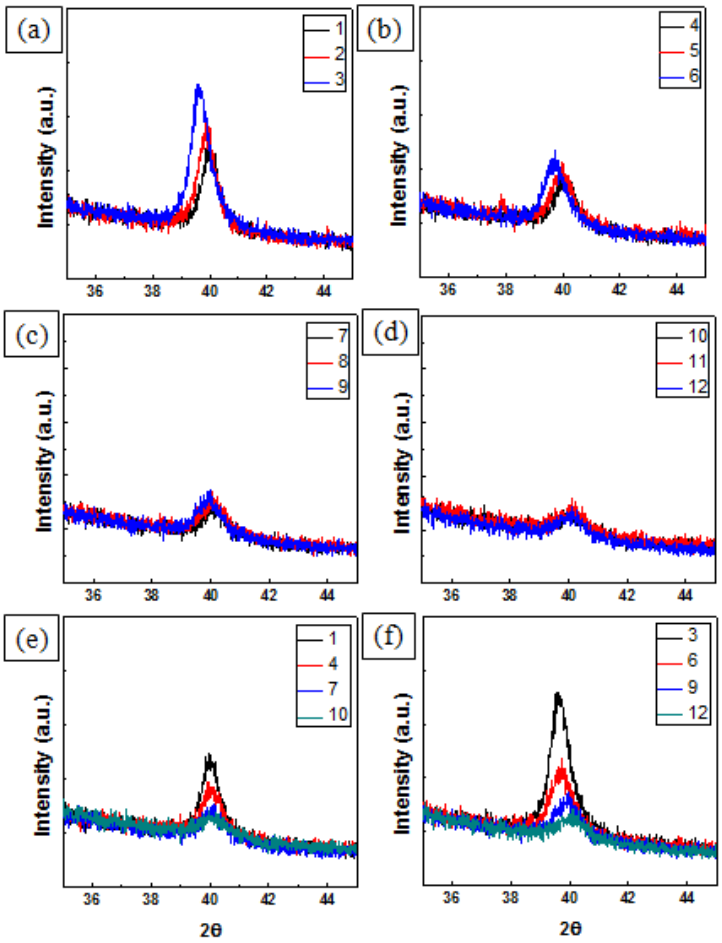

Figure 5-3. XRD spectra of gradient Pd and Pt composition on Si wafer according to different locations.

The changes in peak position and intensity were confirmed by EDS analysis. As summarized in Table 5-3, the amounts of Pd and Pt on ZnO NR devices were measured on sample 1 to 6 prepared under 15 sec deposition time. Different amounts of Pd and Pt were observed according to the position without substrate rotation as expected. From the XRD results, more amount of Pd was observed at the samples located near upper left location (under the Pd target) comparing with the samples located in lower right location (away from the Pd target). Therefore, compositionally gradient structure of catalysts on the ZnO NR devices was successfully deposited by co-sputter method.

Table 5-3. EDS results of the combinatorial catalysts on ZnO devices for 15 sec.

	Pd	Pt
	At %	
1	0.28	0.57
2	0.42	0.37
3	0	0.66
4	0.55	0.41
5	0.68	0.52
6	0	0.64

5.3 Gas sensing performance

Gas sensing performance of the pure ZnO NR was firstly conducted as a reference. The operating temperature was 200 °C and 300 °C and no gas reaction was observed with ZnO NR gas sensors below 200 °C. The gas response of the ZnO NR at 200 °C was measured to 2.0 and the gas response of the sensor at 300 °C was measured to 3.3. The higher value was observed at higher temperature because more electron can be activated to react with surface oxygen [5,6]. Few electrons were available at lower temperature below 200 °C, and the gas reaction did not occur.

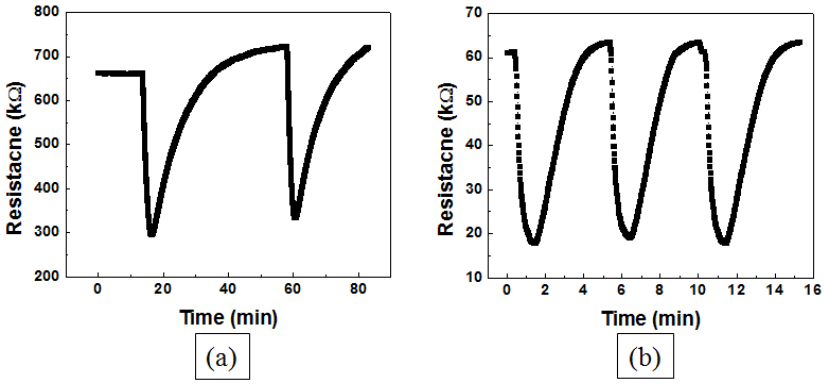

Figure 5-4. Gas sensing profiles of pure ZnO NR devices to 100 ppm of ethanol at (a) 200 °C and (b) 300 °C.

The Pd catalyst tuned ZnO NR gas sensors demonstrated gas sensing behaviors to to enhance sensitivity. Figure 5-5 shows the gas sensing behaviors of Pd deposited ZnO NR sensors for 15 sec and Figure 5-6 shows that of Pd deposited ZnO NR sensors for 30 sec under 100 ppm ethanol at different operating temperatures. The ZnO sensors with Pd for 15 sec showed good n-type gas sensing behaviors and the gas response at 100 °C was 3.9, the gas response at 200 °C was 25.7, and the gas response at 300 °C was 10.0, which was extremely improved comparing with the pure ZnO NR sensors. Also, the Pd catalyst with 15 sec deposition enabled to lower the operating temperature from 200 °C to 100 °C. However, room temperature gas detection was not achieved with 15 sec deposited Pd - ZnO NR sensors. Pd with sec deposition on ZnO NR sensors show different behaviors. At higher temperature such as 200 °C and 300 °C, the sensors showed n-type gas sensing behaviors but at room temperature, the transition behavior was observed. Meanwhile, the gas response was reduced from 3.3 (300 °C) to 1.1 (100 °C) with decreasing the temperature for transition. Then, the gas response was recovered to 1.2 at room temperature with p-type behavior. This transition was unique observation in terms of change in sensing type by operating temperature [7]. The summary of the Pd catalyst tuned ZnO NR sensors was given as shown in Figure 5-7.

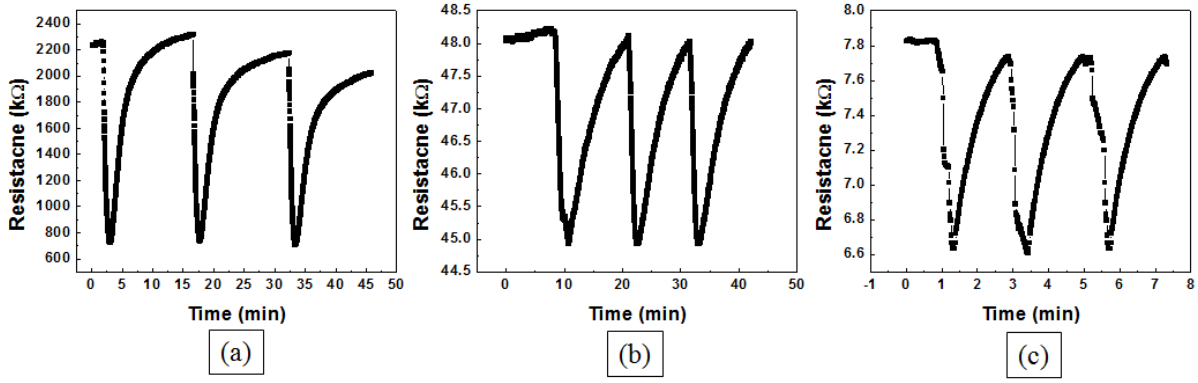

Figure 5-5. Gas sensing profiles of Pd with 15 sec deposition on ZnO NR devices under 100 ppm of ethanol at (a) 100 °C, (b) 200 °C, and (c) 300 °C.

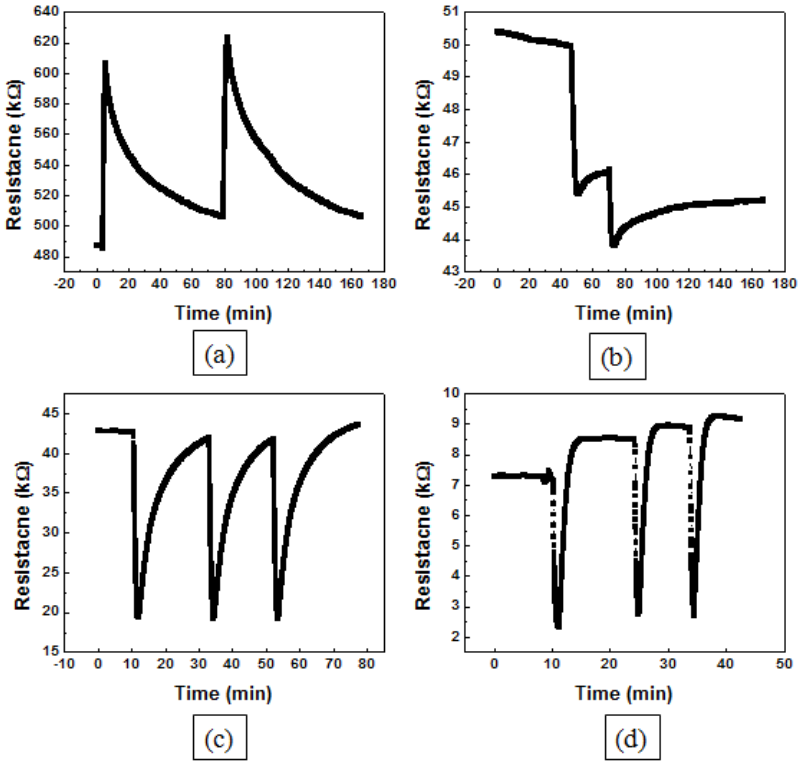

Figure 5-6. Gas sensing profiles of Pd 30 with sec deposition on ZnO NR devices under 100 ppm of ethanol at (a) RT, (b) 100 °C, (c) 200 °C, and (d) 300 °C.

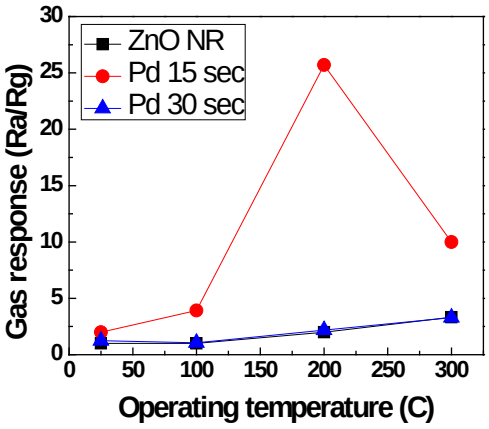

Figure 5-7. Comparison of gas response of pure ZnO NR device and Pd assisted ZnO NR devices according to operating temperature.

The Pt catalyst assisted ZnO NR gas sensors were demonstrated as a way to improve sensitivity. Figure 5-8 shows the gas sensing profiles of Pt with 15 sec deposition on ZnO NR devices and Figure 5-9 shows the gas sensing profiles of Pt with 30 sec deposition on ZnO devices according to different operating temperatures. All gas sensing behaviors with Pt catalyst assisted ZnO gas sensors showed n-type behavior. The gas response was changed with operating temperature. Increase in gas sensing behavior was observed with the increase of operating temperature as the reactive sites increased. As proven in Pd catalyst devices, higher gas response was observed at Pt with 15 sec deposition on ZnO NR devices rather than Pt with 30 sec as shown in Figure 5-10. The highest gas response was observed at Pt with 15 sec deposition on ZnO NR operating at 200 °C. Then, it started to degrease at the higher temperature.

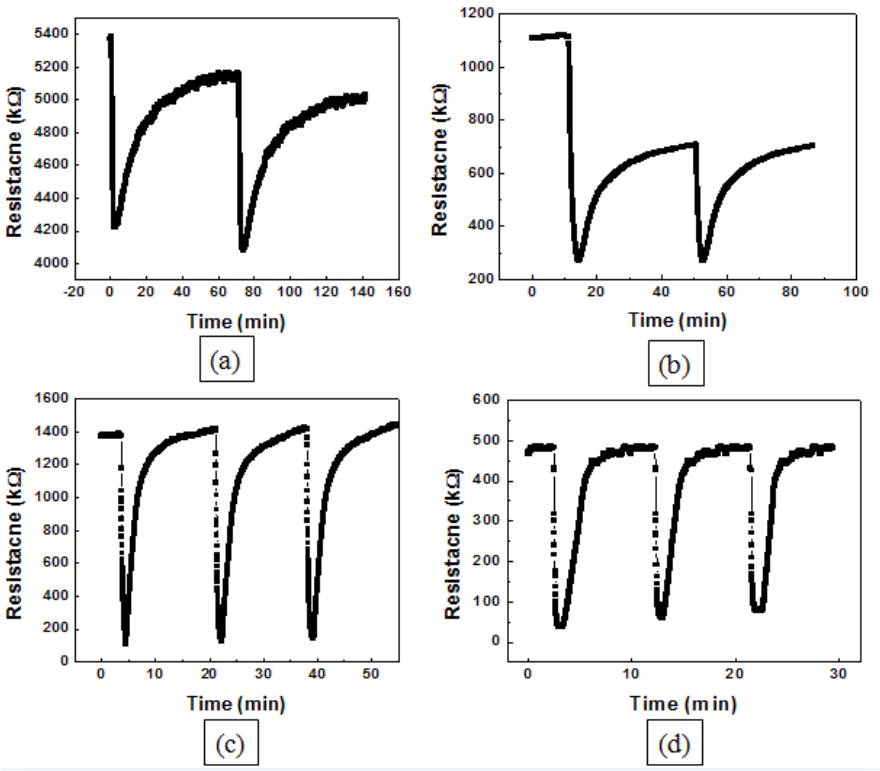

Figure 5-8. Gas sensing profiles of Pt 15 with sec deposition on ZnO NR devices under 100 ppm of ethanol at (a) RT, (b) 100 °C, (c) 200 °C, and (d) 300 °C.

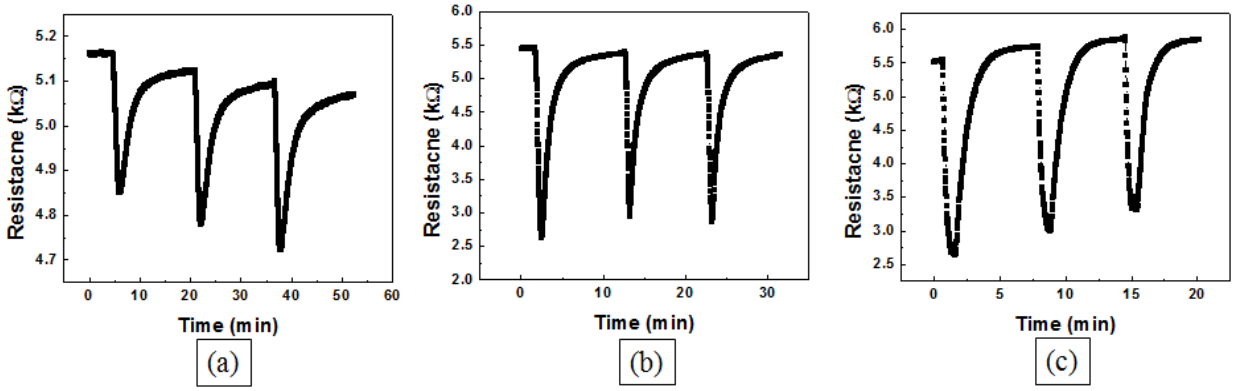

Figure 5-9. Gas sensing profiles of Pt 30 with sec deposition on ZnO NR devices under 100 ppm of ethanol at (a) 100 °C, (b) 200 °C, and (c) 300 °C.

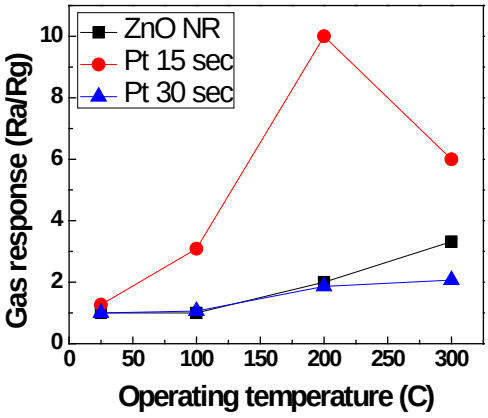

Figure 5-10.Comparison of gas response of pure ZnO NR device and Pt assisted ZnO NR devices according to operating temperature.

After confirming gas sensing behaviors by catalyst assisted ZnO NRs, one condition to show compositionally gradient structure was selected to compare the gas sensing performances. 0.68 Pd + 0.52 Pt sample (sample 5) was chosen to perform to detect 100 ppm of ethanol gas. As shown in Figure 5-11, the sample 5 shows n-type gas sensing behaviors at different temperatures. Additionally, the gas sensing response increased with operating temperature. Even though this combinatorial catalyst assisted ZnO NR devices enabled to improve the gas sensing response and reduce the operating temperature to 100 °C, room temperature detection was still not achieved. The overall comparison of different devices was given in Figure 5-12. The samples of Pt with 15 sec, Pd with 15 sec, and 0.68 Pd + 0.52 Pt assisted ZnO NR devices enabled to enhance the gas sensing behaviors compared with pure ZnO NR devices. Both gas sensing response and sensing rate were improved. The catalyst assisted ZnO NR reacted with 100 ppm ethanol gas faster than the pure ZnO NR devices. However, degration in gas sensing response was observed probably due to thicker coating of catalysts that might cover sensing materials. Therefore, desired properties by combinatorial structure of Pd and Pt would need thinner layer of catalysts with controlled dispersion on

sensing materials.

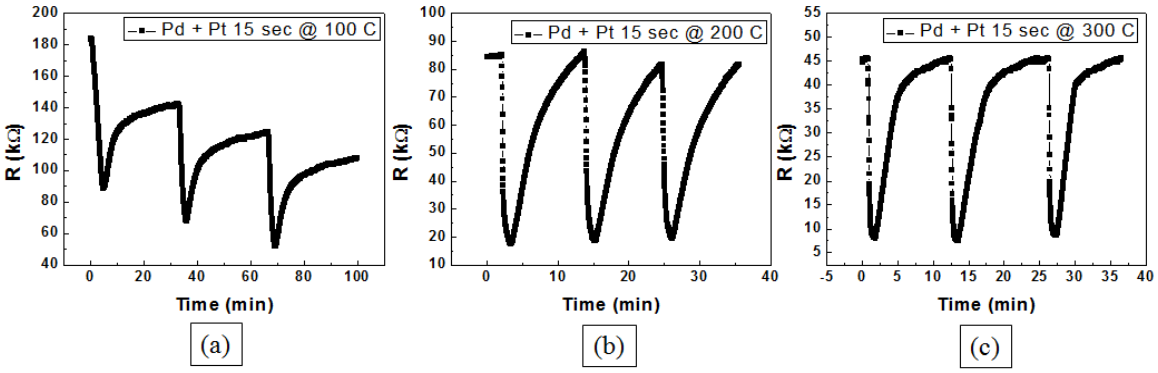

Figure 5-11. Gas sensing profiles of combined Pt and Pd catalysts on ZnO NR devices according to different operating temperature: (a) 100 °C, (b) 200 °C, and (c) 300 °C.

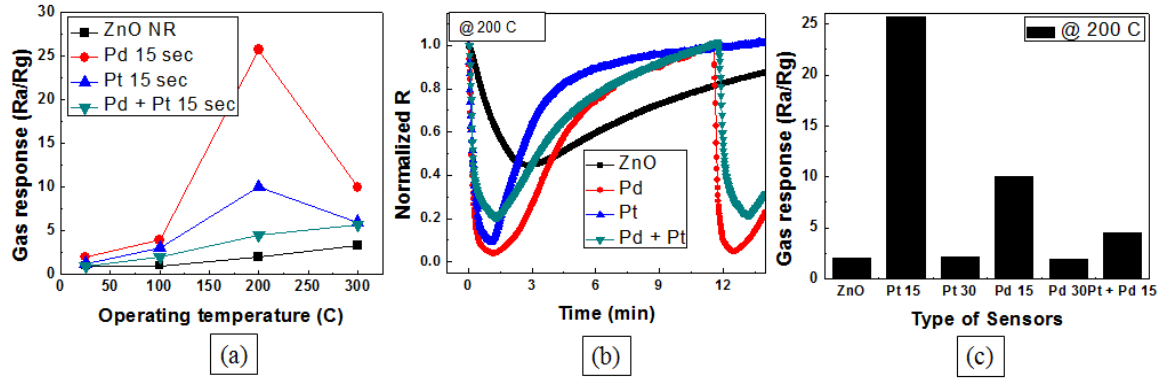

Figure 5-12. (a) comparison of the gas sensing responses of different gas sensing devices at different operating temperatures, (b) gas sensing profiles of different gas sensing devices and 200 °C, (c) and comparison of gas sensing responses of different gas sensing devices at 200 °C.

5.4. Conclusions

Deposition of catalysts on ZnO NR gas sensing devices was successfully conducted by gas sensing behaviors by catalyst assisted ZnO NRs, one condition to show compositionally gradient structure was selected to compare the gas sensing performances. 0.68 Pd + 0.52 Pt sample (sample 5) was chosen to perform to detect 100 ppm of ethanol gas. As shown in Figure 5-11, the sample 5 shows n-type gas sensing behaviors at different temperatures. Additionally, the gas sensing response increased with operating temperature. Even though this combinatorial catalyst assisted ZnO NR devices enabled to improve the gas sensing response and reduce the operating temperature to 100 °C, room temperature detection was still not achieved. The overall comparison of different devices was given in Figure 5-12. The samples of Pt with 15 sec, Pd with 15 sec, and 0.68 Pd + 0.52 Pt assisted ZnO NR devices enabled to enhance the gas sensing behaviors compared with pure ZnO NR devices. Both gas sensing response and sensing rate were improved. The catalyst assisted ZnO NR reacted with 100 ppm ethanol gas faster than the pure ZnO NR devices. However, degration in gas sensing response was observed probably due to thicker coating of catalysts that might cover sensing materials. Therefore, desired properties by combinatorial structure of Pd and Pt would need thinner layer of catalysts with controlled dispersion on sensing materials.

References

[1] Ahn H, Park H, Joo J-C, Kim D-J. Volatile gas sensing properties of phase and composition gradient SnOx thin films by combinatorial sputter deposition. *ECS Solid State Letters.* 2013;2(1):P11-P13.

[2] Kang DH, Kim JH, Park JH, Yoon KH. Characteristics of (Pb 1-x Sr x) TiO 3 thin film prepared by a chemical solution processing. *Materials research bulletin.* 2001;36(1):265-276.

[3] Chin Y-H, Dagle R, Hu J, Dohnalkova AC, Wang Y. Steam reforming of methanol

over highly active Pd/ZnO catalyst. *Catalysis Today.* 2002;77(1):79-88.

[4] Consonni M, Jokic D, Murzin DY, Touroude R. High performances of Pt/ZnO catalysts in selective hydrogenation of crotonaldehyde. *Journal of Catalysis.* 1999;188(1):165-175.

[5] Wang C, Yin L, Zhang L, Xiang D, Gao R. Metal oxide gas sensors: sensitivity and influencing factors. *Sensors.* 2010;10(3):2088-2106.

[6] Morrison SR. Selectivity in semiconductor gas sensors. *Sensors and actuators.* 1987;12(4):425-440.

[7] Lupan O, Ursaki V, Chai G, et al. Selective hydrogen gas nanosensor using individual ZnO nanowire with fast response at room temperature. *Sensors and Actuators B: Chemical.* 2010;144(1):56-66.

CHAPTER 6. EXPLORATION OF ALTERNATIVE MATERIALS TO ACHIEVE ROOM TEMPERATURE DETECTION.

6.1. Deposition of graphene oxide

6.1.1. Deposition condition of graphene oxide by coating methods

Three types of coating methods were investigated to coat graphene oxide (GO) films uniformly. Drop coating, spin coating, and electrophoretic deposition (EPD) were conducted with commercial GO suspensions in an aqueous system. GO suspensions of 0.5 g/L, 5.0 g/L and 6.2 g/L were used.

Spin coating was performed to explore coating coverage on metal/ceramic substrates. Spin coating method for uniform coating of GO thin films is widely used, but the coating conditions can vary according to solvent types and dispersed solid materials. Two primary factors to determine spin speed in GO coating appear to be solvent types and solution concentrations [1,2]. To examine the effect of the concentration on wettability, three GO solutions with 6.2 g/L, 5.0 g/L, and 0.5 g/L were employed to coat a thin layer of GO at three different speeds. The used spin speeds were 500, 800, and 1600 rpm, but coating time was kept for 30 sec. Figure 6-1 shows partially covered GO on the surface of metal electrode, but GO was not coated on the surface of ceramic substrate. Due to different wettability between GO and the substrates, GO film was not coated on the Si wafer without the use of a metal electrode [3]. Partial coverage of the GO films was observed at a low concentration of GO solution such as 5.0 g/L. Even at 0.5 g/L solution, no deposited layer was observed on the substrate. As the concentration of GO solution decreased, the degree of coverage appeared to

decrease. The coverage may become worse as the GO concentration decreases because of weak wettability of the solution causing more dispersion in water suspension. To overcome this limitation, the control of the spin coating condition should be required or alternative methods for uniform coating should be explored [4].

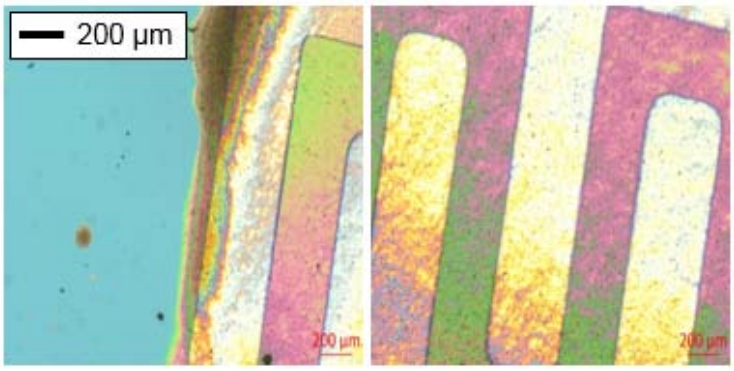

Figure 6-1. Graphene oxide deposition by spin coating with 6.2 g/L of GO in water: spin speed were 500, 800, and 1600 rpm for 30 sec each.

As discussed in chapter 3, the condition of spin coating was adjusted according to solution concentration. Due to lower concentration of our GO solutions, compared with reported references (12.5 g/L of GO solution was mostly used), the rpm was reduced after preliminary coating tests on glass substrates. The spin speed was reduced to 125, 200, and 400 rpm for 30 sec consequently, which is approximately 25% in rpm compared with the reference conditions. As shown in Figure 6-2, no GO layer was observed at 0.5 g/L due to low concentration and weak wettability regardless of spin speed. However, a thin layer of GO was well formed on glass substrates at 5.0 g/L with lower rpm conditions. In the case of high GO concentration of 6.2 g/L, the higher rpm conditions were required to spread out the solution uniformly. Three incremental steps of spin coating conditions, which increase speed, were necessary to prevent the solution from leaving from the substrate. The coating

conditions should be determined according to the concentration of GO. In this study, lower concentration of GO was applied considering the wettability and surface tension [3].

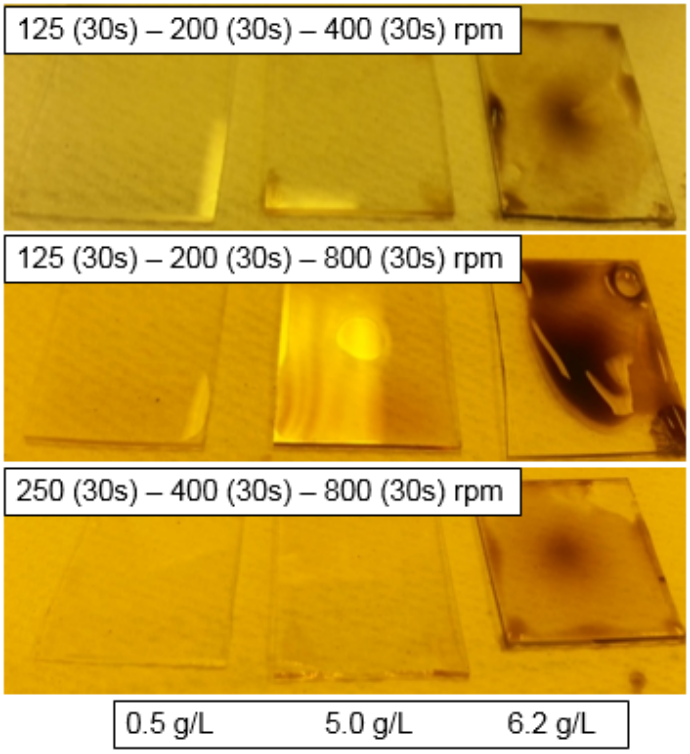

Figure 6-2. Deposition of GO on glass substrates by spin coating according to spin conditions.

While the spin coating conditions were controlled to deposit uniform and thin GO films, an alternative method to deposit GO films was explored. The alternative method was called drop coating (Figure 6-3). One mL of GO solution was dropped onto a substrate and dried overnight to evaporate solution and to leave GO only. The solution did not spread out on substrates but remained as a droplet due to its high surface tension. At higher concentrations of GO solution such as 6.2 g/L and 5.0 g/L, darker films were observed, but GO films became transparent at low concentration of 0.5 g/L GO solution. The drop coating may be a good coating method to deposit uniform GO films; however, thicker films of the order of tens of micrometers were commonly deposited. Since gas sensing properties exhibit better

performance with thin films or nanostructures [5], the drop coating may not be the best method for gas sensor application. Spin coating seems to be a much more reasonable method to obtain a thinner layer with consistent properties. In the case of 0.5 g/L GO solution, we used drop coating to obtain a transparent and thin layer for comparative study with spin coating.

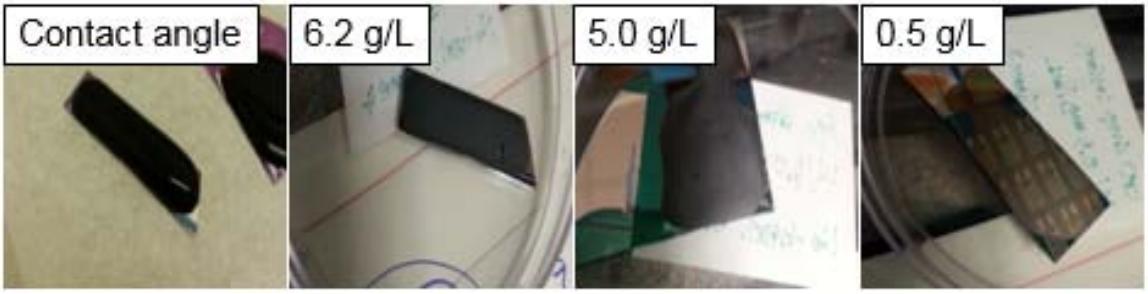

Figure 6-3. Deposition of GO films on SiO_2/Si wafer by drop coating at different concentrations: before evaporation with 6.2 g/L and after evaporation with 6.2 g/L, 5.0 g/L and 0.5 g/L from left to right.

To overcome the limitation of drop coating method, electrophoretic deposition (EPD) was investigated to control thickness (Figure 6-4). GO films were coated on stainless steel by EPD at different concentrations: 0.5 g/L and 5.0 g/L. Bias and time during EPD were 10 V and 3 min at lower concentration and 10 V and 1 min at higher concentration. Deposited films appeared to be uniform even at low voltage condition. In spite of short deposition time used for the higher concentration, the film was thicker than expected. The same experiment was conducted on electrode patterned polyimide substrate. Unlike stainless steel, the conductive electrodes do not fully cover this substrate, but uniform GO films were obtained from the substrate under the same EPD conditions described previously. To control the thickness of GO films, the applied voltage was controlled to 5 V. This voltage was enough to

coat GO on a piece of stainless steel, but not sufficient to cover the interdigitated electrodes on the polyimide films.

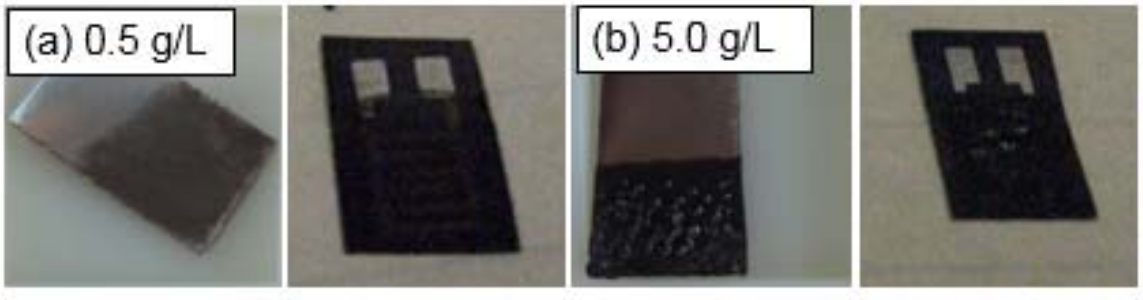

Figure 6-4. Coating condition of graphene oxide films as changing concentration of suspensions: (a) 0.5 g/L on stainless steel (left) and polyimide film (right) and (b) 5.0 g/L on stainless steel (left) and polyimide film (right).

Table 6-1 briefly summaries the advantages and disadvantages of each deposition method. Even though the spin coating requires multiple steps to coat uniform layers due to wettability issue, the spin coating was used for gas sensing applications owing to easy formation of thinner and uniform films.

Table 6-1. Summary of advantages and disadvantages of each deposition method.

	Advantages	Disadvantages
Spin coating	Thinner layer formation Uniform film formation	Complicated steps Wettability issue at lower concentration
Drop coating	Simple approach	Hard to control thickness

	All range of concentrations	Rough surfaces
Electrophoretic deposition	Uniform film formation	Electrolysis
	Easy to control thickness	Thicker layer formation

6.1.2. Reduction of Graphene oxide

Reduction process of GO was conducted in a reduction environment by introducing Ar gas into a furnace. For this study, a series of samples were prepared using different concentrations: 0.5 g/L, and 5.0 g/L. The reduction temperature was examined ranging from room temperature to 200 °C for one hr. GO films deposited via spin coating became darker after heat treatment, but they still maintained continuous films on the substrates. each deposition method. Even though the spin coating requires multiple steps to coat uniform layers due to wettability issue, the spin coating was used for gas sensing applications owing to easy formation of thinner and uniform films.

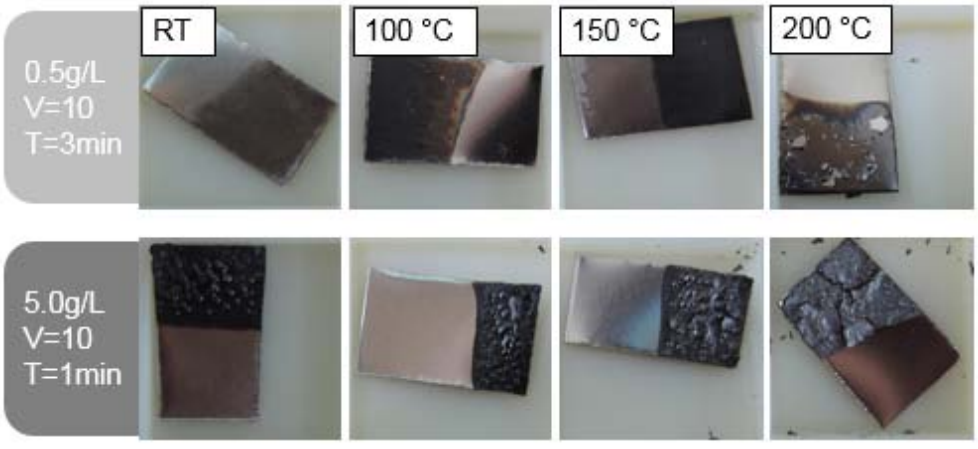

Figure 6-5. Images of graphene oxide film conditions coated by electrophoretic deposition (EPD) as changing heat treatment temperature from RT to 200 °C.

6.1.3. Characterization of reduced graphene oxide

SEM characterization was first performed to examine morphology and topography of the GO films under different coating conditions. As depicted in Figure 6-6, the morphologies of GO films deposited via different coating methods with 5.0 g/L suspension were compared. The spin-coated GO film showed a relatively flatter surface (0.55 μm in thickness) than that of the dip coated film (10 μm in thickness) and the film deposited via EPD (1 μm in thickness). A unique characteristic of EPD processes was observed as shown in Figure 6-6 (c) where small particles existed randomly on the film surfaces. The particle size was around 0.5 μm, which matched the flake size in GO suspension. This confirms that EPD process is one of colloidal deposition processes that use particles/flakes from the suspensions [8].

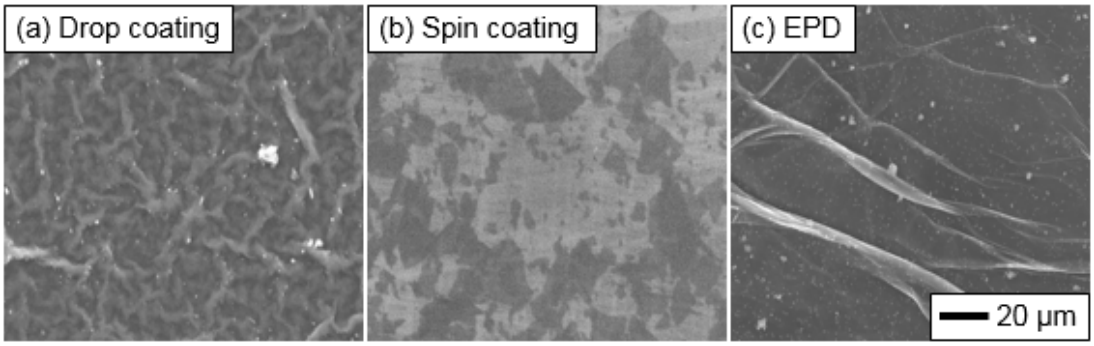

Figure 6-6. SEM images of the morphology of the graphene oxide thin layer deposited via different methods: (a) drop coating, (b) spin coating, and (c) EPD with 5.0 g/L concentration.

Figure 6-7 shows morphological changes according to suspension concentration. As described, different concentrations of suspensions were prepared for film deposition: 0.5 g/L, 5.0 g/L, and 6.2 g/L. These films were coated via drop coating for comparative study. The differences in morphologies were clearly observed with increasing concentration. Fairly flat

surfaces became rougher and had more wrinkles with more GO flakes. These results were consistent when comparing the films coated by drop coating or spin coating.

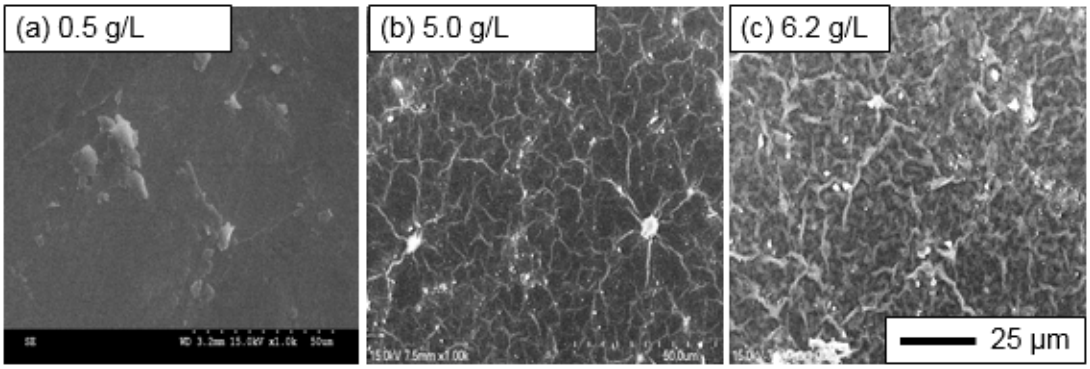

Figure 6-7. SEM images of the morphology of the graphene oxide films with different concentrations: (a) 0.5 g/L, (b) 5.0 g/L, and (c) 6.2 g/L deposited via drop coating.

To explore the effects of heat treatment on morphologies, 5.0 g/L GO films deposited via spin coating were examined as shown in Figure 6-8. Each sample was heat treated at different temperatures: room temperature, 100 °C, and 200 °C. The change of film morphology was observed obviously with increasing temperature. The SEM images did not clearly show isolated single-layer of GO flakes due to multiple stacking of GO and r-GO flakes in the films. The GO film showed more wrinkled surface due to solvent evaporation from coated suspension leaving agglomerated GO flakes. The reduced-GO film after thermal annealing became flatter and thinner. This change may result in decreased thickness because the interlayer gap between each GO layer becomes narrower as solvent evaporates and oxygen functional groups are eliminated [9,10].

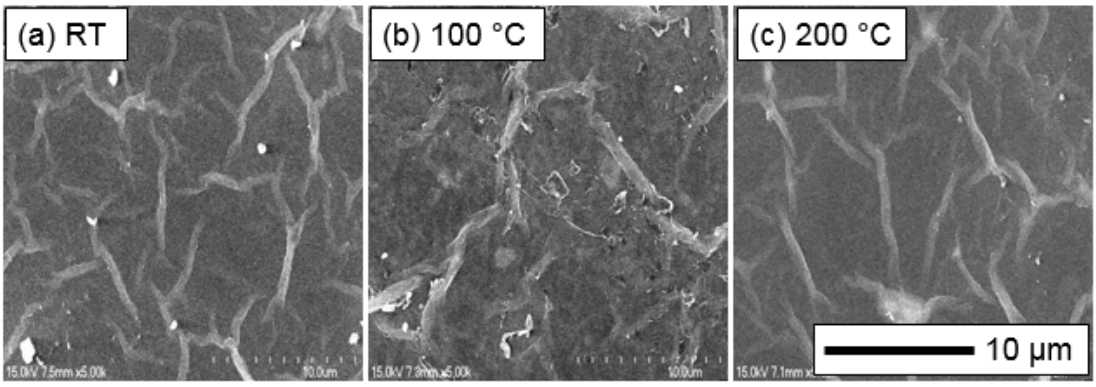

Figure 6-8. SEM images of 5.0 g/L graphene oxide films deposited via spin coating and heat treated under different temperatures.

The crystalline phase of GO was characterized in Figure 6-9 according to drop coating, spin coating, and EPD deposition methods. As shown in the graphs, a peak was observed where 2θ is around 10°, indicating (002) plane of GO when the GO thin films were dried at room temperature [9]. GO thin films showed different intensity of the (002) plane depending on coating methods. The change in the XRD peak intensity, $I_{\text{drop coating}} > I_{\text{EPD}} > I_{\text{spin coating}}$, corresponds to the SEM results in Figure 6. The (002) peak intensity of GO films was also changed by solution concentration. Larger amounts of GO at higher concentrations resulted in thicker film and higher intensity as shown in Figure 6-10.

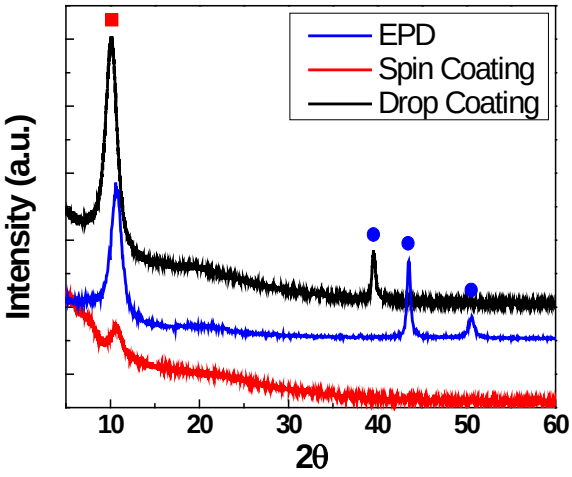

Figure 6-9. XRD patterns of the graphene oxide thin layer deposited via different methods: drop coating, spin coating, and EPD. Red square indicates GO (002) peak and blue dots represent substrate peaks.

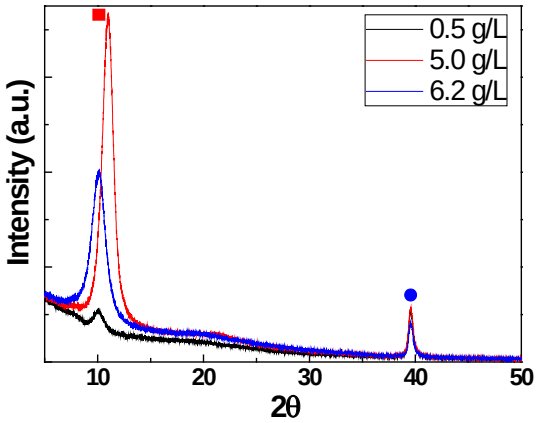

Figure 6-10. XRD patterns of graphene oxide thin layer deposited with different concentrations by drop coating: 0.5 g/L, 5.0 g/L, and 6.2 g/L Red square indicates GO(002) peak and blue dot represents substrate peak.

The evolution of GO to r-GO by thermal reduction at different temperatures was examined by XRD as shown in Figure 6-11. GO films by spin coating was prepared using 5.0 g/L solution, and reduction temperature was varied from RT to 200 °C. GO phase was

observed at 10° of 2θ [9,10]. The intensity of the GO peak after thermal reduction was reduced, and the peak corresponding to graphene phase was observed at 20 ° of 2θ [11]. This XRD result shows that the interlayer distance of the GO films decreased from 8.10 Å (2θ = 10.9 °) to 4.43 Å (2θ = 20 °) after thermal reduction. This decrease results from the elimination of oxygen-containing groups such as intercalated H_2O molecules and various oxide groups on the graphene sheets [11]. These values are quite comparable to those in the literature where the interlayer distance of GO is in the range of 5 to 9 Å, and that of graphene is about 3.4 Å [12].

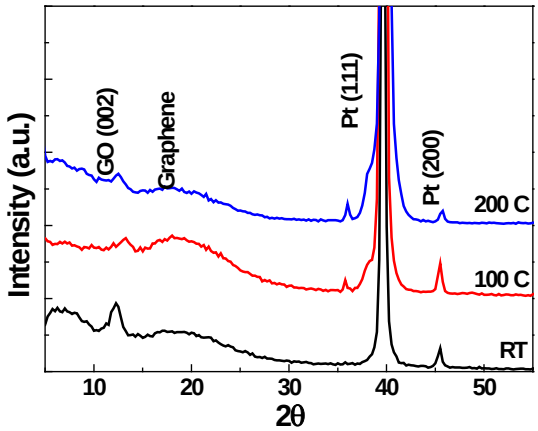

Figure 6-11. XRD patterns of 5.0 g/L graphene oxide deposited by spin coating. Reduction temperature was varied: room temperature, 100 °C and 200 °C

Such a peak position observed in GO and graphene or r-GO can correspond to interlayer distance according to Bragg's law. If (002) planes of graphite or multi-layered graphene are given as in Figure 6-12 (a), the interlayer distance is denoted as d_{002}. The change of XRD patterns formed during the GO reduction, as well as the resultant GP, can be explained via a simple and intuitive concept for various types of interlayer distances of graphene and GO is

shown in Figure 6-12 (b) through Figure 6-12 (e). Because GP layers have intrinsic nano curvature distortions (Figure 6-12 b) existing in a two-dimensional single crystalline structure, the interlayer distance of GP (d_{GP}) is slightly larger than that of the bulk graphite. The reported d_{GP} and graphite are ~3.4 [12] and 3.3483.360 Å [13], respectively. When GO or thermally reduced graphene has defects such as nanoholes (d_{Df}) (Figure 6-12 c), the interlayer becomes increased. In addition, GO and GP having oxide groups of COx with a sp^3 bond (d_{Ox}) (Figure 6-12 d) show even longer distance, and GO has the largest interlayer distance (d_{GO}) because of its intercalated H_2O molecules and various oxide groups (Figure 6-12 e). The d_{GO} value is in the range of ~5 to 9 Å, depending on the number of intercalated water molecules. The interlayer distance order is $d_{GO} > d_{Ox} > d_{Df} > d_{GP} >$ graphite.

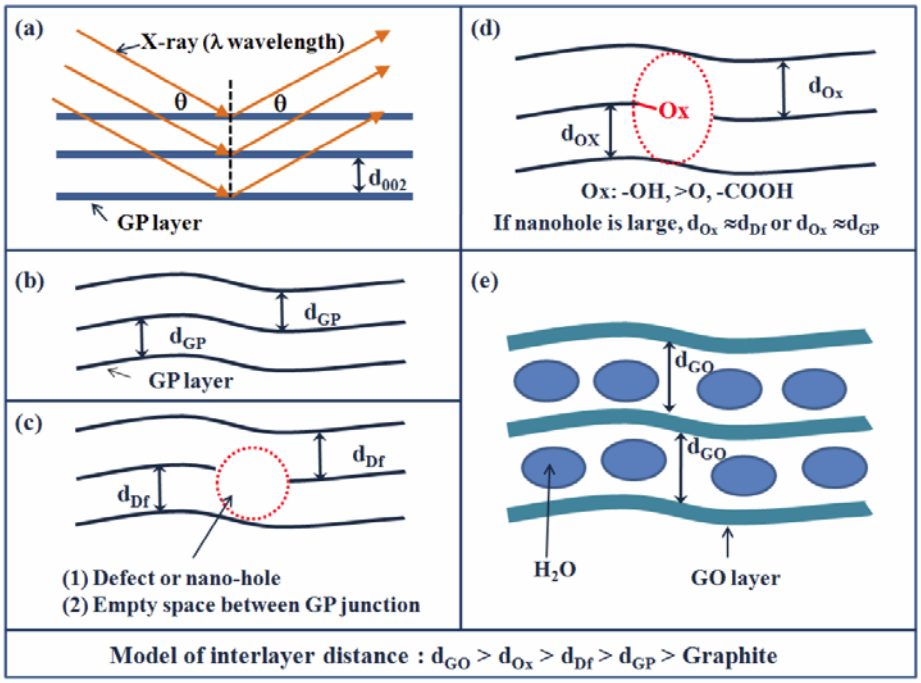

Figure 6-12. Bragg's law for GP or graphite (002) planes (a), and models for d_{002} of GO (e) and thermally reduced GP (b-d). [14]

Figure 6-13 to Figure 6-14 show the structure and phase information of GO and r-GO

films analyzed by Raman spectra. Figure 6-13 shows the GO films coated by the drop coating according to the concentration change from 0.5 g/L to 6.2 g/L. From the Raman spectra, the D and G peaks of GO were obtained at 1342 and 1571 cm^{-1} indicating vibrations of carbon atoms with sp^3 electron configuration and the in-plane vibration of sp^2 bonded carbon atoms respectively [15,16]. As the concentration increases from 0.5 g/L to 6.2 g/L, the intensities of D and G peaks increased indicating the higher concentration of GO phase. However, the ratio of D and G peaks seemed to be constant as the solution concentration changes. Figure 6-14 presents the 5.0 g/L GO films coated via different coating methods such as drop coating, spin coating, and EPD. Similar to concentration effect, the D and G peaks of each GO film seemed to be related to concentration and thickness of the films. However, overall peak position and ratio of D and G are consistent with the property of GO.

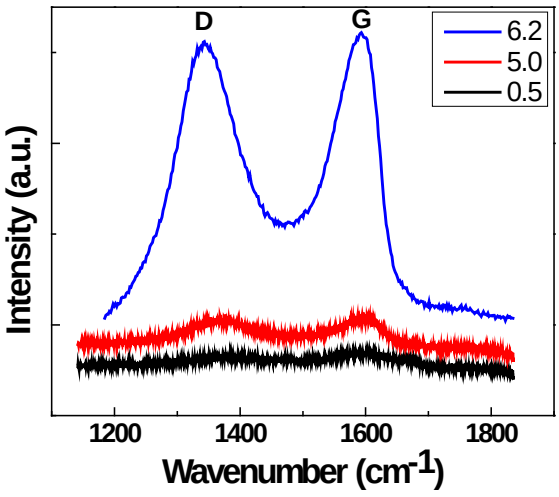

Figure 6-13. Raman spectra of graphene oxide thin layer prepared with different concentrations via drop coating: 0.5 g/L, 5.0 g/L, and 6.2 g/L

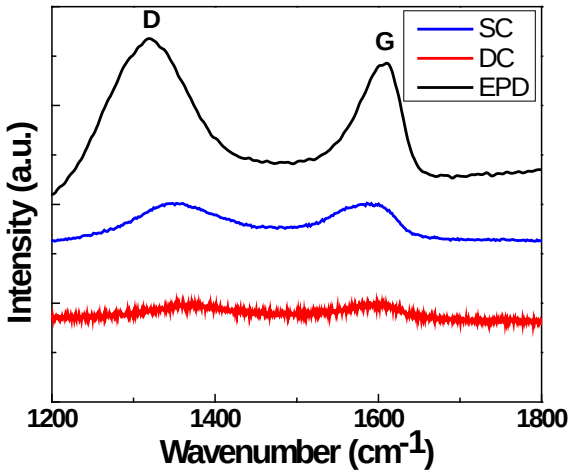

Figure 6-14. Raman spectra of graphene oxide thin layer prepared via different coating methods: drop coating, spin coating, and EPD.

The Raman spectra also showed the change of bond structure as changing the heat treatment temperature as shown in Figure 6-15. The 5.0 g/L GO films deposited via EPD were analyzed to confirm the structure change. After thermal reduction at 200 °C, the intensity of G peak was slightly decreased. The increased of I_D/I_G ratio of r-GO films compared to GO films can present reduced sp^3 bonds and the oxidized molecular defects [16,17,18]. Information on GO and r-GO peaks are analyzed as checking D, G, and 2D peaks. D and G peaks are located near 1340 cm^{-1} and 1600 cm^{-1} respectively. D peak is generated due to oxygen groups, and Graphene peak originates g peak. Both peaks are observed in 0.5 g/L GO, 5.0 g/L, and 6.2 g/L films regardless the coating methods. After heat treatment, structure change is confirmed by checking the shift of each peak. Especially, 2D peak near 2600 cm^{-1} is supposed to shift to 2700 $cm^{-1,}$ and it was confirmed in Figure xx right figure. As increasing the temperature, 2D peak was shifted to right as decreasing the intensity.

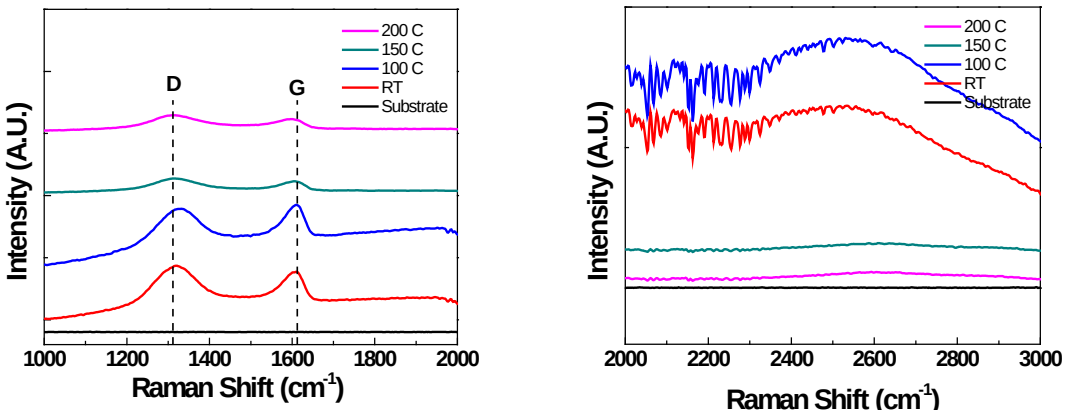

Figure 6-15. Raman spectra of graphene oxide as changing heat treatment condition from RT to 200 °C. D and G peaks are indicated in left and 2D peak is shown in right.

FTIR results presented the change of the oxygen contents and bonding structure from GO to r-GO (Figure 6-16). Peak positions for both GO and r-GO films were similar, but the intensities were different. Peaks at 3400, 1700, 1400, and 1100 cm^{-1} indicating O-H, C=O, O-H, and C-O stretching vibration decreased after thermal reduction of GO film due to the evaporation of the functional groups [10,19]. The peak corresponding to C=C from 1616 to 1580 cm^{-1} shifted and the ratio of C=O peak to C=C peak decreased after thermal reduction. Such change may occur when some electron-withdrawing groups such as oxygen-containing functional groups bind to aromatic rings after reduction [20].

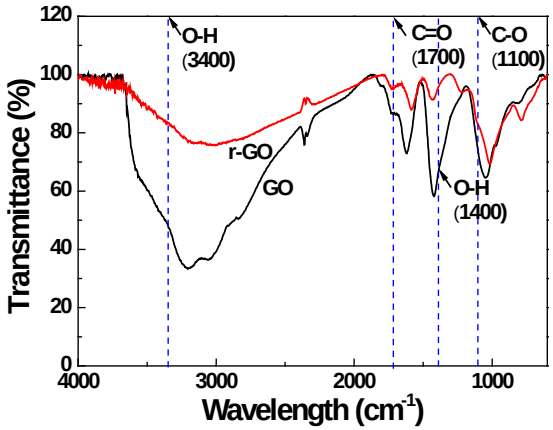

Figure 6-16. FTIR spectra: graphene oxide (black) and reduced graphene oxide (r-GO) films.

The degree of reduction in GO was analyzed by XPS as shown in Figure 6-17. GO film showed the low ratio of C/O = 2.57 and the film after thermal reduction, r-GO showed the increased ratio of C/O = 4. The value of C/O ratio does not reach the case of highly reduced GO (~10) and may be considered as partially reduced GO. But the similar range of C/O ratio values was reported in thermally reduced GO. Ren et al. [20] reported C/O = 6.8 in r-GO film reduced at 200 °C for 12 hr, and Yang et al. [18] had C/O = 3.9 value in their GO film reduced at 200 °C for 30 min. Figure 6-17 also showed the decrease of two main peaks, i.e. C-C (single bond, ~285.9 eV) and C-O (hydroxyl and epoxy, ~286.6 eV) as the film turned to r-GO from GO. Minor peaks indicating C=O (carbonyl, ~287.9 eV) and O=C-O (carboxyl, ~289.2 eV) were also decreased after thermal reduction. The remarkable increase in C=C peak (double bond, ~285 eV) was observed, which indicates the recovery of the sp^2 structure.

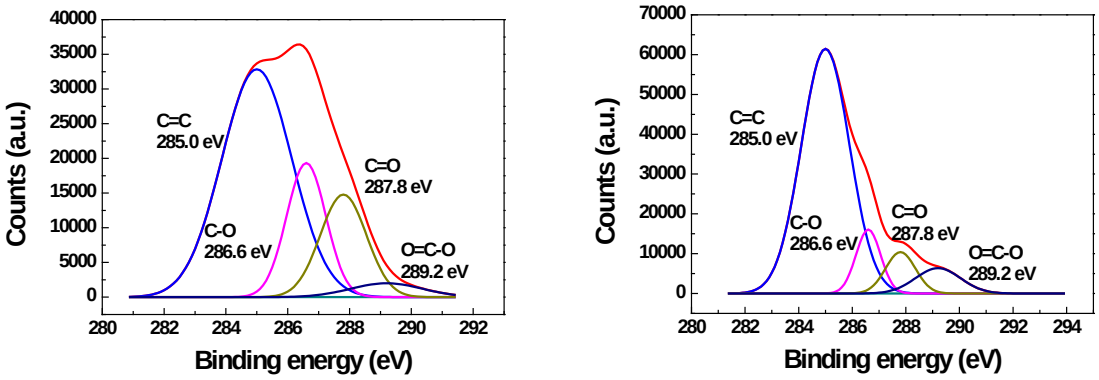

Figure 6-17. XPS spectra of (a) GO and (b) r-GO films at 200 °C.

During thermal treatment, the change of functional groups was confirmed by FTIR and XPS analysis. To check energy consumption to eliminate and/or form bonding in GO films, DSC technique was used. As shown in Figure 6-18, the operating temperature increased from RT to 400 °C. The DSC data have several exothermal and endothermal peaks. The exothermal peaks are due to the decomposition of oxygen functional groups from GO sheet. Especially, the peak at 227 °C is remarkable reported in other references. Some endothermal peaks occurred due to break of the double/single bonds to evaporate oxygen functional groups. The energy consumption at 227 °C corresponds to the change in gas sensing behaviors by GO and r-GO sensors.

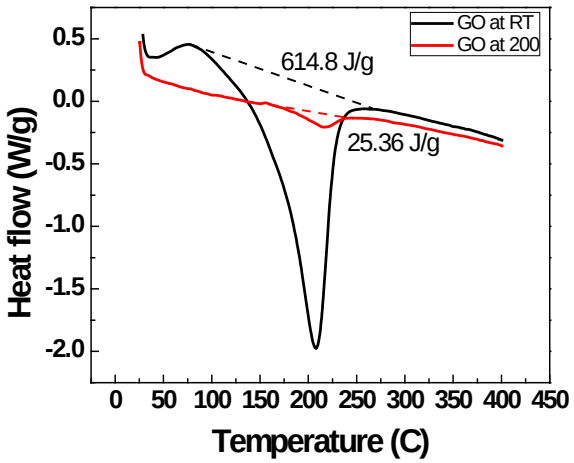

Figure 6-18. DSC analysis of graphene oxide as increasing temperature from RT to 400 °C.

6.2. Electrical and gas sensing properties

The electrical properties of the prepared GO thin films were analyzed by measuring the initial resistance of the films as plotted in Figure 6-19. The initial resistance of pure GO film prior to any treatment was measured to be around 2.0 MΩ. However, the initial resistance of the r-GO film was dropped to several hundred kΩ when reduction temperature increased to 100 °C. After increasing the temperature to 500 °C, the r-GO films became a modified graphene film with good conductivity. The initial resistance decreased with the increase of reduction temperature because the sp^2 bonds were recovered from sp^3 bonds as the functional groups were eliminated [9,19]. Therefore, elimination of oxygen functional groups results in decreased distance between graphitic domains, which enhances charge transport via variable ranges of hopping and/or creates continuous graphitic paths for charge transport [23].

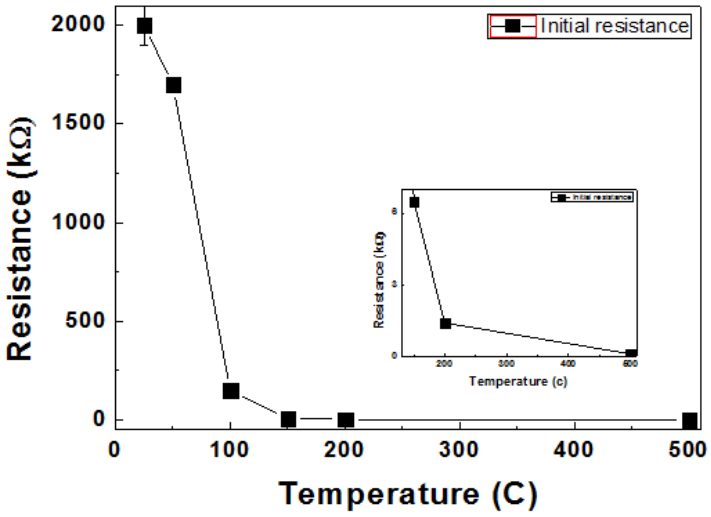

Figure 6-19. Initial resistance of graphene oxide films at different reduction temperature.

Electrical properties of GO/r-GO films influenced by reduction processes were analyzed by evaluating gas sensing performance of ethanol and formaldehyde gasses. From the literature, r-GO is reported as a p-type semiconductor [21]. However, a semiconducting type of GO has been rarely specified. Figure 6-20 shows the gas sensing performance of non-treated GO films deposited by drop coating according to different concentrations. As shown in Figure 6-20 the initial resistances increased as the film concentrations decreased. Under an ethanol atmosphere, the resistance decreased, and n-type sensing behaviors were observed at room temperature regardless of GO concentration. The samples showed the response time of around 36 sec on ethanol gas.

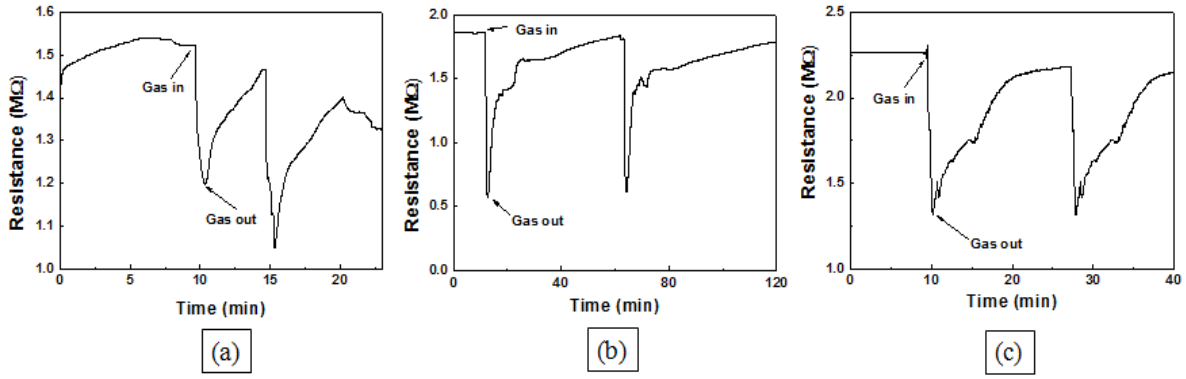

Figure 6-20. Ethanol gas sensing behaviors of GO film coated by drop coating according to concentrations and dried at RT: (a) 6.2 g/L, (b) 5.0 g/L, and (c) 0.5 g/L

Gas sensing properties of GO films were also explored using formaldehyde as shown in Figure 6-21. Two main differences were observed: gas response and response rate. Firstly, the gas response of GO sensors in formaldehyde gas was less than that of GO sensors in ethanol gas. Secondly, the response time and rate became slower in formaldehyde gas as compared with the properties of ethanol. These differences may enable the development of a single chip to provide selectivity between gases.

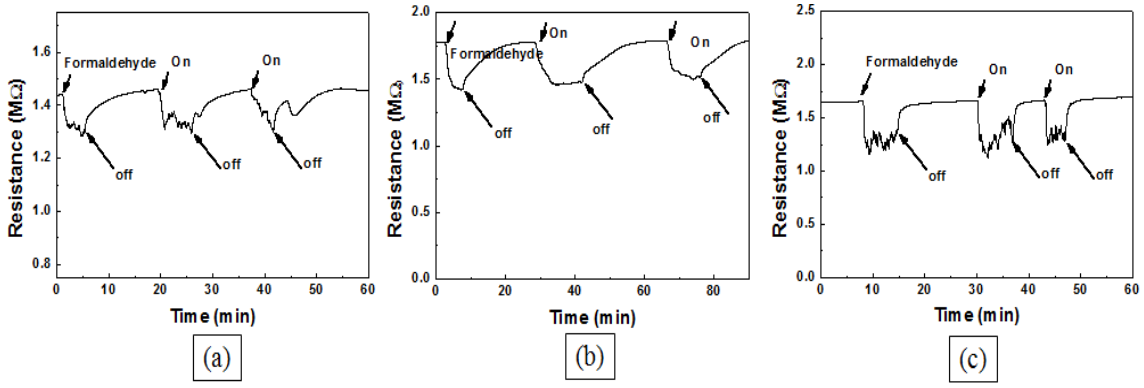

Figure 6-21. Formaldehyde gas sensing behavior of GO film coated by drop coating according to concentrations and dried at RT: (a) 6.2 g/L, (b) 5.0 g/L, and (c) 0.5 g/L.

The effects of heat treatment on GO films were characterized by measuring resistance profiles at room temperature. Once the GO films went through heat treatment at 100 °C for 2 hrs, p-type behavior was observed. The initial resistance decreased dramatically from 1.5 MΩ to 150 kΩ as the sp^2 carbon-carbon bond was recovered, and the functional groups were eliminated [21]. The r-GO film reduced at 100 °C for 2 hrs became a p-type semiconductor having hole-dominant electron transfer behavior instead of an n-type semiconductor having electron dominant electron transfer behavior. This p-type behavior of r-GO may be due not only to the polarization of adsorbed molecules but also to defects introduced on the graphene sheets during the preparation or reduction processes [24]. Therefore, the defect-induced changes in electronic properties, altered from n-type to p-type semiconducting with structural deformations, contribute to effective adsorption of reduction gasses such as ethanol on the surface of r-GO [23].

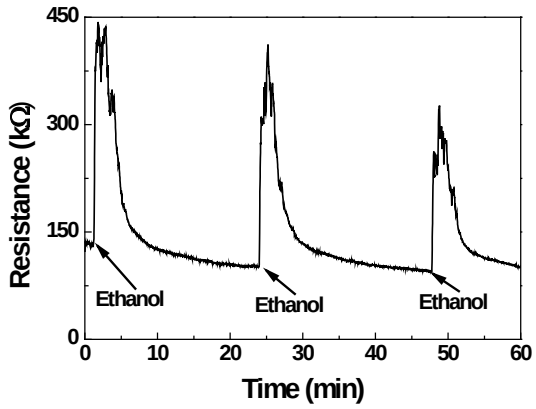

Figure 6-22. Ethanol gas is sensing the behavior of 6.2 g/L GO film coated by spin coating and heat treated at 100 °C for two hr.

Transition behavior was observed by measuring gas sensing performances while changing heat treatment temperature as shown in Figure 6-22. For further study, thermal annealing

temperatures were changed in sequence as shown in Figure 6-23. Under lower temperature such as RT and 100 °C, the resistance of the GO films was dropped as ethanol gas was introduced, indicating n-type gas sensing behavior. However, under higher thermal annealing temperature above 150 °C, the increased resistance of r-GO films was observed with ethanol gas, which correlates with a p-type sensing behavior. This change in gas sensing behaviors can be attributed to the change of a charge carrier from an electron to hole when the number of functional groups, contributing to the number of reactive sites, changes [22,23]. The response times of GO and r-GO films in sensing ethanol gas showed less than 2 min to reach the saturated signal point. The sensitivity changed from 6.21 to 3.32 with the phase change from GO (RT) to r-GO (200 °C). Such decrease of gas response may indicate the reduction of functional groups from GO films, which means the decrease of the reactive sites on GO films [22]. This trend also supports the recovery of sp^2 bonds by eliminating functional groups from the GO films.

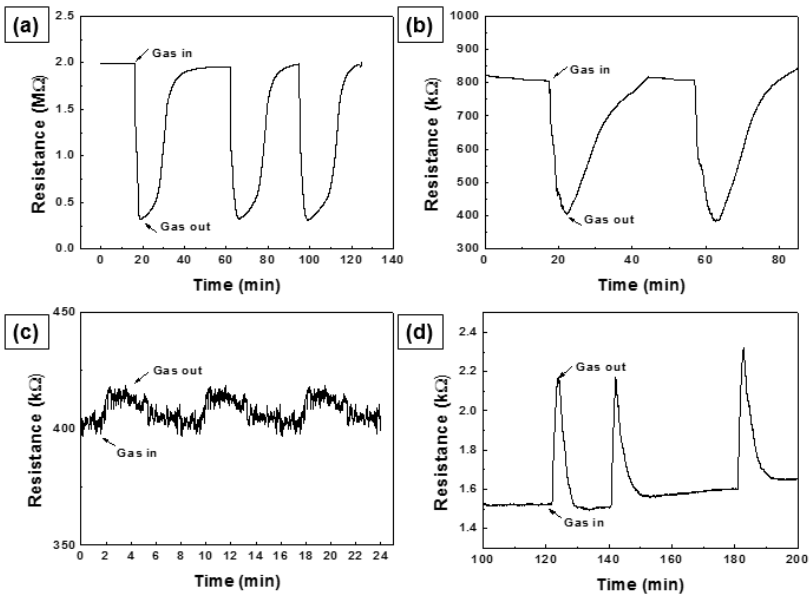

Figure 6-23. Ethanol gas sensing behavior of 6.2 g/L GO film coated by spin coating and reduced at different temperature for 1 hr: (a) RT, (b) 100 °C, (c) 150 °C, and (d) 200 °C.

The gas sensing behaviors of GO sensor were explained by two possible mechanisms as shown in Figure 6-24. One mechanism is explained by recovery of carbon double bond having weak bond strength. These bonds are easily reacted and recovered with surface oxygen and gases, and the gas response can be improved even at room temperature. Another mechanism is supported by reaction of gases with oxygen functional groups. These functional groups are involved to the reaction; however, this reaction is reported as semi-permanent reaction. Therefore, it contributes to the degradation in gas sensing after several cycles.

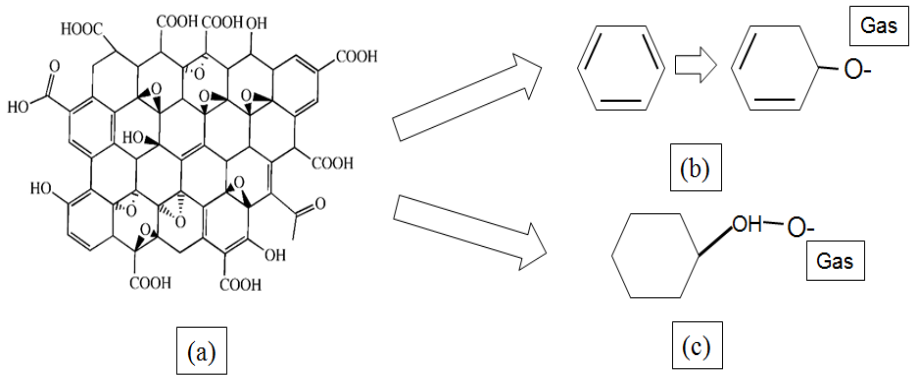

Figure 6-24. Gas sensing mechanisms of GO: (a) surface chemistry, (b) mechanism 1, and (c) mechanism 2.

6.3. Summary and Conclusions

Graphene oxide films were uniformly deposited on various substrates through different deposition methods: drop coating, spin coating, and electrophoretic deposition. While deposited films via drop coating showed thicker and rougher layers, those via spin coating provided thinner and flatter layers when the same concentrated solution was used. Among deposition methods, EPD was considered as an easily controllable method to vary film thickness. Thermal reduction was performed under Ar atmosphere to explore changes in GO

properties. Evaporation of solvents was observed and elimination of oxygen functional groups was estimated by the shift in XRD peak. DSC analysis also proved the solvent evaporations during temperature change. Analysis of the films through FTIR and XPS clarified the change of the amounts of oxygen functional groups as heat treatment temperature changed.Non-treated GO films and heat treated GO films were prepared to measure initial resistance and gas sensing properties. Initial resistance values were changed according to solution concentrations and reduction temperature. Initial resistance increased with decreasing the concentrations and increasing the heat treatment temperature. The results were related with the change and the amounts of functional groups on GO surfaces as proven by material analysis. The fabricated gas sensors with GO films were tested using resistance profile measurement with different gases: 100 ppm of ethanol and 100 ppm of formaldehyde. All gas sensing measurements were conducted at room temperature. Non-treated GO films showed n-type gas sensing behaviors to both gases; however, p-type gas sensing behaviors were observed at higher heat treatment condition (above 150 °C or 100 °C for longer heat treatment time). Other behaviors such as gas responses, response rate, and recovery time were changed depending on heat treatment temperature and types of gases. Higher gas responses and faster reactions were observed with ethanol gas rather than with formaldehyde. Also, slower gas responses were detected as the heat treatment temperature increased. GO and r-GO films were demonstrated as promising candidates for room temperature gas detection with fairly good gas responses. Furthermore, transition behavior from n-type to p-type gas sensing is also very interesting for selective gas sensing.

References

1. Becerril HA, Mao J, Liu Z, Stoltenberg RM, Bao Z, Chen Y. Evaluation of solution-processed reduced graphene oxide films as transparent conductors. *ACS nano.*

2008;2(3):463-470.

2. Wu J, Becerril HA, Bao Z, Liu Z, Chen Y, Peumans P. Organic solar cells with solution-processed graphene transparent electrodes. *Applied Physics Letters.* 2008;92(26):263302.

3. Kim F, Cote LJ, Huang J. Graphene Oxide: Surface Activity and Two-Dimensional Assembly. *Advanced Materials.* 2010;22(17):1954-1958.

4. Sharma S, Ganguly A, Papakonstantinou P, et al. Rapid microwave synthesis of CO tolerant reduced graphene oxide-supported platinum electrocatalysts for oxidation of methanol. *The Journal of Physical Chemistry C.* 2010;114(45):19459-19466.

5. Azad A, Akbar S, Mhaisalkar S, Birkefeld L, Goto K. Solid-state gas sensors: A review. *Journal of the Electrochemical Society.* 1992;139(12):3690-3704.

6. Zalalutdinov MK, Robinson JT, Junkermeier CE, et al. Engineering graphene mechanical systems. *Nano letters.* 2012;12(8):4212-4218.

7. Xiao L, Damien J, Luo J, Jang HD, Huang J, He Z. Crumpled graphene particles for microbial fuel cell electrodes. *Journal of Power Sources.* 2012;208:187-192.

8. Besra L, Liu M. A review on fundamentals and applications of electrophoretic deposition (EPD). *Progress in materials science.* 2007;52(1):1-61.

9. Zhu Y, Murali S, Cai W, et al. Graphene and graphene oxide: synthesis, properties, and applications. *Advanced Materials.* 2010;22(35):3906-3924.

10. Marcano DC, Kosynkin DV, Berlin JM, et al. Improved synthesis of graphene oxide. *ACS nano.* 2010;4(8):4806-4814.

11. Pei S, Zhao J, Du J, Ren W, Cheng H-M. Direct reduction of graphene oxide films into highly conductive and flexible graphene films by hydrohalic acids. *Carbon.* 2010;48(15):4466-4474.

12. Stankovich S, Dikin DA, Piner RD, et al. Synthesis of graphene-based nanosheets via

chemical reduction of exfoliated graphite oxide. *Carbon.* 2007;45(7):1558-1565.

13. Li Z, Hulderman T, Salmen R, et al. Cardiovascular effects of pulmonary exposure to single-wall carbon nanotubes. *Environmental health perspectives.* 2007:377-382.
14. Mikhailov S. Physics and Applications of Graphene-Experiments. *Tech Janeza Trdine, Rijeka, Croatia.* 2011.
15. Fowler JD, Allen MJ, Tung VC, Yang Y, Kaner RB, Weiller BH. Practical chemical sensors from chemically derived graphene. *ACS nano.* 2009;3(2):301-306.
16. Ai K, Liu Y, Lu L, Cheng X, Huo L. A novel strategy for making soluble reduced graphene oxide sheets cheaply by adopting an endogenous reducing agent. *Journal of Materials Chemistry.* 2011;21(10):3365-3370.
17. Wu S, Yin Z, He Q, Huang X, Zhou X, Zhang H. Electrochemical deposition of semiconductor oxides on reduced graphene oxide-based flexible, transparent, and conductive electrodes. *The Journal of Physical Chemistry C.* 2010;114(27):11816-11821.
18. Yang D, Velamakanni A, Bozoklu G, et al. Chemical analysis of graphene oxide films after heat and chemical treatments by X-ray photoelectron and Micro-Raman spectroscopy. *Carbon.* 2009;47(1):145-152.
19. Jeong H-K, Lee YP, Jin MH, Kim ES, Bae JJ, Lee YH. Thermal stability of graphite oxide. *Chemical Physics Letters.* 2009;470(4):255-258.
20. Ren P-G, Yan D-X, Ji X, Chen T, Li Z-M. Temperature dependence of graphene oxide reduced by hydrazine hydrate. *Nanotechnology.* 2011;22(5):055705.
21. Jeong HY, Kim JY, Kim JW, et al. Graphene oxide thin films for flexible nonvolatile memory applications. *Nano letters.* 2010;10(11):4381-4386.
22. Some S, Xu Y, Kim Y, et al. Highly Sensitive and Selective Gas Sensor Using Hydrophilic and Hydrophobic Graphenes. *Scientific reports.* 2013;3.

23. Lu G, Ocola LE, Chen J. Gas detection using low-temperature reduced graphene oxide sheets. *Applied Physics Letters.* 2009;94(8):083111.

24. Kim K, Park HJ, Woo B-C, Kim KJ, Kim GT, Yun WS. Electric property evolution of structurally defected multilayer graphene. *Nano letters.* 2008;8(10):3092-3096.

CHAPTER 7. COMBINATORIAL STRUCTURE OF GRAPHENE OXIDE AND METAL OXIDE FOR SELECTIVE GAS SENSING.

7.1. Deposition of combinatorial structure

The combinatorial structure consisting of graphene oxide (GO) and metal oxide (MO) was prepared: ZnO and SnO_2 were used as representatives of traditional metal oxides. Bimorph structure and multilayer structure were considered to compare and understand gas sensing properties. Moreover, the ratio of the mixture in the combined GO and MO was controlled to explore the effects of compositional gradient on the properties of the composites.

7.1.1. Deposition conditions and characterizations of graphene oxide and ZnO

Bimorph structure of GO and ZnO was prepared: nanostructured ZnO sensing layer was fabricated via sputter deposition and thermally assisted chemical solution method as described in Chapter 3. Then, GO film was deposited via EPD process and on top of the device. Figure 7-1 depicts the schematic diagrams of the bimorph structure and images of the deposited condition of ZnO NRs and GO. GO films were controlled by applied voltage to change film formation. Island type was formed under lower applied voltage, 5V, (Figure 7-1 (a)) and fully covered films were deposited on the ZnO NRs under higher voltage, 10V (Figure 7-1 (b))).

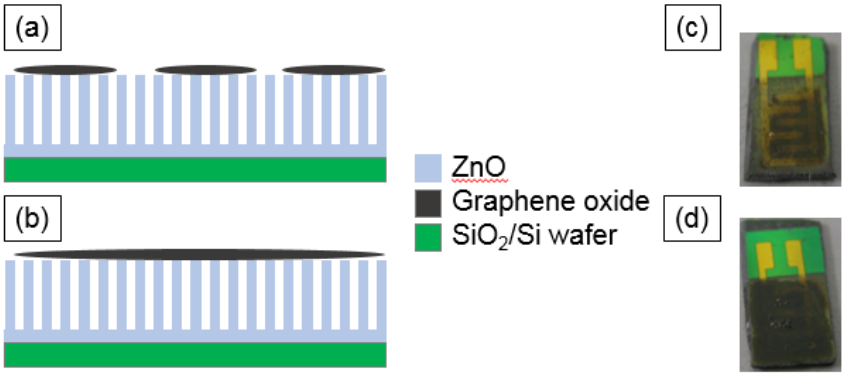

Figure 7-1. Schematic diagrams of ZnO NR and GO mixture: (a) island type and (b) film type, and images of the sensor platforms after deposition: (c) island type and (d) film type.

Morphologies of the films were characterized by SEM as shown in Figure 7-2 (a) and (b). Single or double layers of GO were partially deposited on top of ZnO NRs forming island type film under lower voltage (5 V) in Figure 7-2 (a). Also, fully coated GO film was observed on top of ZnO NRs under higher voltage (10 V) in Figure 7-2 (b). A cross-section view of the bimorph films supported the film formation of GO film on ZnO NRs under higher voltage. This SEM image showed 80 nm of ZnO seed layer, 1.5 μm of ZnO NRs, and 600 nm of GO in the structure. Additionally, the ZnO and GO composites were confirmed by XRD as shown in Figure 7-2 (c). A dominant peak of ZnO crystalline at 34.4 ° indicates c-axis growth. A peak indicating Pt electrode was observed at 39.7 ° [1,2]. At lower angel, around 10 °, a small peak was also detected, and this peak confirmed GO film [3]. This rsult strongly supports the bimorph deposition of ZnO and GO composite on the patterned substrates with Pt electrode.

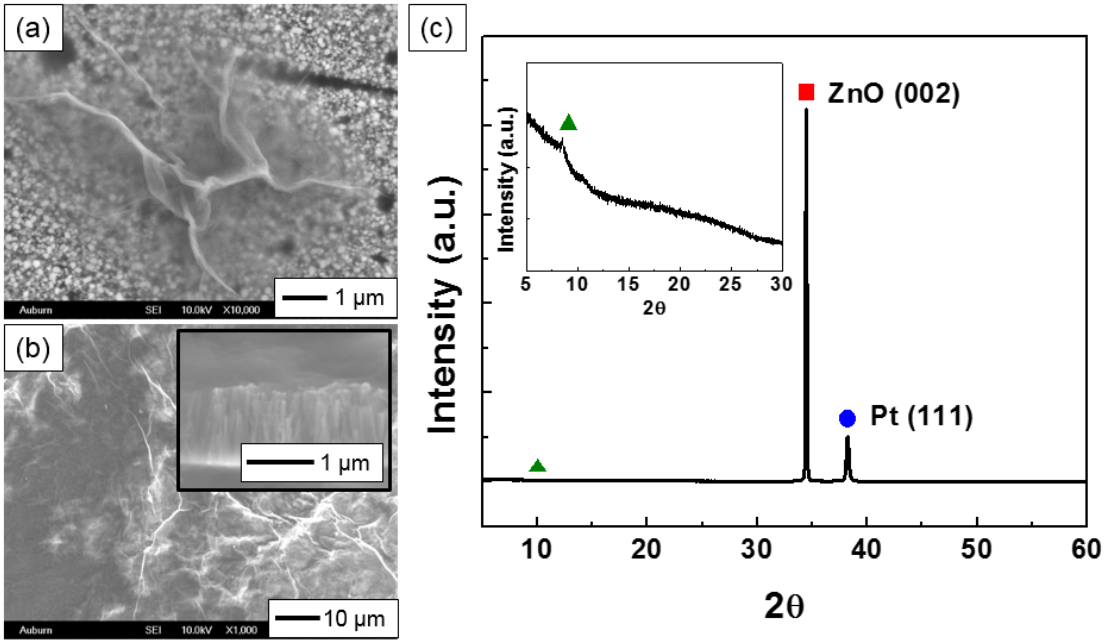

Figure 7-2. SEM images of ZnO NR + GO mixture: (a) island type and (b) film type. (c) XRD spectra of ZnO NR and GO mixture.

7.1.2. Deposition condition and characterization of graphene oxide and SnO_2

A 0.5 g/L GO suspension in an aqueous system and 0.1 wt % of SnO_2 suspension in IPA system were used to fabricate bimorph structure of GO/SnO_2 films. To explore the effect of material on sufrace, two types of films under different deposition sequences were prepared as shown in Figure 7-3 (a) and (b). 10 V for 1 min was applied to coat GO and 100 V for 1 min was provided to coat SnO_2 film.

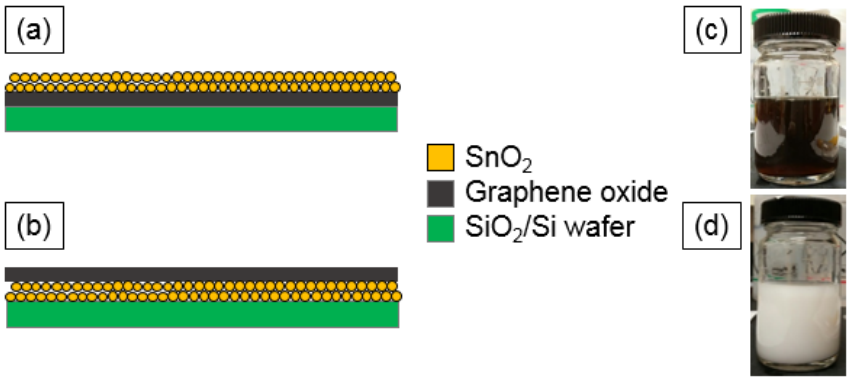

Figure 7-3. Schematic diagrams of SnO_2 and GO mixture: (a) SnO_2 over GO and (b) GO over SnO_2, and images of suspension conditions: (c) 0.5 g/L GO and (d) 0.1 wt % of SnO_2.

Film morphologies and structures were characterized by SEM and XRD respectively as shown in Figure 7-4. Figure 7-4 (a) and (b) depicted that the SnO_2 nanoparticles were formed island type instead of uniformly distributed film. This island formation of SnO_2 may affect the sensing behavior layer. Additionally, clear SnO_2 islands were observed when SnO_2 was deposited later, and opaque particles were shown at thinner GO films when GO was deposited later over the SnO_2 films. It was confirmed by XRD spectra. Strong SnO_2 peaks were detected when the SnO_2 films were located on top of the samples. Moreover, the relative peak intensity of the GO films was changed with film sequence: stronger peaks from the material at the upper position and weaker peaks at under position.

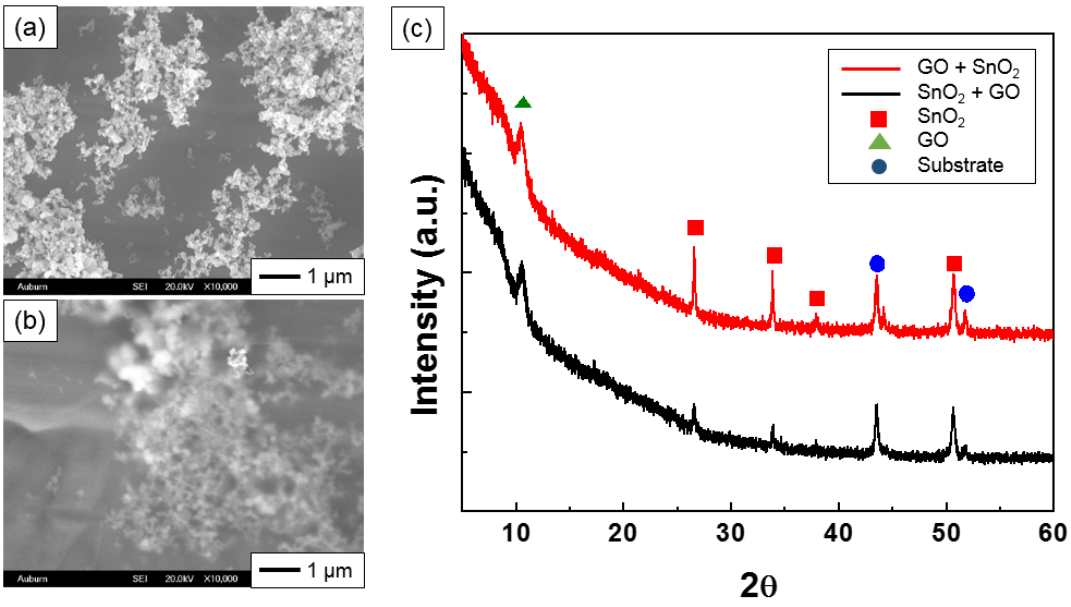

Figure 7-4. SEM images of the combinatorial structures: (a) SnO_2 nanoparticles over GO film and (b) GO film over SnO_2 nanoparticles, and XRD spectra.

Multilayer of GO and SnO_2 composites was prepared by adding SnO_2 nanoparticles in 0.5 g/L GO suspensions. The ratio of GO to SnO_2 was controlled by adjusting the amounts of SnO_2 nanoparticles. Four different suspensions were prepared to explore the ratio effect on gas sensing properties. With increasing the amount of SnO_2 into GO suspension, the color of the suspension was changed as shown in Figure 7-5 (a): from brown color with lower concentration to gray color with higher concentration. Although additional agent to stablize suspension was not added, the mixed suspensions remained as stable as the suspensions before mixture. Multilayer structure of the composites was estimated as depicted in Figure 7-5 (b). Well-dispersed suspensions supported the formation of a multilayer of GO and SnO_2 without distinct regions.

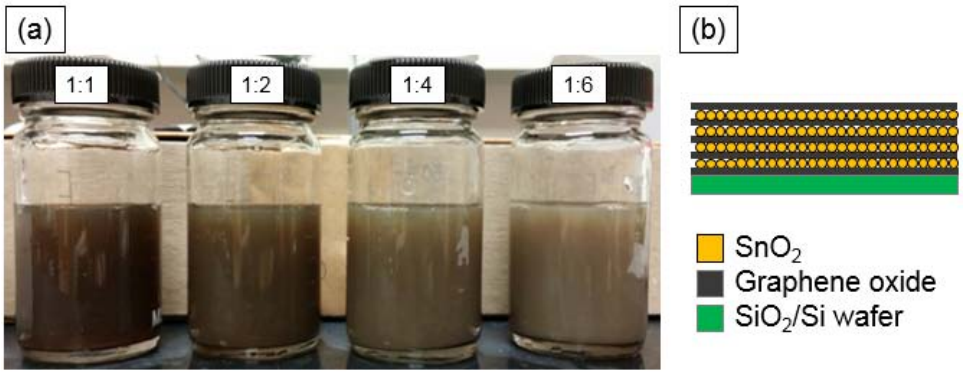

Figure 7-5. (a) Images of suspension conditions of the mixture according to the ratio of GO to SnO_2 and (b) Schematic diagram of estimated structures.

The effect of mixture ratio in the suspensions was firstly checked by measuring deposited weight and Sn amount in Figure 7-6. The increase in deposition weight was observed with increasing the amount of SnO_2 nanoparticles. This trend corresponded to EDS results shown in Figure 7-6 (b). More amount of Sn was detected as more SnO_2 nanoparticles were added by applying higher voltage. This increase indicates that there were more chances to gain SnO_2 nanoparticles on the surface of the films as more amount of SnO_2 existed in the suspensions.

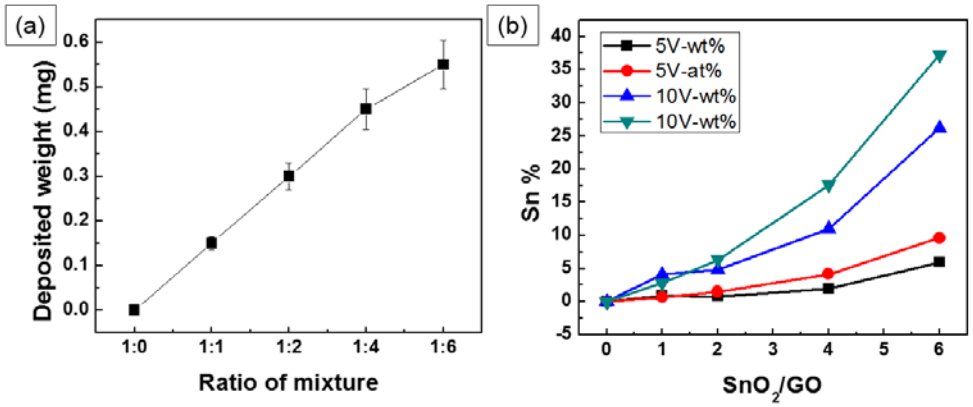

Figure 7-6. (a) Deposition weight of the combinatorial structure according to the ratio of mixture of GO to SnO_2 and (b) EDS results of Sn % of the films.

The numerical results in Figure 7-6 were confirmed by SEM characterization as shown in Figure 7-7. Figure 7-7 (a) to (d) depicted the surface morphologies of the films by change in ratio of mixture. Figure 7-7 (e) described the cross section of the 1:6 mixture of the film to confirm film thickness and multilayered structure. The surface morphologies supported more amounts of SnO_2 nanoparticles with an increase of the ratio. Thin GO layers were observed in the layers of the nanoparticles. Moreover, the multilayer of the mixture was clearly observed in the cross section view. Distinct GO films and nanoparticles were randomly located in the 1.14 μm thick film. This observation could advise that the EPD process is eligible to obtain well-dispersed mixture suspensions by attracting both GO flacks and SnO_2 nanoparticles to the same charged electrodes for multilayered nanostructure.

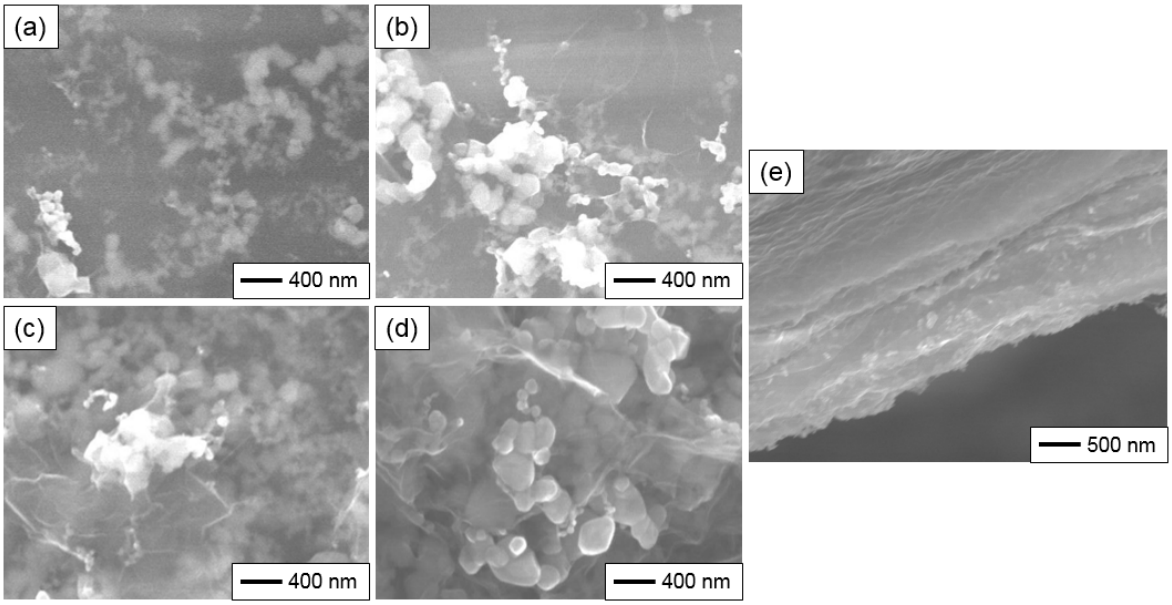

Figure 7-7. SEM images of the combinatorial structures: top view of (a) 1:1, (b) 1:2, (c) 1:4, and (d) 1:6 of GO to SnO_2 and (e) cross section view of 1:6 sample.

XRD characterization was performed to support the SEM results. As shown in Figure 7-8, three types of materials were detected. GO peak was observed near 15° and 28°, 34°, 38°, 51°,

and 53° indicating SnO_2 nanoparticles, and two substrate peaks were observed at 43° and 52° [4,5]. Additionally, four samples under different deposition conditions were compared. Stronger peaks were detected as more SnO_2 nanoparticles were added to the suspensions, which correspond to the SEM results.

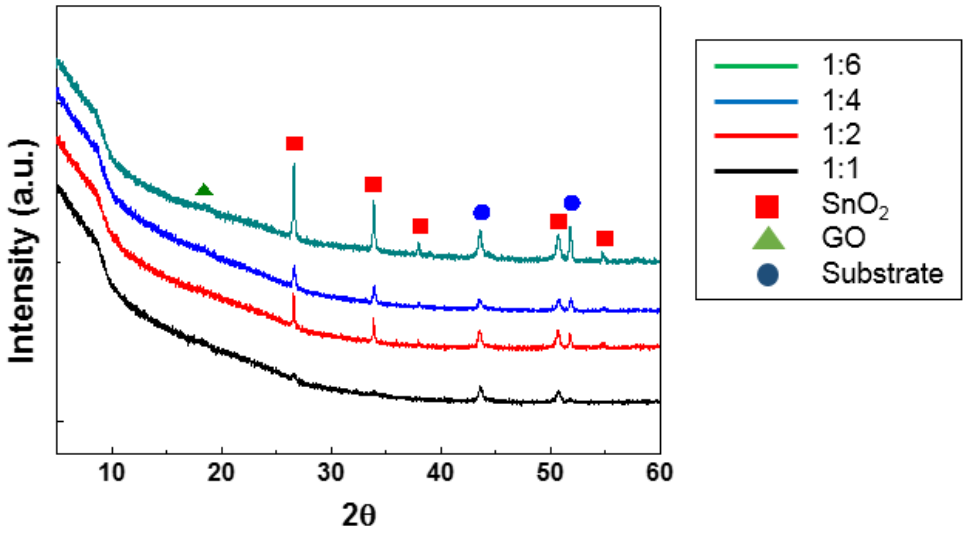

Figure 7-8. XRD spectra of the GO and SnO_2 combinatorial structure according to the ratio.

Thermal analysis of the GO and SnO_2 composites was also conducted to explore the change in surface morphology and properties. After heat treatment of the samples, SEM figures showed the change in the surface topography as changing the ratio of GO to SnO_2. The morphology changes were also analyzed before/after heat treatment of the films at 100 °C under Ar atmosphere as shown in Figure 7-9. The films became rougher as increasing the amount of SnO_2 and temperature due to thickness change by solvent evaporation during heat treatment.

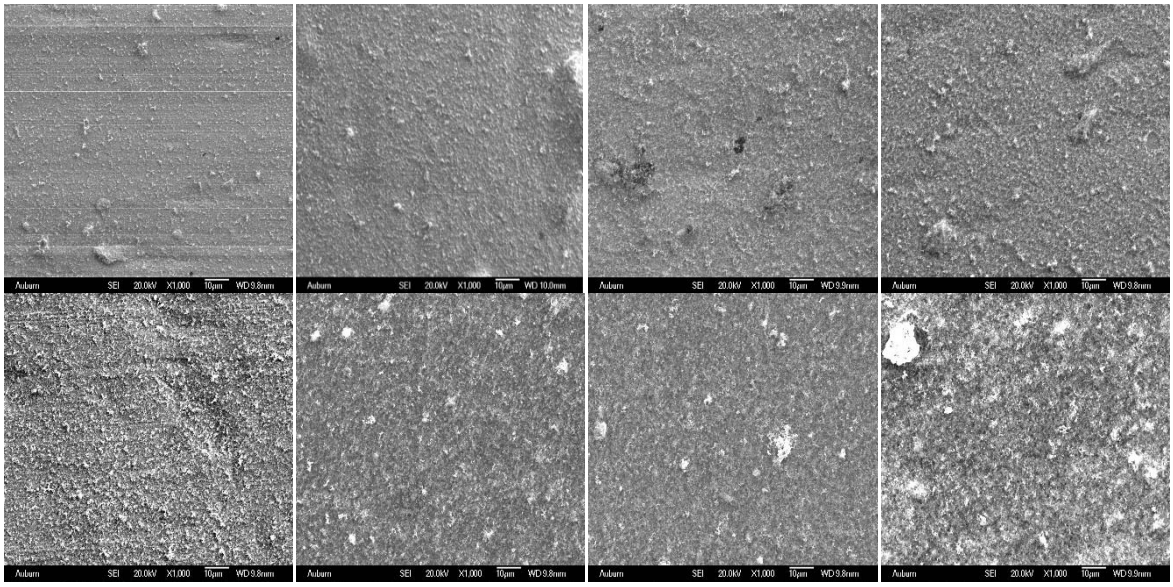

1:1 of GO to SnO_2 1:2 of GO to SnO_2 1:4 of GO to SnO_2 1:6 of GO to SnO_2

Figure 7-9. SEM images of GO + SnO_2 mixture before (top) and after (bottom) heat treatment at 100 °C (1,000 magnification).

Structure of the composite films were examined by XRD as depicted in Figure 7-10 After heat treatment at 100 °C under Ar atmosphere, structure change was not observed in SnO_2 nanoparticles. However, the peak shift and the change in peak intensity of GO were detected due to the change of carbon bonds. This result is consistent with the SEM results.

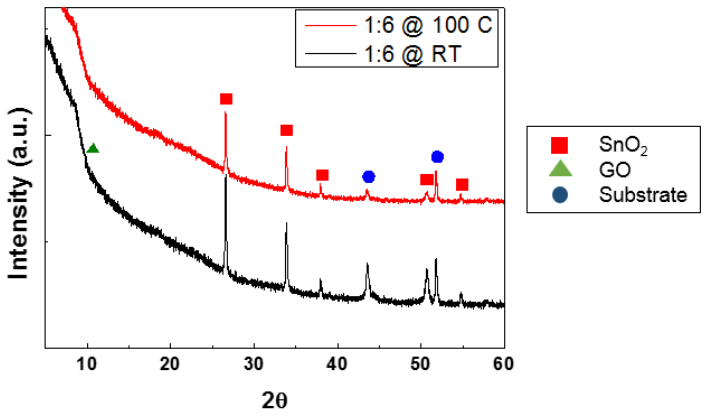

Figure 7-10. XRD spectra of 1 to 6 of GO and SnO_2 mixture after heat treatment at 100 °C.

In mixed suspensions, GO flakes and SnO_2 nanoparticles require different electrical field to attract [6]. Unlike SnO_2 nanoparticles, the GO flakes are attracted to the positive electrode favorably resulting in higher deposition yield. However, since the mixed suspensions consisting of nanoparticles and flakes are dispersed randomly, both materials move to the same direction but in different speed by applied voltage as shown in Figure 7-11. Owing to large surface area and faster movement of GO flakes, the flakes convey SnO_2 nanoparticles to the electrode together even at lower voltage conditions. This process can explain the formation of multilayer structure from mixed suspensions.

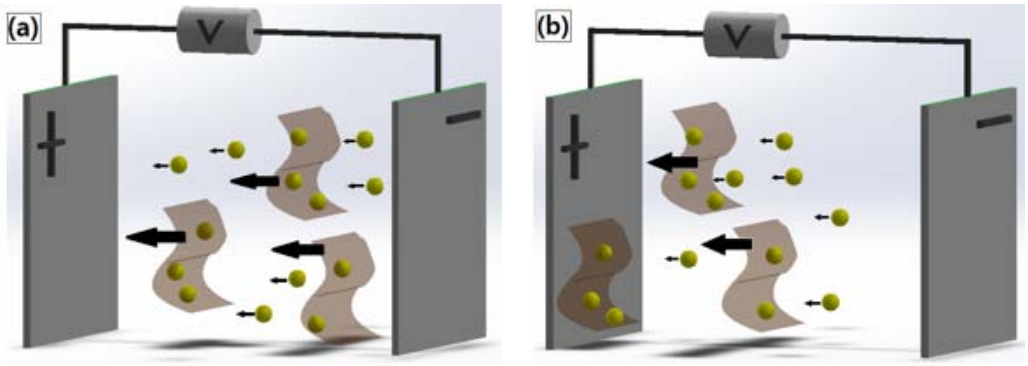

Figure 7-11. Schematic diagrams of movement of particles in the GO and SnO_2 mixture suspensions.

7.2. Electrical and gas sensing properties

Gas sensing performance was conducted with bimorph structure of GO and SnO_2 at room temperature. For feasibility study, pure GO and SnO_2 based sensors were prepared to sense 100 ppm ethanol gas. Figure 7-12 shows the gas sensing behaviors of pure GO films and SnO_2 films on Pt electrode patterned polyimide. GO films were responded to ethanol gas

at room temperature, and the sensitivity (R_i/R_g) was calculated as 1.26. However, SnO_2 films did not show any response towards ethanol gas at room temperature. It is well known that typical metal oxide gas sensors do not react with any types of gases on their surface at room temperature because of energy band gap [7,8]. To activate the reaction sites on the surface of metal oxide, elevating temperature is required to decrease the Fermi energy level to react with surface gases [9]. On the other hand, GO films are easily react with gases at room temperature due to their weak π bonding among double carbon bonding as well as the oxygen functional groups on the film surface [10]. However, the GO film requires certain energy to remove the adsorbed gases on the surfaces and therefore, the recovery time of the GO sensors took longer than typical metal oxide gas sensors [11].

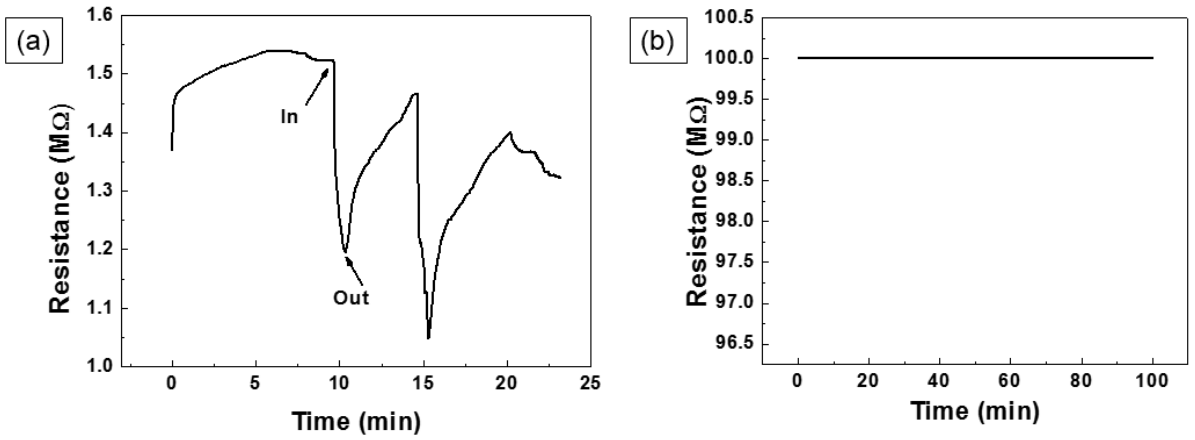

Figure 7-12. Gas sensing behaviors of GO and SnO_2 sensors towards 100 ppm of ethanol gas: (a) 0.5 g/L GO film and (b) SnO_2 film.

The bimorph structure GO and SnO_2 films was analyzed to investigated how they interacted each other. Figure 7-13 shows the overall gas sensing behaviors of two structures. GO and SnO_2 films reacted with ethanol gas showing n-type gas sensing behavior. However, the initial resistance of the bimorph structures was measured differently: GO over SnO_2 films

showed several tens of kilo-ohm whereas the SnO_2 over GO films showed several mega-ohm range of initial resistance. Also, the sensors react with ethanol gases rapidly but the recovery rates were different. The resistance of the GO over SnO_2 sensors recovered quickly once introduced gas was stopped, but the SnO_2 over GO sensors took longer time to recover initial resistance. The result may provide idea on the gas sensing mechanism of the GO and SnO_2 sensors based on the mobility of main charge carriers and main participating materials.

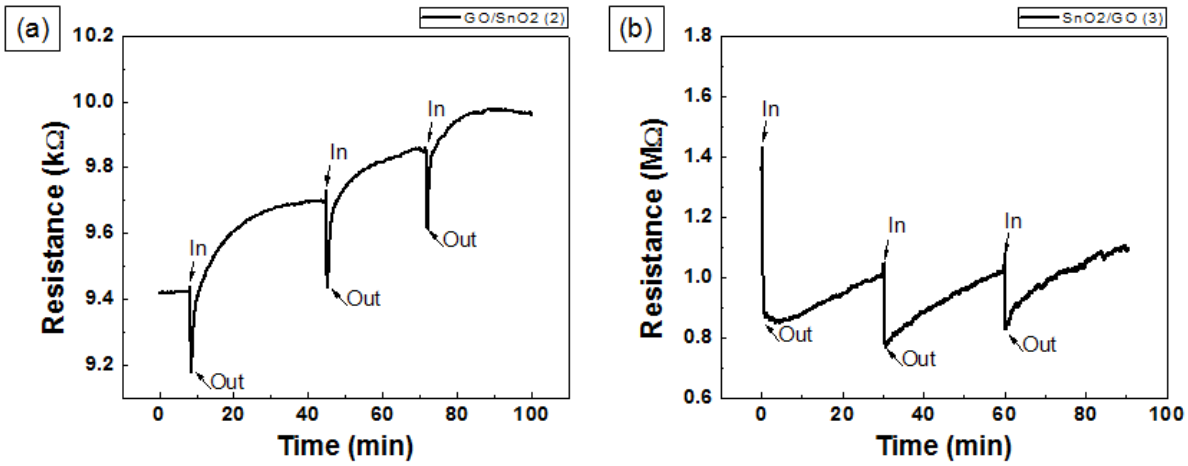

Figure 7-13. Gas sensing behaviors of GO and SnO_2 bimorph structure sensors towards 100 ppm of ethanol gas: (a) GO over SnO_2 film and (b) SnO_2 over GO film.

Table 7-1. Comparisons of gas sensing behaviors of GO and SnO_2 bimorph structure according to its sequence.

	GO over SnO_2	SnO_2 over GO
Initial resistance	~ kΩ	~ MΩ
Sensitivity	Lower, 1.013	Higher, 1.31
Recovery time	Faster	Slower

The catalytic effect of GO and SnO_2 composite on gas sensing properties was clearly observed on mixture structure as well as a combinatorial structure with the change in mixture ratio. The devices were tested at 100 ppm of formaldehyde at room temperature. GO and SnO_2 based sensors were responded as the resistance decreased with the introduced gas showing n-type gas sensing behavior. The gas response of the GO and SnO_2 sensors increased comparing with the pure GO sensors, however, decrease in gas response was also observed after the amount of SnO_2 increased over 1:4 ratio of GO to SnO_2. Additionally, the sensors responded to gas faster after mixing SnO_2 particles in the GO films. This enhancement in gas response and response rate proved that the SnO_2 would serve as catalyst in GO [12,13].

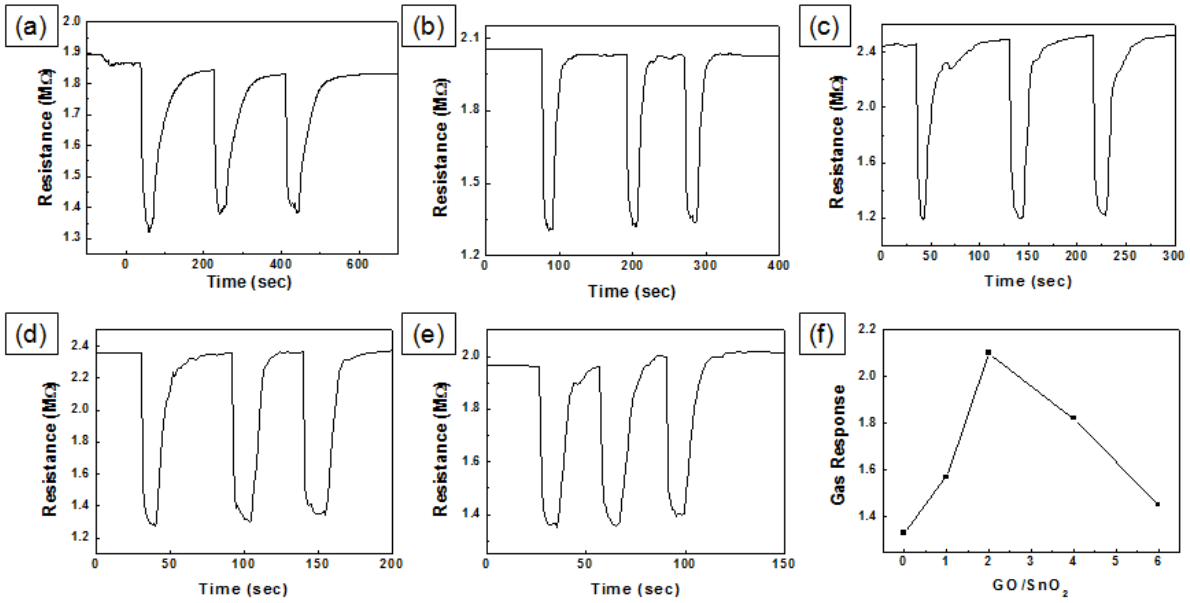

Figure 7-14. Gas sensing behaviors of GO and SnO_2 multilayer sensors towards 100 ppm of formaldehyde gas: (a) 1:0, (b) 1:1, (c) 1:2, (d) 1:4, (e) 1:6, and (f) gas responses according to the mixture ratio.

Second set of gas sensing performance to explore the combinatorial structure was

performed with the same gas, 100 ppm of formaldehyde but all samples were heat treated at 100 °C to check the temperature effect. The gas sensing response of the pure GO film was measured slightly higher than that of the mixture. However, the overall tendency showed the catalytic behavior of SnO_2 in GO films. The response values with 100 ppm formaldehyde to the heat treated GO films were smaller than those to the non-treated GO films. In the case of gas sensing behavior including response rate and recovery rate, it took longer time to get recovered with fluctuation period in this case.

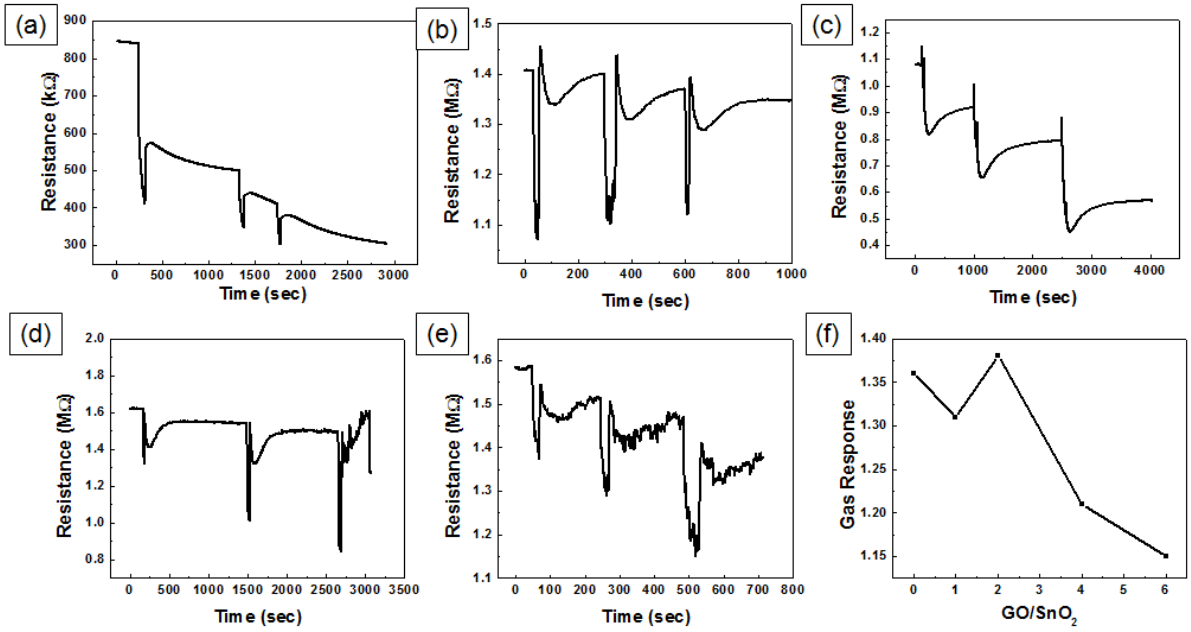

Figure 7-15. Gas sensing behaviors of GO and SnO_2 multilayer sensors treated at 100 °C towards 100 ppm of formaldehyde gas: (a) 1:0, (b) 1:1, (c) 1:2, (d) 1:4, (e) 1:6, and (f) gas responses according to the mixture ratio.

Enhancement in gas selectivity was investigated by using styrene. Difference between formaldehyde and styrene is existence of benzene group: styrene has and formaldehyde does not. Firstly, the gas sensing behavior of GO and SnO_2 sensors showed different gas sensing behavior. Once the gas introduced into the chamber, the initial resistance started to increase

showing p-type gas sensing behavior. It seemed to be good observation to distinguish the type of gas with one sensor array. However, under styrene atmosphere, the catalytic effect was also observed. According to the mixture ratio, the gas response increased and decreased at the point of 1:2 ratio of GO to SnO_2.

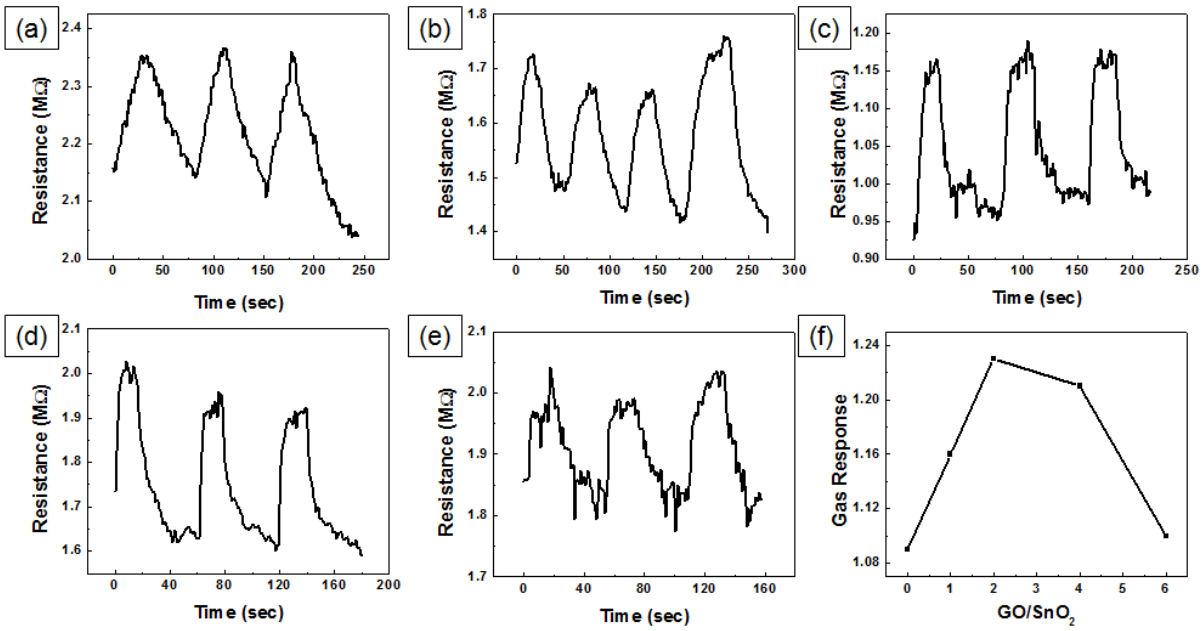

Figure 7-16. Gas sensing behaviors of GO and SnO_2 multilayer sensors towards 100 ppm of styrene gas: (a) 1:0, (b) 1:1, (c) 1:2, (d) 1:4, (e) 1:6, and (f) gas responses according to the mixture ratio.

The combinatorial structure of GO and SnO_2 composites showed catalytic behavior on gas sensing performance with the change in ratio. In Figure 7-17, normalized gas sensing behaviors were summarized according to the ratio of the composites to formaldehyde gas. It clearly showed that the enhancement of gas sensing behavior with an increase in the amount of SnO_2 also degradation behavior after certain amount of the nanoparticles. Moreover, there were gas response changes. With more amounts of the nanoparticles in the composites, shorter gas response rate was observed, which means the SnO_2 into the GO promotes the gas

reaction on the surface. This tendency followed the gas sensing response simultaneously. The overall observation of the gas sensing behavior of the composites corresponds to the catalytic effect of the mixture.

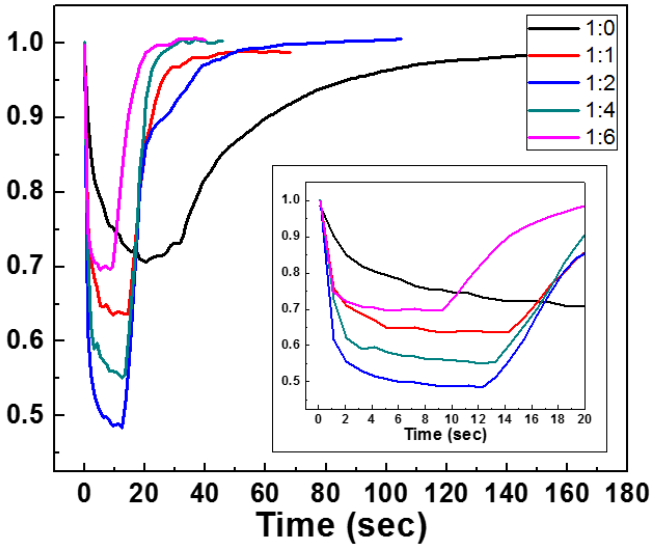

Figure 7-17. The catalytic effect of the GO + SnO_2 composite to 100 ppm formaldehyde gas.

7.3. Summary and Conclusions

Development of combinatorial structure with GO nanosheets and metal oxide nanoparticles (ZnO and SnO_2) was investigated to explore effects on gas sensing behaviors, especially on gas selectivity. Bimorph structure of GO and ZnO/SnO_2 was prepared to compare with multilayer structure. In the case of GO and ZnO mixture, well-grown ZnO NRs were etched into the acid GO suspensions. Therefore, it seemed to be hard to construct GO and ZnO bimorph structure in this current system. However, catalytic effects and compositional effects of GO and SnO_2 were successfully investigated. The samples were prepared via EPD process, then, bimorph structure and multilayer structure were clearly observed in SEM images. After gas sensing test, enhancement in gas responses were detected

after mixing GO and SnO_2 particles. Additionally, different gas responses were measured according to the mixture ratio of GO to SnO_2. These trends support the catalytic behaviors. Moreover, different gas sensing behaviors were observed with styrene gas: n-type gas sensing behavior with formaldehyde gas and p-type gas sensing behavior with styrene gas. This change may contribute to investigating to develop single sensor array to detect multiple gases in the future.

References

1. Ahn H, Park J-H, Kim S-B, Jee SH, Yoon YS, Kim D-J. Vertically aligned ZnO nanorod sensor on flexible substrate for ethanol gas monitoring. *Electrochemical and Solid-State Letters.* 2010;13(11):J125-J128.
2. Zhou Z, Zhao Y, Cai Z. Low-temperature growth of ZnO nanorods on PET fabrics with two-step hydrothermal method. *Applied Surface Science.* 2010;256(14):4724-4728.
3. Zhu Y, Murali S, Cai W, et al. Graphene and graphene oxide: synthesis, properties, and applications. *Advanced materials.* 2010;22(35):3906-3924.
4. Ding J, Yan X, Li J, et al. Enhancement of field emission and photoluminescence properties of graphene-SnO2 composite nanostructures. *ACS applied materials & interfaces.* 2011;3(11):4299-4305.
5. Zhang DF, Sun LD, Yin JL, Yan CH. Low-Temperature Fabrication of Highly Crystalline SnO2 Nanorods. *Advanced materials.* 2003;15(12):1022-1025.
6. Besra L, Liu M. A review on fundamentals and applications of electrophoretic deposition (EPD). *Progress in materials science.* 2007;52(1):1-61.
7. Ozgur U, Hofstetter D, Morkoc H. ZnO devices and applications: a review of current status and future prospects. *Proceedings of the IEEE.* 2010;98(7):1255-1268.

8. Korotcenkov G. Metal oxides for solid-state gas sensors: What determines our choice? *Materials Science and Engineering: B.* 2007;139(1):1-23.

9. Morrison SR. Selectivity in semiconductor gas sensors. *Sensors and actuators.* 1987;12(4):425-440.

10. Lu G, Ocola LE, Chen J. Gas detection using low-temperature reduced graphene oxide sheets. *Applied Physics Letters.* 2009;94(8):083111.

11. Ko G, Kim H-Y, Ahn J, Park Y-M, Lee K-Y, Kim J. Graphene-based nitrogen dioxide gas sensors. *Current Applied Physics.* 2010;10(4):1002-1004.

12. Song H, Zhang L, He C, Qu Y, Tian Y, Lv Y. Graphene sheets decorated with SnO2 nanoparticles: in situ synthesis and highly efficient materials for cataluminescence gas sensors. *Journal of Materials Chemistry.* 2011;21(16):5972-5977.

13. Mao S, Pu H, Chen J. Graphene oxide and its reduction: modeling and experimental progress. *Rsc Advances.* 2012;2(7):2643-2662.

CHAPTER 8. SUMMARY AND FUTURE WORKS

8.1. Summary of research

Investigation of gas sensors to detect VOC gases was conducted with functional nanomaterials on flexible and wearable substrates. One of traditional metal oxide, ZnO, was investigated owing to its excellent semiconducting properties and proven gas sensing properties. For the ZnO sensing material to be deposited on wearable substrates, alternative process method was explored because most coating methods of ZnO demand higher process temperature. Therefore, four deposition methods were examined to coat ZnO seed layer on diverse wearable substrates: sputter deposition, sol-gel coating, electrophoretic deposition (EPD), and dip-pad-cure (DPC) methods. Among these coating methods, DPC coating was only performed at lower temperature (150 °C) providing stable ZnO formation and its uniform coverage on fabrics. ZnO nanostructures were also successfully fabricated on various wearable substrates such as cotton, nylon and PET via this chemical solution method. Optical and electrical properties of ZnO nanostructure grown by DPC coating were comparable of properties of ZnO nanostructure. Therefore, the growth of ZnO nanostructures via this chemical solution growth can be a proper approach to embed functional ZnO nanostructures into various fabrics for developing functional garments at low temperature. However, well grown ZnO nanostructure on garments was not sufficient for gas sensors because the ZnO nanostructure still requires elevated operating temperature for activation to react with surface oxygen.

To achieve operating temperature of ZnO gas sensing devices on wearable substrates, exploration of gradient structure with metallic catalysts was considered. In addition to effort

to lower sensing temperature, the design of multiple catalyst with gradient structure was explored to improve gas selectivity. Deposition of the catalysts on ZnO NR gas sensing devices was successfully conducted by sputter method. Pd and Pt catalysts improved the gas sensing behaviors such as gas response, gas response rate, and selectivity. Enhancement in gas sensing behaviors was observed with proper amount of catalysts, but degradation of the gas sensing behaviors was also found with large amount of the catalysts. Improvement was owing to the increase in activated sites and modification of the Fermi energy level, but the degradation was due to blockage of the activate sites by excessive catalysts. Combinatorial structure, i.e. gradient composition of the catalysts was also conducted to explore the interaction between different catalysts according to mixture ratio. The combinatorial structure was successfully deposited via co-sputter deposition. Evidently, the used catalyst and their gradient influenced gas sensing behaviors.

However, the catalyst did not reach to perform room temperature gas sensing, which means higher sensing temperature is still limit to fabricate wearable gas sensing devices. Therefore, an alternative and new sensing material, graphene oxide (GO) was investigated. Even though a single layer of GO is well known as an insulating material, it was reported that multilayer of GO has semiconducting properties due to the surface defects along and inside of the layers. Thus, GO can be a promising candidate as a sensing layer for room temperature gas sensors as reduced-GO (r-GO) does. For the fabrication of gas sensors, deposition of GO was firstly conducted via different methods: drop coating, spin coating, and EPD. Deposited films were characterized by SEM and XRD. The films deposited via drop coating were thicker and rougher, the films via spin coating were thinner and flatter, and the films via EPD were thicker. As a comparison between GO and r-GO, thermal reduction under Ar atmosphere was performed to explore changes in GO properties. Evaporation of solvents and elimination

of oxygen functional groups were examined by XRD peak shift and peak change from FTIR and XPS. Moreover, the electrical properties of non-treated GO films and heat treated GO films were confirmed via measurement of initial resistance and gas sensing properties. Then, room temperature gas sensing with GO and r-GO was demonstrated with 100 ppm of ethanol and formaldehyde gasses. Gas responses, response rate, and recovery time were changed depending on the heat treatment temperature, and types of gases. Additionally transition of gas sensing behavior was observed, i.e. non-treated GO films showed n-type gas sensing behaviors with both gases while p-type gas sensing behaviors were observed at higher heat treatment condition (above 150 °C or 100 °C for longer heat treatment time). Room temperature sensing of GO and its transition behavior from n-type to p-type gas sensing behaviors are important observation for gas sensing applications.

Lastly, single chip array sensor with a combinatorial structure with GO nanosheets and metal oxide nanoparticles (ZnO and SnO_2) was investigated to realize selective sensing of multiple gases. Bimorph structure and intercalation structure of GO and ZnO/SnO_2 were prepared by EDP to explore the interaction between two oxide materials. Enhancement in gas responses was observed after mixing GO and SnO_2 particles. Additionally, different gas responses were measured according to the mixture ratio of GO to SnO_2. These trends can be explained by catalytic behaviors. Moreover, different gas sensing behaviors were observed with different types of gases: n-type gas sensing behavior with formaldehyde gas and p-type gas sensing behavior with styrene gas. This change may contribute to developing a single chip array sensor to detect multiple gases in a small scale without complicated assembly procedure.

8.2. Future works

GO gas sensors at room temperature and GO/SnO_2 composites were successfully performed to adapt the sensors on wearable substrates. However, the sensing mechanisms were still unclear. Therefore, the study of electron transfer in GO layers and the interaction between GO and SnO_2 layers should be concentrated. Then, the embedment of electrodes on wearable devices has technical challenges with current electrode patterning systems (sputtering on shadow mask and micro-fabrication method) due to rough and disconnected surfaces. Therefore, printing conductive materials for electrode can be performed so that the electrode materials can be penetrated into the fibers without disconnection.